An Optimised Model for the Terminal Velocities of Isolated Bubbles in Magma

DAVID ALISTER SQUIRRELL

An Optimised Model for the Terminal Velocities of Isolated Bubbles in Magma

D. A. Squirrell

Department of Earth Sciences, Durham University

2024

This thesis is submitted in fulfilment of the requirements for the degree MSc by Research in Volcanology

Abstract

The rise of single, uncoupled bubbles in a Newtonian liquid medium is a well constrained phenomenon that occurs in a variety of scenarios. Their velocity is an important variable in volcanic eruption modelling, in which overpressures and fragmentation driven by bubble nucleation, growth, and degassing have been proposed as possible eruption mechanisms. Recent work has synthesised a parameterisation for rising rates across all bubble shape regimes. This thesis tests the empirical model against a larger experimental dataset and specifically within a magmatic regime, to produce an improved parameterisation for volcanic systems. This will aid in the creation of a validated quantitative model for bubble ascent in magma.

Data have been collated from ninety-one experimental studies carried out on rising bubbles. Experiments have primarily been carried out using low viscosity (<1 Pa.s) and relatively low density (<2000 kg m^{-3}) fluids. These are poor analogues for magmatic conditions. To constrain the dataset to relevant magmatic conditions, several dimensionless numbers were used. The Reynolds number (Re), the ratio of inertial to viscous forces in the fluid, defines whether the flow will be laminar or turbulent. The Eötvös number (Eö), describing the effect of surface tension, and the Morton number (M), characterising the shape of the rising bubble. The motion of isolated bubbles rising can then be described within three distinct regimes: the spherical, ellipsoidal and spherical-cap regimes, with boundary conditions between each of these regimes identified by the dimensionless parameters. Scaling analysis of magma rheology shows that bubbles remain in the spherical regime within volcanic conduits. This is visualised on an Eö-Re plot, with bubbles occurring within silicate melts having a Re number of less than 1. Consequently, the following parameterisations are suggested for the terminal velocity of individual bubbles rising in magma:

$$v_b = \frac{1}{\sqrt{\frac{144{\mu_f}^2}{g^2{\rho_f}^2 d^4} + \frac{{\mu_f}^{4/3}}{0.202^2 g^{5/3}{\rho_f}^{4/3} d^3}}}$$

v_b is the bubble terminal velocity, d is the diameter the bubble, ρ_f and μ_f are the fluid density and absolute viscosity respectively, and g is the acceleration due to gravity.

Constraining the experimental dataset collected to magmatic analogues within the relevant bubble rising regimes shows that highly viscous magmas, such as low temperature rhyolites, are poorly represented. Viscoelastic analogues could be used; however, these produce experimental difficulties. Further studies of isolated bubbles rising in highly viscous magmatic analogues would help optimise this equation further for use in eruption modelling.

Table of Contents

Acknowledgements

Firstly, I'd like to thank my supervisors, Ed Llewellin and Fabian Wadsworth for their support and patience throughout this seemingly never-ending project. Your advice, guidance and reassurance have been really appreciated. Thanks, must also go to the wider student support team including Grant Slater, Louise Bowron and Janice Oakes. So much of your work comes in students' toughest times at university, but your positive and friendly attitude seems endless. It makes so much difference knowing that someone is looking out for us, and I can't put into words how much I appreciate the work you do behind the scenes.

I'd also like to thank my partner Izzy Friedlander. The past few years seem to have been a series of unfortunate events, but they've also been some of the best times thanks to you! There's not a chance I'd be here without the love and patience you've shown me. Hopefully we can now start the next chapter in our lives.

Finally, to my parents, Sally and Michael Squirrell. I may not say it enough, but I truly appreciate how much you have done to support me, especially when I have fought against it. I only hope that I can raise my future children with as much support, love, and care that you have. Because of you both, I can aim for the stars.

Statement of Copyright

List of Figures

List of Tables

Nomenclature

Notation	Variable
a	Spherical-cap Radius
$A_{b,xy}$	Cross-sectional Area of Bubble in the x-y plane
A_m, B_m	Melt Constants
C_d	Drag Coefficient
d_{eb}	Equivalent Spherical Bubble Diameter
E	Aspect Ratio
g	Acceleration due to Gravity
G_∞	Shear Modulus at Infinite Frequency
k	Ratio of Bubble to Fluid Absolute Viscosity
K	Wall Effect Correction Factor
p	Pressure
p_0	Reference Pressure at Stagnation Point
Δp	Pressure Difference across Gas-Fluid Interface
r_{eb}	Equivalent Spherical Bubble Radius
R_1, R_2	Principal Radii of Curvature
T	Temperature
T_m	Melt Temperature
u_f	Fluid Velocity
u_b	Bubble Velocity
Δu_z	Difference in Bubble to Fluid Velocity in z axis
V_b	Bubble Volume
v_b	Bubble Terminal Velocity
$\dot{\gamma}$	Shear Strain Rate
λ	Wall Diameter Ratio
μ	Apparent Viscosity
μ_0	Intrinsic Viscosity
μ_b	Bubble Absolute Viscosity
μ_f	Fluid Absolute Viscosity
μ_r	Relative Viscosity
ρ_b	Bubble Density
ρ_f	Fluid Density
ρ_x	Crystal Density
$\Delta\rho$	Difference in Fluid to Bubble Density
σ	Surface Tension
τ_r	Viscous Relaxation Time
ϕ	Gas Volume Fraction
ϕ_x	Crystal Volume Fraction

Notation	Equation
$C_{b,HR}$	Hadarmard-Rybczynski solution for Drag Coefficient
f_{sc}	Park Scaling Factor for Contaminated Bubbles
$RE_{Optimised}$	Optimised Park solution for Reynolds Number
$v_{b,BR}$	Baz-Rodríguez solution for Bubble Terminal Velocity
$v_{b,DT}$	Davies & Taylor solution for Bubble Terminal Velocity
$v_{b,E}$	Ellipsodal solution for Bubble Terminal Velocity
$v_{b,HR}$	Hadarmard-Rybczynski solution for Bubble Terminal Velocity
$v_{b,Magmatic}$	Magmatic solution for Bubble Terminal Velocity
$v_{b,Optimised}$	Optimised Park solution for Bubble Terminal Velocity
$v_{b,P}$	Peebles solution for Bubble Terminal Velocity
$v_{b,Park}$	Park pure solution for Bubble Terminal Velocity
$v_{b,SC}$	Spherical-cap solution for Bubble Terminal Velocity
$v_{b,St}$	Stokes solution for Bubble Terminal Velocity
$v_{b,W}$	Wallis solution for Bubble Terminal Velocity

Notation	Statistical Method
$MAPE$	Mean Absolute Percentage Error
$wMAPE$	Weighted Mean Absolute Percentage Error
w_iMAPE	Weighted Mean Absolute Percentage Error per Interval
$w_{sf}MAPE$	Weighted Mean Absolute Percentage Error per Study Fluid
n	Number of Datapoints
n_{sf}	Number of Studied Fluids
δ_v	Relative Error in Velocity
$\delta_{\log(v)}$	Relative Error in Logarithm (Base 10) of Velocity

Notation	Dimensionless Number
Ca	Capillary Number
Eö	Eötvös Number
M	Morton Number
Re	Reynolds Number
We	Weber Number

1. Introduction

Volcanic eruptions are driven by bubbles that nucleate when volatile species exsolve from the magma. The conditions for bubble nucleation primarily depend upon the magma composition, volatile concentration, the volume fraction of suspended crystals, and the decompression rate (Gardner et al., 2023). Bubble ascent in magma can increase pressure and stress within the volcanic conduit, triggering eruptive activity. The growth of bubbles drives this ascent. Under the non-isobaric and isothermal conditions within a volcanic conduit, ascent-driven decompression occurs, accelerating the rise of both the magma and bubbles within it, potentially inducing fragmentation (Melnik & Sparks, 1999; Papale, 1999; Gonnermann & Manga, 2003; Gonnermann, 2015; La Spina et al., 2022). Exsolution of volatiles from the melt into the bubbles due to a saturation gradient further increases the bubble size or pressure, driving magma ascent (Sparks, 1978; Sparks, 1983; Pyle & Pyle, 1995; Woods & Cardoso, 1997; Wallace et al., 2015). Outgassing of these volatiles through decoupled bubbles can reduce the explosivity of eruptions (Eichelberger et al., 1986; Cassidy et al., 2018). The processes involving bubbles that occur during the rising of magma define the eruptive behaviour of the volcano as the magma approaches the surface (Sparks, 2003; Gonnermann & Manga, 2007; Vergniolle & Gaudemer, 2015; Spina et al., 2019; Crozier et al., 2022; Weaver et al., 2022). Consequently, accurately modelling bubble ascent within the conduit is essential for understanding eruptive dynamics.

Various formulae to describe the terminal rising velocity of bubbles under different bubble shape regimes have been proposed (Stokes, 1851; Allen, 1900; Hadamard, 1911; Rybczynski, 1911; Boussinesq, 1913; Davies & Taylor, 1950; Moore, 1965; Mendelson, 1967; Wallis, 1974; etc.). More recently, these equations have been combined into parameterisations (Jamialahmadi et al., 1994; Bozzano & Dente, 2001; Baz-Rodríguez et al., 2012; Park et al., 2017) to remove the circular dependency of the velocity and bubble regime. However, these models have not been explicitly tested against magmatic conditions. The datasets they test against are generally

limited to 5-10 studies, focused on water, mixtures of glycerol, or oils as the liquid phase. These fluids are poor magmatic analogues. Analysis of a model's fit to experimental data primarily rely on water, even when other fluids were used for comparison, leading to potential bias when assessing models (e.g., Moore, 1965; Collins, 1967; Wallis, 1974; Wegener & Parlange, 1973; Karamanev, 1994; Nguyen, 1998; Bozzano & Dente, 2001; Rodrigue, 2001, 2002, 2004; Clanet et al., 2003; Kulkarni & Joshi, 2005; Baz-Rodriguez et al., 2012; Amirnia, 2013; Park et al., 2017; Kure, 2021; Kosior et al., 2023). The simplicity of the experimental setup by using water as the fluid medium can allow for greater precision and the results can then be directly compared to the array of previous studies carried out with highly purified water. However, model validation should still consider a range of fluids. A clear research gap exists in testing models for the terminal velocities of isolated bubbles using a more extensive and varied experimental dataset, especially fluids analogous to magma.

Models for the terminal velocities of isolated bubbles under magmatic conditions have been proposed (Prousevitch et al., 1993; Lensky et al., 2004; Huber et al., 2014; Coumans et al., 2020), but testing these experimentally is difficult. Many additional factors can influence bubble growth and ascent within conduits, increasing the complexity of the problem. Magma is a multiphase, viscoelastic material in which bubbles are constantly interacting with each other. Impurities, including surfactants, are present, and there are external influences such as the conduit wall and pressure oscillations. Producing a simplified parameterisation for the terminal velocity of rising bubbles will help reduce the complexity of modelling the eruptive processes in volcanoes. Therefore, this study aims to compile existing experimental data on bubble ascent, evaluate current bubble terminal velocity models against this more extensive and varied dataset, and then produce a validated quantitative model for bubble ascent in magma.

2. Current Theory

The motion of bubbles rising in liquid columns has been extensively studied due to its impact on countless industrial processes. Research generally focuses on specific sections of a bubble's "lifespan": nucleation, growth, interaction, and breakup. Each of these stages involves different characteristic values, which makes compiling datasets containing all the relevant information for bubble rising terminal velocity challenging. To effectively analyse bubble terminal velocity models, it is essential to first identify the key variables relevant to each model.

Due to the varied focus of previous studies, experimental setups are very inconsistent, with different independent variables being controlled depending on their specific research objectives. Bubble terminal velocity data stretches back as far as the work by Allen (1900), while studies on rising bubbles reach the 1850s (Stokes, 1851). Our understanding of the forces involved has developed since then. Consequently, it is crucial to identify and incorporate these additional forces into the data collection process, as they may have influenced the accuracy and relevance of published experimental data.

2.1 Bubbles

2.1.1 Forces on a Rising Bubble

In this study, the focus is single gas bubbles rising at terminal velocity in a boundless, homogenous Newtonian liquid under isobaric and isothermal conditions with no mass transfer taking place. Taking this simplified frame of reference, the forces acting upon the bubble are as follows,

$$F_{bubble} = F_{buoyant} - F_{drag}. \tag{1}$$

2.1.2 Single Bubble Terminal Velocity

Using Newton's second law, an expression for the bubble rise velocity in the z-axis can be created:

$$\frac{d}{dt}(m_b u_{b,z}) = (\rho_f - \rho_b)V_b g - \frac{1}{2}\rho_f \Delta {u_z}^2 C_d A_{b,xy}. \tag{2}$$

Δu_z is the flow velocity of the bubble relative to the fluid in the z-axis, V_b is the volume of the bubble, $A_{b,xy}$ is the cross-sectional area of the bubble in the $x-y$ plane, and C_D is the drag coefficient, a dimensionless quantity used to describe the resistance of the object to its movement through a fluid. ρ is the density and g is the acceleration due to gravity.

When a bubble reaches terminal velocity (v_b), it has no acceleration; therefore, equating the drag and buoyant forces produces the following expression for the terminal velocity of the bubble relative to the fluid:

$$v_b = \sqrt{\frac{2(\rho_f - \rho_g)V_b g}{\rho_f C_d A_{b,xy}}} - u_f. \tag{3}$$

To calculate the terminal velocity, the cross-sectional area of the bubble ($A_{b,xy}$), and therefore its shape, must be calculated. Taking a stationary bubble in a liquid medium, the pressure difference across the gas-liquid interface (Δp) can be given by the Young-Laplace equation,

$$\Delta p = -\sigma\left(\frac{1}{R_1} + \frac{1}{R_2}\right), \tag{4}$$

in which σ is the surface tension and R_1 and R_2 are the principal radii of curvature.

As a gas bubble rises in a liquid medium, the forces are no longer homogenous across the gas-liquid interface, and the bubble shape may be deformed. Consequently, the frontal cross-sectional area of the bubble ($A_{b,xy}$) may vary, changing the terminal velocity of the bubble and, in turn, the coefficient of drag. This is problematic as Equation (3) falls into a circular dependency and cannot be used to calculate bubble terminal rise velocity.

2.1.3 Bubble Regimes

To produce a functional equation for the terminal rise velocity of a bubble, rising bubbles can be categorised into shape regimes. This allows the calculation of the frontal cross-sectional area for each different bubble shape, independent of the bubble velocity. Feeding these formulas back into Equation (3) produces separate equations for each rising regime between the critical points at which the shape changes. These can then be combined to produce a parameterisation for the terminal velocity of the bubble.

There are three distinct bubble rising regimes, as seen in Fig. 1, each based upon which forces are dominant in creating the shape of the bubble.

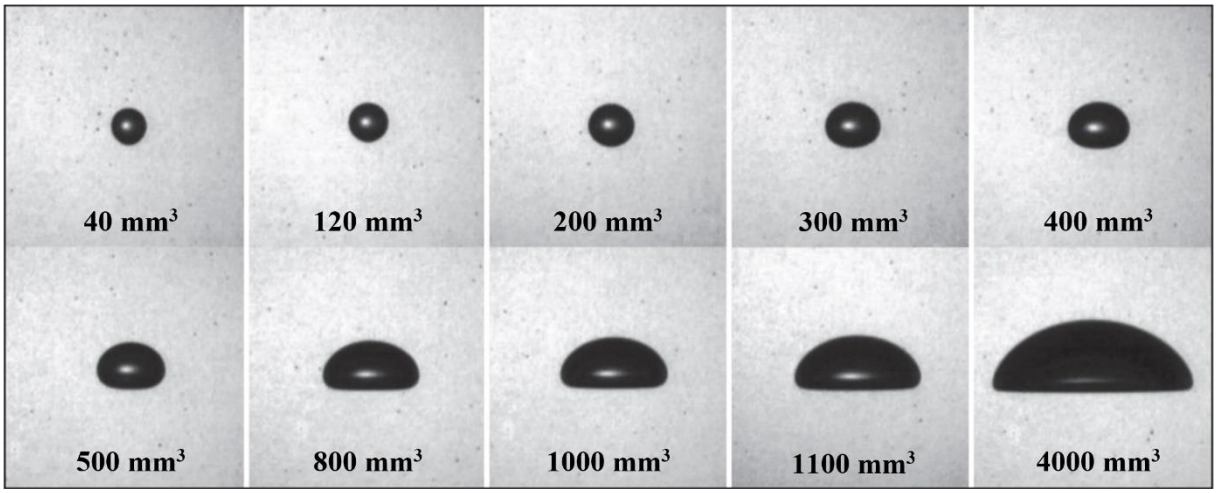

Figure 1. Evolution of bubble shape regimes as bubble volume increases from 40 to 4000 mm³ in an ethylene glycol–Carbopol mixture. The top row covers the spherical to ellipsoidal regimes, progressing into the spherical-cap regime on the bottom row. Adapted from Chelate (2004), copyright Universidad Nacional Autonoma de Mexico.

2.1.3.1 Spherical

In the spherical regime (also known as the Stokes regime), viscous and/or interfacial forces are dominant. Given the uniform nature of these forces acting upon the bubble, the surface area of the bubble is minimised, forming the shape of a sphere. Using the Navier-Stokes equation for a bubble in the spherical regime, Hadamard (1911) and Rybczynski (1911) both independently derived the following simplified equation:

$$p = p_0 + \mu_f u_b \frac{(2+3k)}{2r^2(1+k)},$$

(5)

with,

$$k = \frac{\mu_b}{\mu_f},$$

(6)

where p is the pressure, p_0 is the reference pressure (a constant), μ_f is the fluid absolute viscosity, μ_b is the bubble absolute viscosity, u_b is the bubble velocity, and r is the equivalent spherical radius. Integrating the pressure over the surface of the bubble gives:

$$C_{d,HR} = \frac{4\mu_f}{\rho u_b r}\left(\frac{2+3k}{1+k}\right).$$

(7)

For a bubble at terminal velocity, there must be no net force; therefore, balancing the forces in Eq. 2 and substituting in the above equation for C_d leads to,

$$v_{b,HR} = \frac{2gr^2\Delta\rho}{3\mu_f}\left(\frac{1+k}{2+3k}\right).$$

(8)

For most gas-fluid systems, the bubble viscosity is significantly lower than the fluid viscosity, therefore $k \to 0$, producing the Hadamard-Rybczynski equation for terminal velocity,

$$v_{b,HR} = \frac{gr^2\Delta\rho}{3\mu_f}.$$

(9)

2.1.3.2 Ellipsoidal

In the ellipsoidal regime, interfacial forces and inertial forces are dominant and of similar magnitude. The shear force created by the fluid moving around the bubble starts to overcome the surface tension, elongating the bubble in the $x-y$ plane. Slight asymmetries in the pressure field around the bubble are then amplified, causing the bubble to rotate.

When an anisotropic object rotates as it moves through a fluid, it creates pressure differences on either side, inducing a lift force commonly referred to as the "Magnus effect." These additional forces produce helical or oscillatory motion of the bubble through the fluid (shown in Figure 2), reducing the z component of its velocity. The onset of path instabilities for two-phase systems is similar for spherical and anisotropic objects (Fernandes et al., 2007) and is commonly referred to as a critical point, described in terms of the equivalent spherical radius or Reynolds number. Beyond this point, the rising dynamics of the bubble are fundamentally different as the centre of pressure decouples from the geometric centre of the bubble. The rotational dynamics of the bubble and the oscillatory variation of the wake compound exaggerate the path instability of the bubble rise (Zhou et al., 2017; Will et al., 2021).

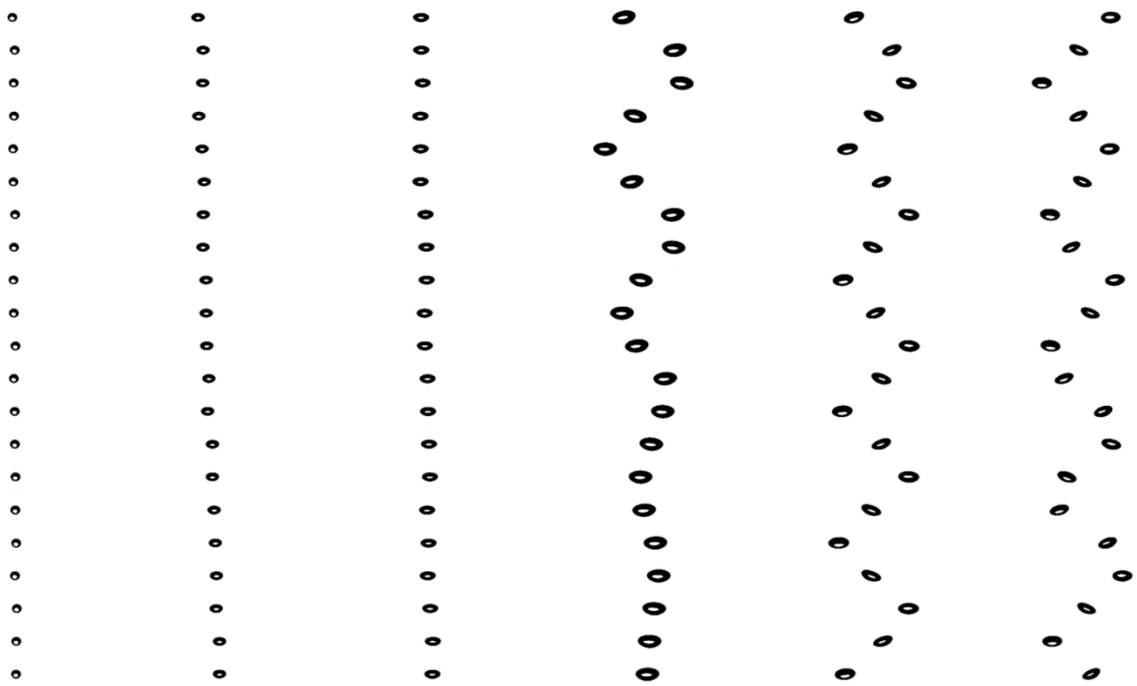

Figure 2. Rising trajectories of oxygen bubbles in deionized water at 23°C. The equivalent spherical bubble radius varies from 0.38mm to 0.87mm (left to right). Image from Kure et al. (2021), copyright AIP Publishing

As the bubble deviates from a rectilinear path, the study of the terminal velocity becomes empirical due to the multitude of additional forces to consider. Peebles (1952) suggested one of the first equations for this shape regime,

$$v_{b,P} = 1.35\sqrt{\frac{\sigma}{r\rho_f}}. \tag{10}$$

However, being an empirical equation, it is limited by the dataset used. Later studies indicated that bubbles in high-viscosity fluids move much slower than the terminal velocity calculated by Equation (10). Mendelson (1967) approached the issue from a wave perspective, due to the oscillatory nature of the motion. Using Mendelson's equation as a base, Clift, Grace, and Weber (1978) suggest the following equation for the ellipsoidal regime, using empirical constants to adjust the curve (plotted in Figure 3):

$$v_{b,E} = \sqrt{\left(\frac{2.14\,\sigma}{\rho_f d_{eb}}\right) + 0.505 g d_{eb}}, \tag{11}$$

where d_{eb} is the equivalent diameter of a spherical bubble. Considering just the surface tension term, Equation (11) is similar to that initially proposed by Peebles, however, the additional term provides a better fit of experimental data closer to the spherical-cap regime.

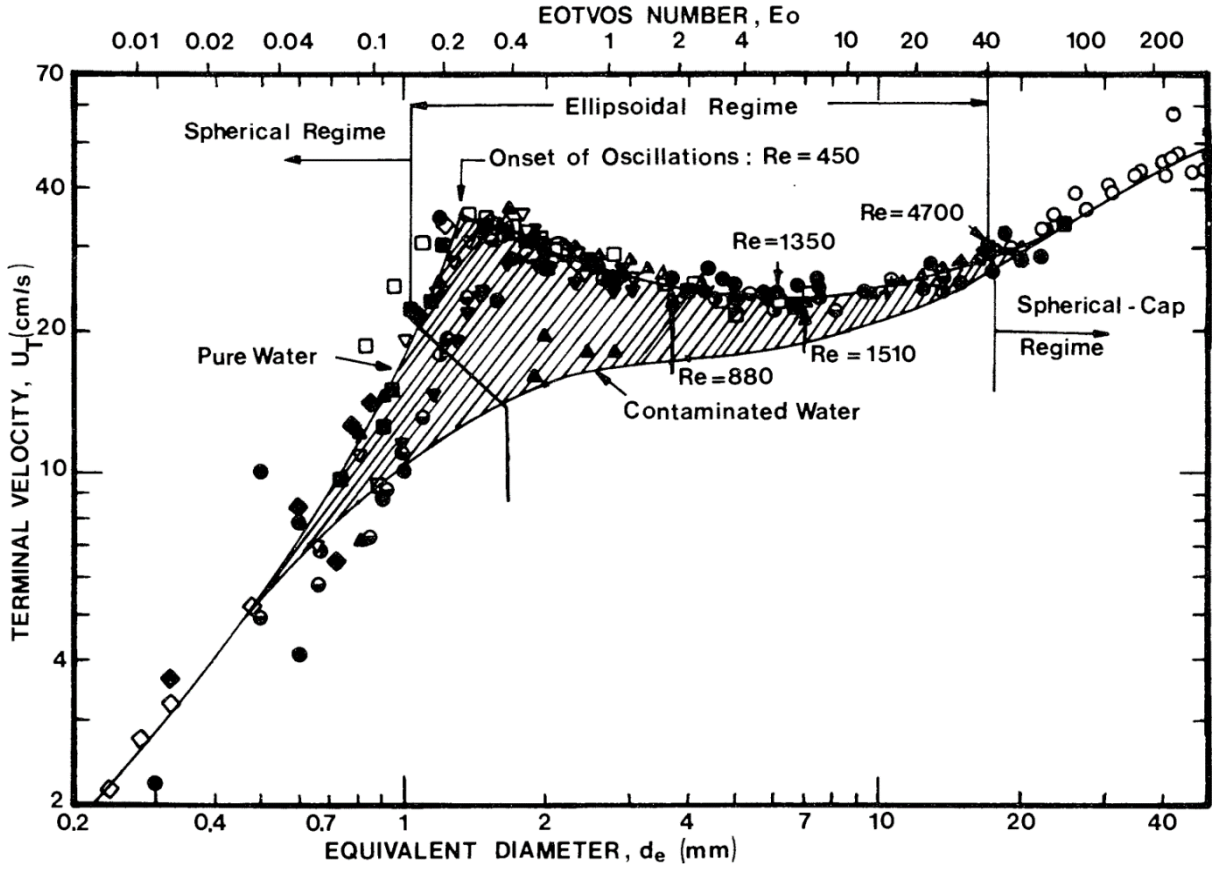

Figure 3. The terminal velocity of air bubbles in water at 20°C highlights the impact of each bubble regime on the rising velocity and onset of path instabilities. Adapted from Clift et al. (1978), copyright Academic Press.

2.1.3.3 Spherical-cap

In the spherical-cap regime, the inertial forces are dominant. By considering the fluid flow around the leading edge of the bubble, we can use Bernoulli's principle to calculate the pressure distribution and therefore the terminal velocity,

$$p - p_0 = ga\rho_f(1 - cos\theta) - \frac{9}{8}\rho_f {v_b}^2 \, sin^2 \, \theta,$$

(12)

where a is the radius of the spherical-cap. For relatively large bubbles, we can consider the pressures across the thin interior boundary layer. The slowly moving interior fluid imposes a pressure across this layer (Davies & Taylor, 1950; Harper & Moore, 1968), which is supported by internal circulation measurements (Wairegi, 1974). The following equation can then be determined,

$$p - p_0 = ga\rho_b(1 - cos\theta).$$

(13)

Equating Equation (12) with Equation (13) and then considering the stagnation point at the leading edge of the bubble, at which $\theta \to 0$, produces the Davies and Taylor equation (Davies & Taylor, 1950):

$$v_{b,DT} = \frac{2}{3}\sqrt{\frac{ga\Delta\rho}{\rho_f}}.$$

(14)

For most fluid-gas systems, $\frac{\Delta\rho}{\rho_f} \to 1$ which can simplify Equation (14) further, however, bubbles entering the spherical-cap regime are not always spherical, displaying eccentricity and path instabilities. As the bubbles increase in velocity and radius, they become geometrically similar, with a wake angle of approximately 50° (Davenport et al., 1967; Wu, 1972; Clift et al., 1978). Therefore, we can convert the spherical-cap radius a to the equivalent spherical diameter d_{eb},

$$v_{b,SC} = 0.711\sqrt{gd_{eb}}.$$

(15)

2.1.4 Dimensionless Numbers

To compare bubbles under a variety of conditions, dimensionless numbers, which characterise the ratio of forces upon the bubble, can be used. These numbers enable the production of universally applicable limits of bubble regimes to model rising bubble terminal velocities and flow patterns. Therefore, dimensionless numbers will be used to scale experimental data across the range of fluid and bubble properties. The ratios between the viscous, interfacial, and inertial forces upon a bubble can be described by the dimensionless numbers indicated in Table 1.

Ratio	**Inertial**	**Viscous**	**Interfacial**
Inertial	*d*, *u*, *a*	Reynolds Number	Weber Number
Viscous	Reynolds Number $^{-1}$	μ	Eötvös Number
Interfacial	Weber Number $^{-1}$	Eötvös Number $^{-1}$	σ

Table 1. The dimensionless number characterising each ratio of forces on a bubble.

2.1.4.1 Reynolds Number

The Reynolds number (Re) is the ratio of inertial to viscous forces within a fluid, defining whether the flow will be laminar or turbulent around a particle (Stokes, 1851; Reynolds, 1883). Laminar flows, in which the fluid moves past the particle (or vice versa) relatively undisturbed due to the high ratio of viscous to inertial forces, have a low Reynolds number. In this thesis, the Reynolds number will be expressed as,

$$Re = \frac{u_b \rho_f d_{eb}}{\mu_b}. \tag{16}$$

When considering bubbles rising in fluids, the equivalent spherical bubble diameter d_{eb}, is used as the characteristic length; however, other studies use the radius. As the bubble shape changes, the leading edge retains a curved profile unless breakup occurs. The leading edge is dominant (but not isolated) in the calculation of the forces upon the bubble. Therefore, the equivalent spherical bubble diameter is the best approximation available.

2.1.4.2 Weber Number

The Weber number (We) is the ratio between the inertial force and the interfacial force. It is of particular importance when considering multiphase flows such as foams, crystal mushes, and suspensions. Considering single bubble systems, the Weber number is the ratio of inertia to surface tension and is described as,

$$We = \frac{{u_b}^2 \rho_f d_{eb}}{\sigma}. \tag{17}$$

2.1.4.3 Eötvös Number

The Eötvös number (Eö), also referred to as the Bond number (Bo), describes the ratio of inertial forces to interfacial forces (Eötvös, 1886). A high ratio $>> 1$ signifies inertial forces are dominating. In the case of a rising bubble, a high Eötvös number therefore indicates that the bubble is more likely to have an increased cross-sectional area in the direction of travel. The Eötvös number is given by,

$$\text{Eö} = \frac{\Delta \rho g {d_{eb}}^2}{\sigma}. \tag{18}$$

2.1.4.4 Morton Number

Instead of describing a ratio of forces, as presented by the dimensionless numbers in Table 1, the Morton number (M) characterises the shape of a rising bubble (Haberman & Morton, 1953). The Morton number is obtained by,

$$\mathrm{M} = \frac{\Delta\rho g {\mu_f}^4}{{\rho_f}^2 \sigma^3}.$$

(19)

Importantly, the Morton number is independent of the bubble radius or velocity; therefore, it is constant for any bubble-fluid system, irrespective of the bubble volume, shape, and velocity. Consequently, the relationship between the Reynolds number and the Eötvös number can be calculated using the Morton number.

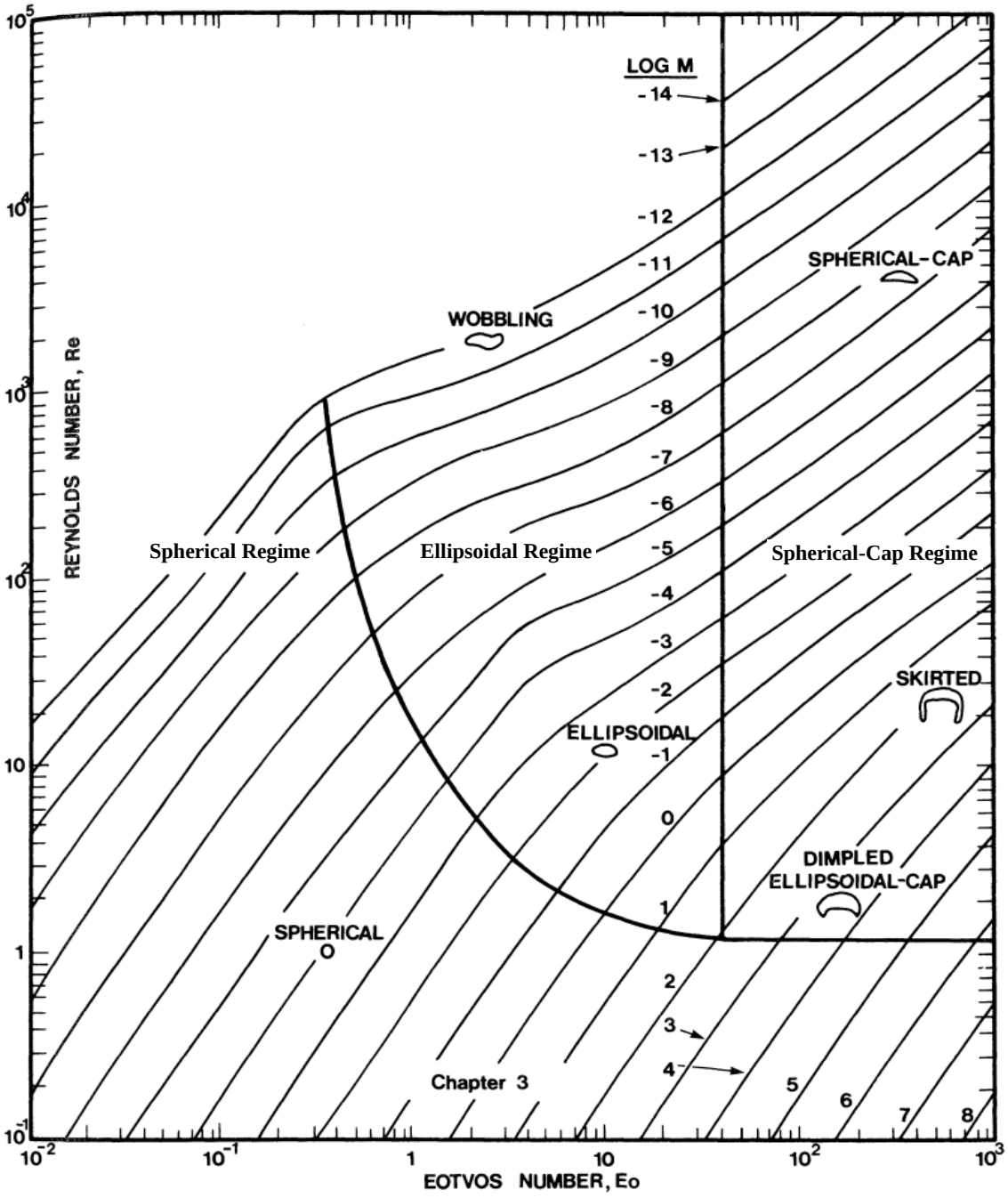

Figure 4. A Grace plot highlighting the different bubble shape regimes and the boundaries between them. Morton number lines are overlaid. Adapted from Clift et al. (1978), copyright Academic Press.

2.1.5 Boundary Conditions

Plotting dimensionless quantities such as the Reynolds number against the Eötvös number for experimental data and overlaying values of the Morton number is a graphical representation referred to as a Grace plot (Grace, 1973). We can use this to define the boundary conditions of different bubble rising regimes, as seen in Figure 4. The Morton number is representative of the specific fluid-bubble system; therefore, when plotting the theoretical Morton number line and experimental dataset on a Grace plot, all the experimental points should fall on the theoretical line. Any consistent deviation can identify when the experimental conditions have varied throughout the study or other factors have influenced the terminal velocity.

2.1.6 Further Considerations

When modelling the terminal velocity of a bubble, we must apply constraints to the situation. There are a myriad of forces that can impact the bubble terminal velocity within a volcanic conduit, and we currently do not have the computing capacity or understanding to account for them all. In practice, these additional forces may have a significant impact on the terminal velocity. Previous work on bubble terminal velocity is also inconsistent in accounting for these forces, and therefore understanding the impact they may have helps identify experiments with systematic errors that must be corrected for or removed from the dataset.

2.1.6.1 Surface-Active Contaminants

Experimental results show that small bubbles in viscous fluids within the spherical regime can act more like rigid spheres, in part due to a lack of internal circulation, consequently obeying Stokes' Law (Stokes, 1851; Bond & Newton, 1928; Clift et al., 1978). If we treat the bubble as a rigid sphere, then $k \to \infty$ and we get the following alternate equation for terminal velocity in the spherical regime:

$$v_{b,St} = \frac{2gr^2\Delta\rho}{9\mu_f}.$$

(20)

Considering larger bubbles within the spherical regime, it has been observed that the Hadamard-Rybczynski equation overestimates the terminal velocity. Several iterations of the equation have been put forward to address this, notably by Boussinesq (1913), Haberman and Morton (1953), Scriven (1960), Levich (1962), and Wallis (1974). These all adjust the constants in the equation, similarly to the Stokes equation, but some through different methods.

The generally accepted theory for these variations from the Hadamard-Rybczynski equation is that surface-active substances accumulate at the interface, rendering it immobile and reducing the surface tension (Frumkin & Levich 1947). If this is the case, then bubbles that are free of surface-active contaminants should display internal circulation, no matter the size. Most experimental studies using extremely pure systems support this theory (Redfield & Houghton, 1965; Maxworthy, 1996; Parkinson et al., 2008; Pawliszak et al., 2019), although some have observed distilled systems to follow Stokes' Law (Detsch, 1991). Consequently, under perfect conditions in which we have a pure fluid, or when we can calculate the impact of the surfactants on the surface tension, the Hadamard-Rybczynski equation is more accurate than Stokes'.

2.1.6.2 Wall Effect

The buoyant force exerted on a bubble can act tangentially to the initial direction of motion, especially as the shape of the bubble is deformed. A transverse migration of the bubble can then occur. This differs from the standard non-rectilinear paths found in elliptical bubbles in that there is a net transverse movement of the bubble. Smaller bubbles tend to migrate towards the walls of a system, whereas larger bubbles migrate to the centre (Zun, 1980; Kariyasaki, 1987; Tomiyama et al., 1993; Serizawa & Kataoka, 1994; Tomiyama et al., 1998; Tomiyama et al., 2002).

The presence of a boundary layer produces further interfacial interactions with the bubble. A "wall force" occurs, reducing the rising velocity of the bubble, and producing additional transverse movement (Vasseur & Cox, 1976; Takemura & Magnaudet, 2003; Zeng et al., 2005; Zaruba et al., 2006; Zeng et al., 2009). Contaminated bubbles add another layer of complexity to the wall force, always being repelled by the wall (Feng, 2017).

The ratio of bubble diameter to container diameter, λ, has a major influence on the magnitude of the wall effect, as do the Reynolds and Eötvös numbers of the system. Experimental and theoretical studies have produced a range of minimum values of λ at which the wall effect begins to have an impact on the rising velocity ($> 2\%$ reduction), varying from 0.3 (Clift et al., 1978) to 0.007 (Countanceau & Thizon, 1979) depending on the system conditions.

When considering magmatic conditions, λ is rarely going to be in the range for the wall effect to have a significant impact on the terminal velocity. The only exception is very close to the surface where extreme decompression-based expansion, or coalescing bubbles, form a slug, also known as a Dumitrescu-Taylor bubble (Dumitrescu, 1943; Davies & Taylor, 1950). However, experimental studies use methodologies that can have far greater values of λ. Increased values of λ are prominent when generating magmatic analogues in high temperature conditions, or using more complex experimental setups, such as rotating containers producing Taylor–Couette flow (Taylor, 1923; Couette, 1990), or an annulus. In these cases, one of the proposed wall effect correction factors (K) may need to be applied (Ladenburg, 1907; Faxén, 1922; Francis, 1933; Rosenberg, 1950; Habermann & Sayre, 1958). In this study, Habermann & Sayre's solution for a circulating sphere travelling in steady motion along the axis of a cylindrical tube at low Reynold's number is the most relevant. It is applicable when $\lambda < 0.6$ in a surfactant free fluid and as $\mu_f \gg \mu_b$ within magmatic conditions, it can be simplified to,

$$K = \frac{1 + 1.1378\lambda^5}{1 - 1.4034\lambda + 1.1378\lambda^5 - 0.72603\lambda^6}. \quad (21)$$

2.1.6.3 Bubble-Bubble Interactions

Bubbles are rarely isolated in real-world scenarios. Interaction between bubbles can produce additional forces to consider, especially when modelling volcanic processes. The drag force is a significant component of the terminal velocity of a bubble. Therefore, when there is a stream of bubbles, the wake dynamics of a leading bubble impacts the drag coefficient of the following bubble (Coppock & Meiklejohn, 1951). An increased bubble frequency is directly correlated to an increase in bubble terminal velocity (Owens, 1921; Sam et al., 1996).

When the gas volume fraction, ϕ, is greater than 2%, there is the possibility of bubble interaction and coalescence (Vergniolle & Gaudemer, 2015; Giachetti et al., 2019). Bubble coalescence increases the velocity of the bubbles as it is proportional to ${r_{eb}}^2$. It also further disrupts the fluid, reducing the drag coefficient on the following bubbles. Coalescence requires the drainage of the melt film surrounding the bubbles (Datta et al., 1950); consequently, the rate of coalescence is dependent on the size of the bubble and fluid viscosity (Gonnermann & Manga, 2007), becoming unlikely for Reynolds numbers ≥10 (Narayanan et al., 1974).

2.2 Magmatic Conditions

To analyse current models of bubble terminal velocities under magmatic conditions, we first need to identify the composition of magma within the conduit and the thermodynamic conditions. Once we understand the conditions, we can constrain the dataset collected to experiments that are well scaled to magmatic conditions. The composition of bubbles affects volcanic processes within the conduit, such as bubble growth, due to a concentration gradient between itself and the surrounding melt; however, the viscosity and density of the bubbles are orders of magnitude smaller than those of the surrounding fluid. Variations in the bubble composition produce minimal impact and therefore can be ignored when modelling the terminal velocity.

2.2.1 Melt Rheology

2.2.1.1 Viscosity

The rheological properties of magmas exhibit substantial variability. Highly silicic melts, such as rhyolites, are composed of a greater weight of orthosilicate anions. The SiO_4 tetrahedral anions that form are linked by Si-O bonds that break and reform, resulting in a highly viscous flow. The presence of additional alkali cations, such as sodium and potassium, forms metal oxides (NaO_2 and K_2O), depolymerising the melt and reducing its viscosity. Different anhydrous melts can be classified on a total alkali silica diagram, as seen in Figure 5.

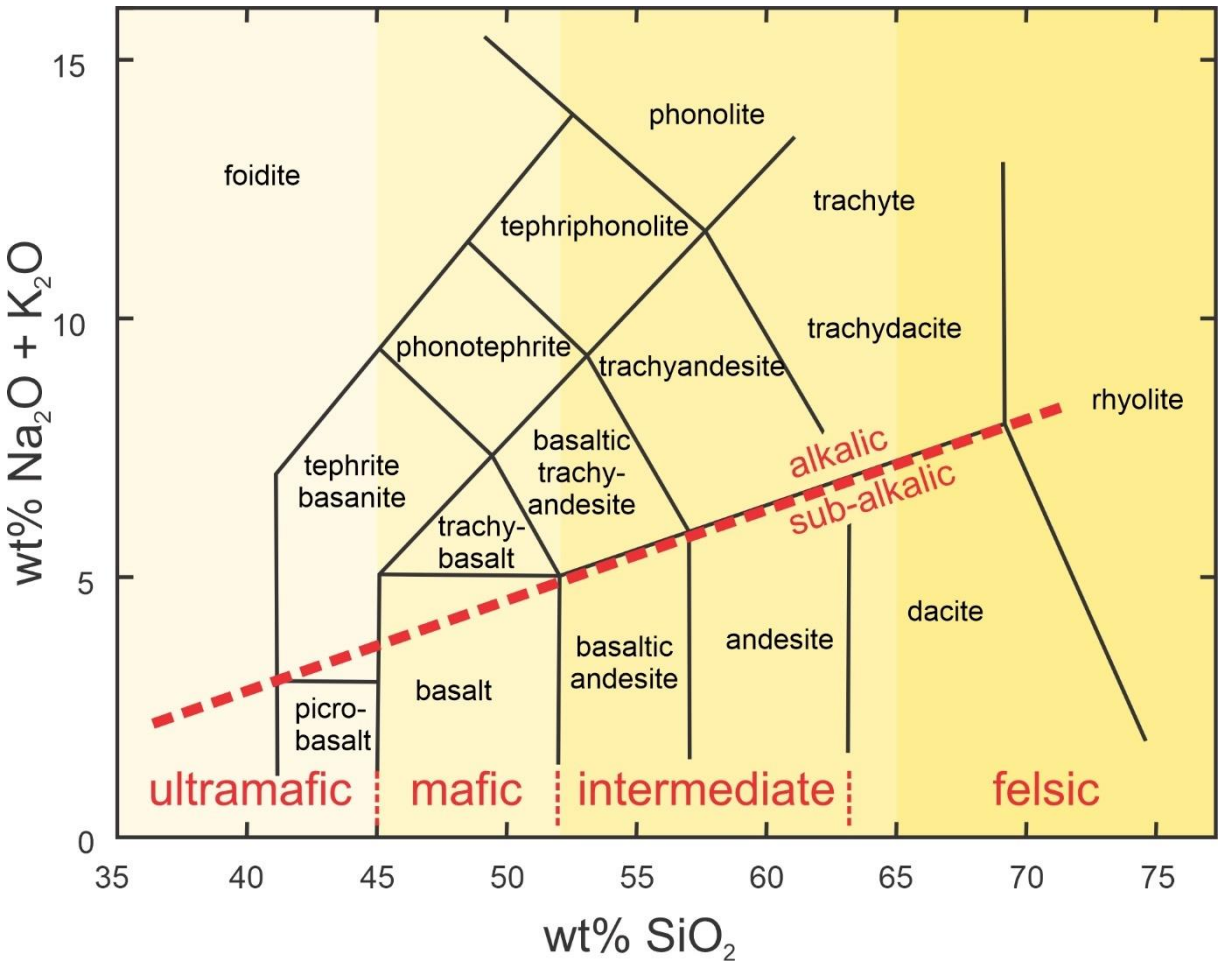

Figure 5. Total alkali silica diagram highlighting the different weightings of SiO_2 and $NaO2 + K_2O$ in anhydrous melts and the resulting classifications. Figure from Perkins (2022), copyright University of North Dakota.

The presence of dissolved volatiles, primarily H_2O and CO_2, causes depolymerisation of the melt. H_2O molecules react with O^{2-} anions, breaking the Si-O bond and producing hydroxide anions, reducing the melt viscosity (Bottinga & Weill, 1972; Behrens & Gaillard, 2006). Dissolved CO_2 also reduces the melt viscosity, but to a lesser extent (Bourgue & Richet, 2001; Zhang et al., 2007). As H_2O is more prevalent than CO_2 in silicic melts, increased dissolved volatiles reduce the viscosity to a greater extent in silicic magmas than mafic magmas, as shown in Figure 6 (Giordano et al., 2006; Hui and Zhang, 2007).

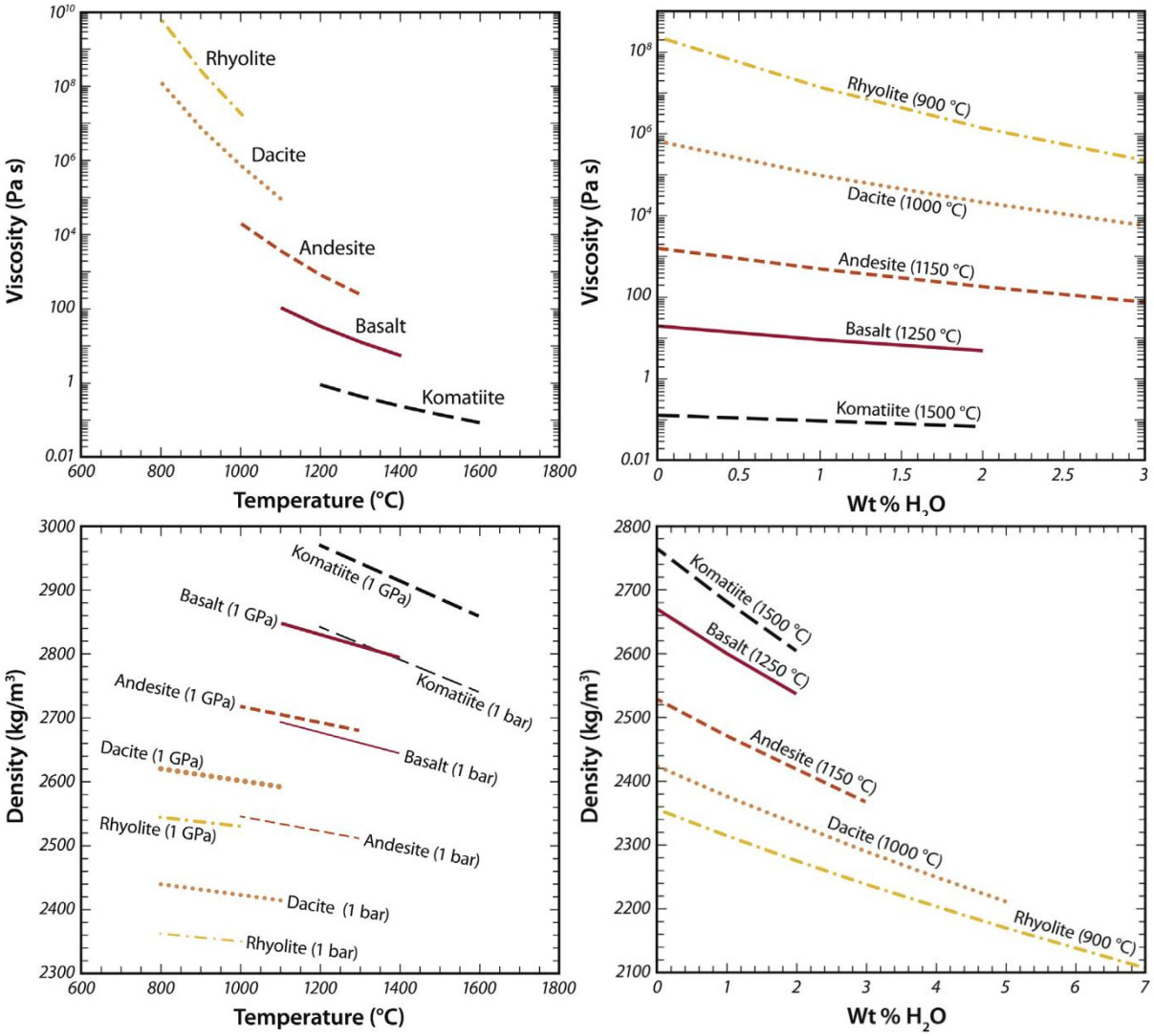

Figure 6. Melt viscosity and density as functions of temperature and H_2O content for a range of melt compositions. Viscosities and densities are calculated for anhydrous melts at a pressure of 10^{-4} MPa (1 bar) when not otherwise listed, using models from Shaw (1972) and Giordano et al. (2008). Adapted from Lesher & Spera (2015), copyright Academic Press.

Silicate melt viscosity also exhibits a strong temperature dependency. Due to the large temperature range found in magma, not all silicate melts follow an Arrhenian temperature-viscosity relationship (Romine & Whittington, 2015). General models have been proposed (Hui and Zhang, 2007; Giordano et al., 2008); however, a simplified Vogel-Fulcher-Tammann equation (Vogel, 1921; Fulcher, 1925; Tammann & Hesse, 1926) using empirical fitting parameters is preferred for computational modelling (Whittington et al., 2009); given by,

$$\log_{10}(\mu_f - \mu_0) = \frac{A_m}{T_m - B_m}, \tag{22}$$

where μ_0 is the viscosity at an infinite temperature, A_m and B_m are melt dependent constants, and T_m is the melt temperature. Low temperatures can therefore increase the melt viscosity exponentially. Due to these factors acting in combination, melt viscosity can vary by many orders of magnitude. Anhydrous rhyolites have been measured with viscosities over 10^{15} Pa.s (Neuville et al., 1993; Zhang, 2003), whereas high-temperature komatiites and peridotite are estimated to be as low as 0.1 Pa.s (Giordano & Dingwell, 2003; Dingwell et al., 2004; Sparks et al., 2006).

The exsolution of bubbles from the melt also impacts the viscosity of magma. As the gas volume fraction increases up to a maximum of 0.5, the viscosity can differ by a factor of 5 to 70. During steady flow conditions in which the shear strain rate is constant, the viscosity will increase. When there is a variable shear strain rate, given by the dimensionless Capillary number, $Ca >> 1$, the viscosity decreases with an increased gas volume fraction (Llewellin & Manga, 2005). The Capillary number is given by,

$$Ca = \frac{\mu_f d_{eb} \dot{\gamma}}{2\sigma}, \tag{23}$$

where $\dot{\gamma}$ is the shear strain rate. Beyond a gas volume fraction of 0.5, the suspension begins to exhibit foam-like characteristics (Mader et al., 2013). As the shear strain rate increases, shear-thinning of the melt can occur, producing an apparent viscosity that is lower than expected

(Webb & Dingwell, 1990; Spina et al., 2016). The shear-thinning is caused by the flow deformation rate exceeding the rate at which the melt structure reorganises when the Si–O bonds break (Moynihan, 1995), called the viscous relaxation time (τ_r), which is given by,

$$\tau_r = \frac{\mu_0}{G_\infty}, \tag{24}$$

where G_∞ is the shear modulus at infinite frequency. As $G_\infty \approx 10\,GPa$ for silicate melts (Bansal & Doemus, 1986), the critical shear strain rate for the onset of non-Newtonian rheology in silicate melts can be estimated as:

$$\dot{\gamma} \approx \frac{10^{-3} G_\infty}{\mu_0}. \tag{25}$$

Therefore:

$$\dot{\gamma} \geq \frac{10^7}{\mu_0}. \tag{26}$$

Finally, suspensions of crystals within the melt increase the viscosity. Crystal volume fractions, $\phi_x > 0.3$, increase the suspension viscosity by multiple orders of magnitude compared to the melt (Lejeune & Richet, 1995; Lavallée et al., 2007). The effect of this on the viscosity can be approximated using the Krieger-Dougherty equation (Krieger & Dougherty, 1959),

$$\mu_r = \left(1 - \frac{\phi}{\phi_x}\right)^{-[\mu]\phi_x}, \tag{27}$$

with:

$$\mu_r = \frac{\mu}{\mu_0}, \tag{28}$$

where $\mu_r$is the relative viscosity, μ is the apparent viscosity, and μ_0 is the intrinsic viscosity, also known as the Einstein coefficient (Einstein, 1906). Further work has been undertaken to combine the equations for suspended particles and bubbles (Costa, 2005; Costa et al., 2009; Mader et al., 2013; Moitra & Gonnermann, 2015); however, it is beyond the scope of this study.

2.2.1.2 Surface Tension

Surface tension is particularly important in the processes of bubble nucleation, growth, and breakup. It occurs due to imbalances between the intermolecular forces at the extremity of a molecule, resulting in internal pressure. Increasing silica content and mafic oxides decreases the surface tension, while the presence of excess alkalis can increase the surface tension (Kozakevitch, 1959; Sharma & Philbrook, 1970; Epelbaum et al., 1973; Bagdassarov et al., 2000; Mangan & Sisson, 2000; Mourtada-Bonnefoi & Laporte, 2002, 2004). The temperature dependence varies with different compositional changes (Murase & McBirney, 1973; Walker & Mullins, 1981; Taniguchi, 1988), but in general, there is a weak positive dependence in the region of $0.00015\ \mathrm{N/m/°C}$ (Weirauch & Ziegler 1996; Bagdassarov et al., 2000). The presence of volatiles, primarily H_2O, is more significant, varying inversely with the surface tension, at a rate of $\sim 0.06\ \mathrm{N/m/wt.\%\ H_2O}$ from an anhydrous fluid to 4.5 wt.% H_2O. The rate of surface tension decreases for H_2O contents greater than 4 wt.% (Mangan & Sisson, 2005; Gardner et al., 2013).

The edge cases of surface tension in silicate melts are found with water-saturated dacites and anhydrous basalt, with surface tension values of 0.042 N/m and 0.389 N/m, respectively. Given that these are single order of magnitude changes to surface tension, the variations in melt composition have minimal impact on the terminal velocity, especially when compared to the vast changes observed in viscosity.

2.2.2 Melt Density

Magma can consist of multiple phases; therefore, the combined density can be calculated by,

$$\rho = (1 - \phi - \phi_x)\rho_f + \phi_x\rho_x + \phi\rho_b. \tag{29}$$

where ϕ_x is the volume fraction of crystals and ρ_x is the crystal density. The melt density, ρ_f, is calculated by summating the mole fractions and molecular mass of each oxide component.

As the volume fraction of volatiles increases, the overall density will decrease, as seen in Figure 6. There is also a temperature dependency. The molecular structure expands as temperature rises due to increased kinetic energy overcoming the intermolecular bonds. Consequently, the density reduces. The temperature variation within volcanic conduits can be significant; however, as with the surface tension, the resulting change in density is within an order of magnitude, ranging from ~ 2000-2800 kg/m^3.

2.2.3 Thermodynamic Conditions

The melt density and rheological properties are temperature dependent, significantly so in the case of viscosity, which has the greatest influence on changes in the terminal velocity. Most conduit flow models assume isothermal conditions for simplicity (Sahagian, 2005; Costa et al., 2007). The walls of the magma conduit are not homogeneous, parallel, or solid. There can be temperature variations within horizontal cross-sections of the conduit due to heat exchange and viscous frictional heating through the conduit's walls (Huppert & Sparks, 1989; Costa & Macedonio, 2003; Mastin, 2004).

The vertical temperature variation is present due to a change in depth through the magma conduit and is of the magnitude of 100 K. As magma ascends through the conduit, the cooling rate is correlated to the degassing rate and, therefore, bubble ascent velocity. Eruptions with longer cooling durations (21-368 s) are measured as having the slowest cooling rates (0.1–1.7°C/s) through analysis of the concentration gradients of MgO melt inclusions produced by olivine crystallisation on inclusion walls (Newcombe et al., 2020; Saper & Stolper, 2020). Similarly, the pressure within the conduit varies with depth, as shown in Figure 7. The pressure variation within the conduit is also of a single order of magnitude until very close to the surface. The exception to this are rapid degassing events, such as an eruption, which causes decompression in the conduit.

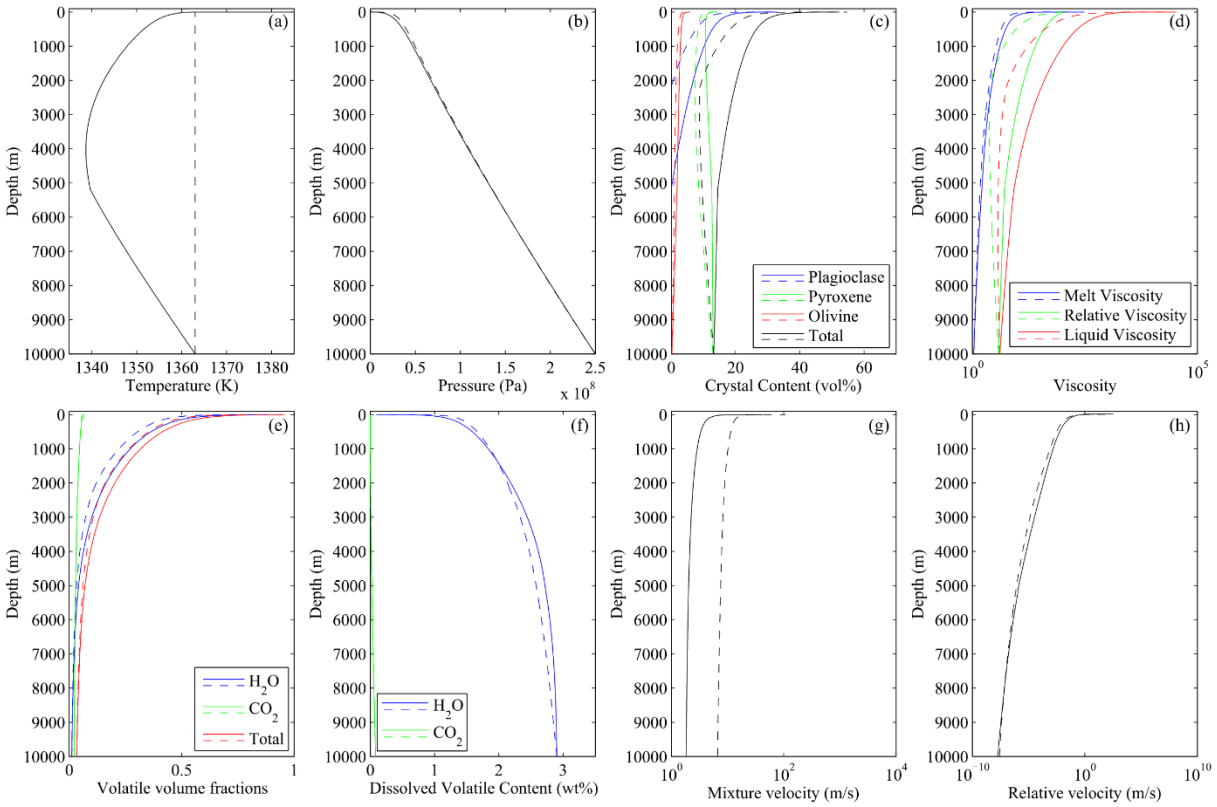

Figure 7. Key magmatic parameters for a basaltic effusive eruption plotted against the depth within the conduit. Figure from La Spina et al. (2015).

3. Methodology

3.1 Data Collation

In this study, a larger dataset than any previous bubble rising study has been compiled, to test the fit of rising bubble terminal velocity models, with over 10,000 individual terminal velocity results. Bubble terminal velocity data stretches back as far as the work by Allen (1900), although published studies on rising bubbles reaches the 1850s (Stokes, 1851). Since then, our understanding of the forces involved has changed, notably, the impact of impurities on surface tension. Systematic error is consequently present in certain data and had to be accounted for, or removed, from this analysis. Studies on Dumitrescu-Taylor bubbles, bubbles within Taylor-Couette flow, drops, and bubbles undergoing significant capillary action were not included in the initial dataset as they are either not relevant, or require significant corrections before they could be included. The full list of studies included in the initial dataset is listed in Table 2 and shown in Figure 8.

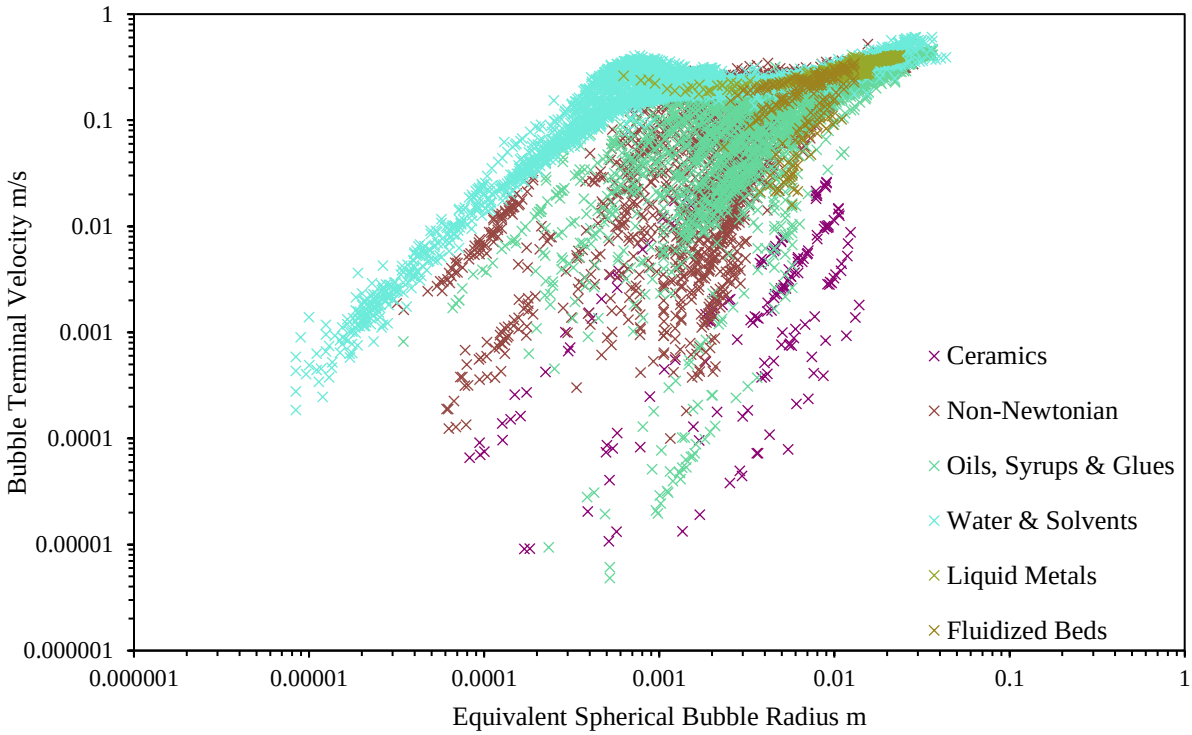

Figure 8. Dataset of every rising bubble terminal velocity compiled in this study, categorised by the fluid medium into six groups of fluids. Studies included are listed in Table 2.

Data has been obtained from published studies and theses, either directly from tables, or using WebPlotDigitizer v4.6 (Rohatgi, 2022) to collect directly from graphs in the work. WebPlotDigitizer v4.6 can automatically extract datasets through calibration of the axis, providing a precision of 15 significant figures. The accuracy of this extracted dataset is dependant on accurate calibration of the axis, and in turn, the accuracy of the graphs produced in the studies. Miscalibration of an axis would create a systematic error for that dataset, shifting all the datapoints, however, as most work is published on logarithmic axis, this shift will not be consistent for every point. To mitigate this potential error when assessing the fit of each model, the deviation is averaged for each two phase system within a study, then averaged for all studies. This method prevents undue influence from studies with large datasets, reducing the impact of systematic error. The velocities and bubble size cover several orders of magnitude, therefore the absolute deviation of the calculated velocities to the experimental velocities have been normalised by the calculated velocity to prevent overweighting the fit to the larger values of velocity.

Manual data extraction was also used; primarily within studies with large, or overlapping datasets, preventing data points being missed or misallocated by the automatic collection alogrithm. Human error will have impacted the data with this method of collection. Visual precision within the software is dependent upon the data range and the spatial resolution of each graph imported, therefore, it cannot be summarily determined. The software has a potential precision greater than a single pixel on the display used and therefore is not a limiting factor.

Fluid characteristics must be obtained in order to determine dimensionsless numbers, as seen in Equations (16)-(19). Not all studies assessed or published these figures. Consequently, known values have been obtained at the temperature listed. In studies where a temperature is not given, fluid parameters at 20°C have been used. Some experiments have plotted other values, such as the Reynolds number or the coefficient of drag. In these cases, where sufficient other values are given, the equivalent spherical bubble radius has been calculated for each data point from these values. Most of these values are provided to just 2 significant figures, and in some cases a single order of magnitude. The uncertainty in these values produces a far greater source of potential error than the method of data collection. Due to this, when assessing the fit of the bubble terminal velocity model, we do not use the dimensionless version as the uncertainty in the fluid parameters would then be compounded.

Table 2. All the studies included in the initial dataset, categorised by the fluid medium into six groups of fluids as displayed in Figure 8. The primary fluid listed is the main component of any solutions, except for non-Newtonian fluids in which the main additive to a water or glycerol base is listed. The focus of the experimental work within the study is listed, usually the dependant variable of the data obtained, but also covering certain independent variables that impact the bubble terminal velocity such as the presence of impurities or surfactants, or the container diameter (wall effect). The range of bubble radii for the group of fluids within each study, and the range of calculated dimensionless numbers are also included for reference.

Study	Primary Fluid	Focus of Experiment	Equivalent Spherical Bubble Radius (mm)	Reynolds number	Eotvos number	Morton number
Ceramics						
Hornyak & Weinberg 1984	Soda-Lime-Silica Glass	Bubble rise velocity	0.39 - 0.78	10^{-7} - 10^{-5}	10^{-1} - 10^{1}	10^{7} - 10^{9}
Jucha et al. 1982	Various	Drag coefficient	0.082 - 5.9	10^{-7} - 10^{1}	10^{-3} - 10^{1}	10^{0} - 10^{7}
Kočárková 2011	Soda-Lime-Silica Glass	Bubble rise velocity	1.4 - 14	10^{-7} - 10^{-2}	10^{0} - 10^{2}	10^{4} - 10^{11}
Non-Newtonian						
Acharya et al. 1977	Various	Bubble rise velocity, regime & drag coefficient	1.1 - 4.9	-	-	-
Almani et al. 2021	Various	Wall effect	0.67 - 1.7	10^{1} - 10^{2}	10^{-1} - 10^{0}	10^{-6} - 10^{-5}
Amirnia et al. 2013	Various	Bubble rise velocity, regime & drag coefficient	0.61 - 9.9	10^{-2} - 10^{2}	10^{-1} - 10^{2}	10^{-4} - 10^{4}
Astarita & Apuzzo 1965	Various	Bubble rise velocity & regime	0.34 - 22	-	-	-
Calderbank et al. 1970	Polyethylene Oxide solution	Bubble rise velocity, regime & mass transfer	1.3 - 28	-	10^{0} - 10^{3}	-
Haque et al. 1988	Carboxymethyl Cellulose solutions	Bubble rise velocity & regime	1.2 - 24	-	10^{0} - 10^{3}	-
Johnson 1969	Polyethylene Oxide solution	Bubble rise velocity & mass transfer	1.2 - 28	10^{-1} - 10^{2}	10^{0} - 10^{3}	10^{-2}
Leal et al. 1971	Peracetic Acid solutions	Bubble rise velocity	1.4 - 15	10^{0} - 10^{1}	-	-
Liu et al. 1995	Polyethylene Oxide solutions	Bubble rise velocity & regime	0.93 - 14	10^{-5} - 10^{0}	10^{0} - 10^{2}	10^{5} - 10^{7}
Loudon 1968	Carboxymethyl Cellulose solutions	Bubble rise velocity & mass transfer	2.7 - 27	10^{0} - 10^{2}	10^{1} - 10^{3}	10^{-1} - 10^{2}
Macedo & Yang 1974	Peracetic Acid solutions	Drag coefficient	0.032 - 0.2	-	-	-
Margaritis et al. 1999	Various	Bubble rise velocity & drag coefficient	0.16 - 16	-	10^{-2} - 10^{2}	-
Miyahara & Yamanaka 1993	Carboxymethyl Cellulose solutions	Bubble rise velocity, regime & drag coefficient	2.0 - 14	-	10^{0} - 10^{2}	-
Räbiger & Vogelpohl 1986	Carboxymethyl Cellulose solutions	Bubble rise velocity & regime	0.71 - 9.0	-	-	-
Rodrigue et al. 1996	Various	Bubble rise velocity & impurities	0.77 - 5.5	10^{-5} - 10^{0}	10^{-1} - 10^{2}	10^{0} - 10^{8}
Zana 1975	Peracetic Acid solutions	Bubble rise velocity, regime & mass transfer	1.5 - 21	10^{-4} - 10^{1}	-	-

Study	Primary Fluid	Focus of Experiment	Equivalent Spherical Bubble Radius (mm)	Reynolds number	Eotvos number	Morton number
Oils, Syrups & Glues						
Allen 1900	Aniline	Motion of spheres in viscous fluids	0.035 - 0.55	10^{-2} - 10^{1}	10^{-3} - 10^{-1}	10^{-7}
Angelino 1966	Various	Bubble rise velocity, regime & wall effect	6.2 - 37	10^{0} - 10^{2}	10^{2} - 10^{3}	10^{-2} - 10^{2}
Astarita & Apuzzo 1965	Glycerol solutions	Bubble rise velocity & regime	0.89 - 23	-	-	-
Bond & Newton 1928	Various	Bubble rise velocity & regime	0.23 - 6.3	10^{-7} - 10^{-2}	10^{-1} - 10^{1}	10^{6} - 10^{10}
Bryn 1933	Glycerol solutions	Bubble rise velocity	0.61 - 8.8	10^{0} - 10^{3}	10^{-1} - 10^{2}	10^{-8} - 10^{-5}
Calderbank et al. 1970	Glycerol solutions	Bubble rise velocity, regime & mass transfer	1.1 - 28	10^{-1} - 10^{2}	10^{0} - 10^{3}	10^{-1} - 10^{1}
Davenport 1964	Polyvinyl Alcohol solutions	Bubble rise velocity, regime & mass transfer	5.8 - 22	10^{1} - 10^{2}	10^{1} - 10^{3}	10^{-3} - 10^{1}
Funfschilling & Li 2006	Glycerol	Bubble rise velocity & regime	1.4 - 7.0	10^{-2} - 10^{0}	10^{0} - 10^{2}	10^{2}
Garner & Hammerton 1954	Various	Bubble rise velocities, impurities & wall effect	0.18 - 7.6	10^{-3} - 10^{0}	10^{-1} - 10^{2}	10^{0} - 10^{2}
Gorring and Katz 1962	Glycerol solution	Drag coefficient	0.20 - 1.5	10^{-1} - 10^{2}	10^{-2} - 10^{0}	10^{-6} - 10^{-5}
Guthrie 1967	Polyvinyl Alcohol solutions	Bubble rise velocity, regime & mass transfer	11 - 27	10^{1} - 10^{3}	10^{2} - 10^{3}	10^{-3} - 10^{1}
Haberman & Morton 1953	Various	Bubble regime, impurities, wall effect & drag coefficient	0.20 - 16	10^{-2} - 10^{2}	10^{-2} - 10^{3}	10^{-4} - 10^{-2}
Jackson et al. 2022	Golden Syrup solution	Bubble rise velocity	0.49 - 2.0	10^{-6} - 10^{-5}	10^{-1} - 10^{0}	10^{9}
Johnson 1969	Glycerol solutions	Bubble rise velocity & mass transfer	1.2 - 28	10^{-1} - 10^{2}	10^{0} - 10^{3}	10^{-1} - 10^{1}
Jucha et al. 1982	Silicone Oil	Drag coefficient	0.28 - 1.5	10^{-1} - 10^{1}	10^{-1} - 10^{1}	10^{-2}
Kojima et al. 1968	Various	Bubble rise velocity & regime	0.82 - 14	10^{-3} - 10^{1}	10^{0} - 10^{2}	10^{-2} - 10^{5}
Kubota et al. 1967	Glycerol solutions	Bubble rise velocity, regime & impurities	0.51 - 5.9	10^{0} - 10^{3}	10^{-1} - 10^{1}	10^{-7} - 10^{-4}
Leal et al. 1971	Mineral Oil	Bubble rise velocity	1.0 - 14	10^{0} - 10^{2}	10^{0} - 10^{2}	10^{-2}
Li & Schneider 1993	Polyisobutene Oils	Bubble rise velocity	3.7 - 5.8	10^{-3} - 10^{0}	10^{1} - 10^{2}	10^{3} - 10^{9}
Liu et al. 2016	Glycerol solutions	Bubble rise velocity & regime	0.24 - 11	10^{-3} - 10^{2}	10^{-1} - 10^{2}	10^{-3} - 10^{1}
Mahmoudi et al. 2019	Kerosene	Bubble rise velocity	0.66 - 6.9	10^{2} - 10^{3}	10^{0} - 10^{2}	10^{-8}
Maxworthy et al. 1996	Glycerol solutions	Bubble rise velocity	0.22 - 5.2	10^{-2} - 10^{3}	10^{-2} - 10^{1}	10^{-10} - 10^{-3}
Miyahara & Yamanaka 1993	Glycerol solutions	Bubble rise velocity, regime & drag coefficient	1.5 - 15	10^{-2} - 10^{1}	10^{0} - 10^{2}	10^{1} - 10^{3}
O'Brien & Gosline 1935	Various Oils	Bubble rise velocity & wall effect	1.2 - 25	10^{1} - 10^{3}	10^{0} - 10^{3}	10^{-5} - 10^{-2}

Study	Primary Fluid	Focus of Experiment	Equivalent Spherical Bubble Radius (mm)	Reynolds number	Eotvos number	Morton number
Oils, Syrups & Glues						
Peebles 1952	Various Oils	Bubble rise velocity & drag coefficient	0.68 - 9.5	10^{0} - 10^{3}	10^{0} - 10^{2}	10^{-11} - 10^{-3}
Räbiger & Vogelpohl 1986	Glycerol solutions	Bubble rise velocity & regime	0.27 - 9	10^{0} - 10^{3}	10^{-1} - 10^{2}	10^{-7} - 10^{-6}
Raymond & Rosant 2000	Glycerol solutions	Bubble rise velocity, regime & drag coefficient	0.84 - 6.4	10^{-1} - 10^{2}	10^{0} - 10^{1}	10^{-6} - 10^{1}
Redfield & Houghton 1965	Dextrose solutions	Mass transfer & drag coefficient	2.2 - 9.2	10^{-2} - 10^{3}	10^{1} - 10^{2}	10^{-6} - 10^{3}
Rodrigue et al. 1996	Glycerol solutions	Bubble rise velocity & impurities	1.1 - 5.5	10^{-2} - 10^{1}	10^{0} - 10^{1}	10^{-2} - 10^{1}
Tadaki & Maeda 1961	Various	Bubble rise velocity, regime & impurities	0.57 - 10	10^{1} - 10^{4}	10^{0} - 10^{2}	10^{-9} - 10^{-4}
Talaia 2007	Glycerol solution	Bubble rise velocity & drag coefficient	9.2 - 19	10^{0} - 10^{1}	10^{2}	10^{2}
Tsuge & Hibino 1977	Various	Bubble regime	0.62 - 1.8	10^{2} - 10^{3}	10^{0} - 10^{1}	10^{-10} - 10^{-6}
Viana et al. 2001	"Viscous Liquid"	Bubble rise velocity & wall effect	5.6 - 21	10^{0} - 10^{1}	10^{2} - 10^{3}	10^{1}
Zana 1975	Glycerol solution	Bubble rise velocity, regime & mass transfer	1.0 - 5.8	10^{-1} - 10^{1}	10^{0} - 10^{1}	10^{-1}
Zhang et al. 2004	Glycerol solution	Bubble rise velocity & drag coefficient	2.2 - 3.0	10^{1}	10^{1}	10^{-2}
Water & Solvents						
Abou-el-Hassan 1983	"Newtonian Fluids"	Bubble rise velocity	1.1 - 5.5	10^{3}	10^{0} - 10^{1}	10^{-11}
Allen 1900	Water	Bubble rise velocity	0.047 - 0.39	10^{-2} - 10^{2}	10^{-3} - 10^{1}	10^{-10} - 10^{-7}
Almani et al. 2021	Water (Distilled)	Wall effect	0.87 - 1.6	10^{3}	10^{0}	10^{-11}
Aybers and Tapucu 1969	Water	Bubble regime & drag coefficient	0.42 - 3.6	10^{2} - 10^{3}	10^{-1} - 10^{1}	10^{-11}
Bachhuber and Sanford 1974	Water	Bubble rise velocity	0.072 - 0.20	10^{0} - 10^{2}	10^{-3} - 10^{2}	10^{-11}
Baird and Davidson 1962	Water (Tap)	Mass transfer & impurities	3.4 - 43	10^{3} - 10^{5}	10^{2} - 10^{3}	10^{-11}
Blandín-Arrieta 1997	Water	Bubble regime	0.95 - 4.3	10^{3} - 10^{5}	10^{0} - 10^{1}	10^{-11}
Bryn 1933	Various	Bubble rise velocity	0.20 - 12	10^{1} - 10^{4}	10^{-1} - 10^{2}	10^{-11} - 10^{-9}
Calderbank & Lochiel 1964	Water	Bubble regime & mass transfer	2.8 - 15	10^{3} - 10^{4}	10^{1} - 10^{2}	10^{-11}
Calderbank et al. 1970	Water (Distilled)	Bubble rise velocity, regime & mass transfer	2.1 - 19	10^{3} - 10^{4}	10^{0} - 10^{2}	10^{-11}
Coppock & Meiklejohn 1951	Water	Bubble rise velocity, mass transfer & orifice diameter	0.093 - 11	10^{0} - 10^{4}	10^{-2} - 10^{2}	10^{-11}
Datta et al. 1950	Water	Mass transfer & orifice diameter	0.13 - 3.7	10^{1} - 10^{3}	10^{-2} - 10^{1}	10^{-11} - 10^{-10}
Davenport 1964	Various	Bubble rise velocity, regime, mass transfer & impurities	4.0 - 24	10^{3} - 10^{4}	10^{1} - 10^{3}	10^{-10} - 10^{-8}
Davies & Taylor 1950	Various	Bubble rise velocity & wall effect	7.1 - 36	10^{3} - 10^{5}	10^{2} - 10^{3}	10^{-10} - 10^{-9}

Study	Primary Fluid	Focus of Experiment	Equivalent Spherical Bubble Radius (mm)	Reynolds number	Eotvos number	Morton number
Water & Solvents						
Detsch 1991	Water (Various)	Bubble rise velocity & impurities	0.011 - 0.52	10^{-2} - 10^{2}	10^{-4} - 10^{-1}	10^{-11}
Dong et al. 2010	Ionic Liquids	Bubble rise velocity, regime & drag coefficient	0.69 - 0.92	10^{-1} - 10^{1}	10^{0}	10^{-5} - 10^{-1}
Duineveld 1995	Water (Distilled)	Bubble rise velocity	0.33 - 0.97	10^{2} - 10^{3}	10^{-1} - 10^{0}	10^{-11}
Garner & Hammerton 1954	Water	Bubble rise velocity, impurities & wall effect	0.063 - 3.9	10^{0} - 10^{3}	10^{-3} - 10^{1}	10^{-11} - 10^{-10}
Gorodetskaya 1949	Various	Bubble rise velocity & impurities	0.16 - 12	10^{1} - 10^{4}	10^{-2} - 10^{2}	10^{-11} - 10^{-7}
Gorring and Katz 1962	Water (Tap)	Drag coefficient	0.19 - 1.0	10^{1} - 10^{3}	10^{-2} - 10^{0}	10^{-11}
Guthrie 1967	Water (Tap)	Bubble rise velocity, regime & mass transfer	11 - 27	10^{4}	10^{2} - 10^{3}	10^{-10}
Guyer & Pfister 1946	Water	Mass transfer	0.90 - 2.4	10^{3}	10^{0}	10^{-11}
Haberman & Morton 1953	Various	Bubble regime, impurities, wall effect & drag coefficient	0.11 - 12	10^{1} - 10^{4}	10^{-2} - 10^{2}	10^{-12} - 10^{-9}
Hoefer et al. 1913	Water	Bubble rise velocity & wall effect	0.16 - 15	10^{1} - 10^{4}	10^{-2} - 10^{2}	10^{-11}
Houghton et al. 1957	Water (Various)	Bubble rise velocity, regime & impurities	0.40 - 2.7	10^{2} - 10^{3}	10^{-1} - 10^{1}	10^{-11} - 10^{-10}
Jamialahmadi & Müuller-Steinhagen 1993	Water	Bubble rise velocity	0.93 - 20	10^{3} - 10^{4}	10^{0} - 10^{2}	10^{-11}
Johnson 1969	Water (Distilled)	Bubble rise velocity & mass transfer	0.35 - 19	10^{2} - 10^{4}	10^{-1} - 10^{2}	10^{-11}
Karamanev et al. 1996	Water (Distilled)	Bubble rise velocity & drag coefficient	3.5 - 3.5	10^{3}	10^{0} - 10^{1}	10^{-12} - 10^{-11}
Kubota et al. 1967	Various	Bubble rise velocity, regime & impurities	0.097 - 6.1	10^{1} - 10^{4}	10^{-2} - 10^{2}	10^{-11} - 10^{-9}
Kure et al. 2021	Water (Distilled)	Bubble rise velocity	0.38 - 0.94	10^{2} - 10^{3}	10^{-1} - 10^{0}	10^{-11}
Leifer et al. 2000	Water (Distilled)	Bubble rise velocity	0.32 - 4.4	10^{2} - 10^{3}	10^{-1} - 10^{1}	10^{-11} - 10^{-10}
Leonard & Houghton 1963	Water	Bubble rise velocity, mass transfer & impurities	1.1 - 9.6	10^{3} - 10^{4}	10^{0} - 10^{2}	10^{-11}
Liu et al. 2015	Water	Bubble rise velocity & regime	0.085 - 5.6	10^{0} - 10^{3}	10^{-2} - 10^{1}	10^{-10}
Loudon 1968	Water (Distilled)	Bubble rise velocity & mass transfer	2.1 - 24	10^{3} - 10^{4}	10^{0} - 10^{2}	10^{-11} - 10^{-10}
Luchsinger 1937	Water	Bubble rise velocity & regime	0.32 - 1.8	10^{2} - 10^{3}	10^{-1} - 10^{0}	10^{-11}
Mahmoudi et al. 2019	Water (Distilled)	Bubble rise velocity	0.66 - 7.3	10^{3} - 10^{4}	10^{-1} - 10^{2}	10^{-11} - 10^{-10}
Maxworthy et al. 1996	Water (Distilled)	Bubble rise velocity	0.21 - 6.7	10^{1} - 10^{4}	10^{-2} - 10^{1}	10^{-11}
Merker et al. 2017	Water	Mass transfer	0.44 - 1.4	10^{2} - 10^{3}	10^{-1} - 10^{0}	10^{-11}

Study	Primary Fluid	Focus of Experiment	Equivalent Spherical Bubble Radius (mm)	Reynolds number	Eotvos number	Morton number
Water & Solvents						
Miyagi 1925	Water	Bubble rise velocity & regime	0.25 - 3.5	10^{2} - 10^{3}	10^{-1} - 10^{1}	10^{-11} - 10^{-10}
Miyahara & Yamanaka 1993	Water	Bubble rise velocity, regime & drag coefficient	0.50 - 13	10^{2} - 10^{4}	10^{-1} - 10^{2}	10^{-11}
O'Brien & Gosline 1935	Water	Bubble rise velocity & wall effect	1.4 - 22	10^{3} - 10^{4}	10^{0} - 10^{2}	10^{-11}
Okawa et al. 2003	Water	Bubble rise velocity & regime	0.33 - 1.8	10^{2} - 10^{3}	10^{-1} - 10^{0}	10^{-12} - 10^{-10}
Okazaki 1964	Water (Distilled)	Bubble rise velocity & impurities	0.16 - 1.3	10^{1} - 10^{3}	10^{-2} - 10^{0}	10^{-11}
Paneni 1969	Water (Distilled)	Bubble rise velocity & mass transfer	4.6 - 8.9	10^{3} - 10^{4}	10^{1} - 10^{2}	10^{-11}
Parkinson et al. 2008	Water (Distilled)	Bubble rise velocity	0.0051 - 0.057	10^{-3} - 10^{0}	10^{-5} - 10^{-3}	10^{-11}
Pawliszak et al. 2019	Water (Distilled)	Bubble rise velocity & impurities	0.023 - 0.75	10^{-1} - 10^{3}	10^{-4} - 10^{-1}	10^{-11}
Peebles 1952	Various	Bubble rise velocity & drag coefficient	0.74 - 7.2	10^{2} - 10^{3}	10^{0} - 10^{2}	10^{-11} - 10^{-9}
Raymond & Zieminski 1971	Water (Distilled)	Mass transfer, impurities & drag coefficient	1.1 - 2.2	10^{3}	-	-
Redfield & Houghton 1965	Dextrose solutions	Mass transfer & drag coefficient	1.6 - 8.2	10^{3} - 10^{4}	10^{0} - 10^{2}	10^{-11} - 10^{-8}
Rosenberg 1950	Water	Bubble regime & drag coefficient	0.34 - 33	10^{2} - 10^{5}	10^{-1} - 10^{3}	10^{-11}
Sam et al. 1996	Water (Various)	Bubble rise velocity & impurities	0.45 - 1.4	10^{2} - 10^{3}	10^{-1} - 10^{0}	10^{-11}
Sanada et al. 2008	Water (Distilled)	Bubble rise velocity, regime, impurities & drag coefficient	0.20 - 0.87	10^{1} - 10^{3}	10^{-2} - 10^{0}	10^{-11}
Shabalin et al. 1939	Water	Mass transfer & drag coefficient	0.19 - 7.2	10^{1} - 10^{4}	10^{-2} - 10^{1}	10^{-11}
Stuke 1952	Water	Bubble rise velocity & impurities	0.33 - 3.0	10^{2} - 10^{3}	10^{-1} - 10^{1}	10^{-10}
Tadaki & Maeda 1961	Various	Bubble rise velocity, regime, impurities & drag coefficient	0.68 - 10	10^{1} - 10^{4}	10^{0} - 10^{2}	10^{-10} - 10^{-6}
Talaia 2007	Water	Bubble rise velocity & drag coefficient	0.69 - 11	10^{2} - 10^{4}	10^{-1} - 10^{2}	10^{-11}
Tomiyama et al. 2002	Water (Distilled)	Bubble rise velocity & impurities	0.31 - 2.7	10^{2} - 10^{3}	10^{-1} - 10^{1}	10^{-11}
Tsuge & Hibino 1977	Various	Bubble regime	0.86 - 1.8	10^{2} - 10^{3}	10^{0} - 10^{1}	10^{-11} - 10^{-7}
Uno & Kitner 1956	Water	Bubble rise velocity & wall effect	3.1 - 11	10^{3} - 10^{4}	10^{1} - 10^{2}	10^{-11}
Wang et al. 2017	Water	Bubble rise velocity & drag coefficient	2.5 - 5.8	10^{3}	10^{1}	10^{-11}
Yan et al. 2017	Water (Distilled)	Bubble rise velocity & drag coefficient	0.93 - 2.3	10^{3}	10^{0}	10^{-11}
Zawala & Niecikowska 2017	Water (Distilled)	Bubble rise velocity & impurities	0.49 - 0.89	10^{2} - 10^{3}	10^{-1} - 10^{0}	10^{-11}

Study	Primary Fluid	Focus of Experiment	Equivalent Spherical Bubble Radius (mm)	Reynolds number	Eotvos number	Morton number
Water & Solvents						
Zdonik 1942	Water (Distilled)	Bubble rise velocity & impurities	0.71 - 2.7	10^{3}	10^{-1} - 10^{1}	10^{-11}
Zhang et al. 2005	Water (Tap)	Bubble rise velocity, regime & drag coefficient	1.4 - 3.1	10^{3}	10^{0} - 10^{1}	10^{-11}
Liquid Metals						
Davenport 1964	Mercury & Silver	Bubble rise velocity, regime & mass transfer	4.0 - 24	10^{4} - 10^{5}	10^{1} - 10^{3}	10^{-13}
Guthrie 1967	Silver	Bubble rise velocity, regime & mass transfer	9.8 - 15	10^{4}	10^{2}	10^{-13}
Mori 1977	Mercury	Bubble rise velocity & regime	0.63 - 3.0	10^{3} - 10^{4}	10^{0} - 10^{1}	10^{-13}
Paneni 1969	Mercury	Bubble rise velocity & mass transfer	3.3 - 12	10^{4} - 10^{5}	10^{1} - 10^{2}	10^{-13}
Wang et al. 2017	Galinstan	Bubble rise velocity & drag coefficient	1.5 - 2.8	10^{3} - 10^{4}	10^{0} - 10^{1}	10^{-13}
Zhang et al. 2005	Galinstan	Bubble rise velocity, regime & drag coefficient	2.2 - 4.2	10^{3} - 10^{4}	10^{0} - 10^{1}	10^{-13}
Fluidized Beds						
Darton & Harrison 1974	Fluidized Sand	Bubble rise velocity & drag coefficient	2.3 - 13	10^{-1} - 10^{2}	10^{1} - 10^{2}	10^{-2} - 10^{3}
Luo et al. 1980	Fluidized Glass	Bubble rise velocity	4.3 - 11	10^{-1} - 10^{0}	10^{2}	10^{4} - 10^{5}

3.2 Statistical Analysis

To compare the fit of different models, the relative error (δ_v) of each bubble velocity datapoint was calculated for each model,

$$\delta_{\log(v)} = \log_{10}(v_{calculated}) - \log_{10}(v_{experimental}).$$

(30)

We can then use the mean of these results to assess the models, taking the mean absolute percentage error ($MAPE$) values. As previously discussed, this can lead to overweighting studies with a greater number of observations, potentially inducing a greater degree of systematic error into the model. Therefore, the weighted mean absolute percentage error ($wMAPE$) can also be used as a metric of statistical forecasting analysis to assess model optimisation, in this case weighted per studied fluid. These statistical methods are given by,

$$MAPE = 10^{2+\frac{1}{n}\sum_{i=1}^{n}|\delta_i|} - 1,$$

(31)

and,

$$w_{sf}MAPE = 10^{2+\frac{1}{n_{sf}}\sum_{j=1}^{n_{sf}}\left(\frac{1}{n}\sum_{i=1}^{n}|\delta_i|\right)_j} - 1.$$

(32)

$n_{sf}$is the number of studies of a fluid such as Glycerol, Distilled Water (Maxworthy et al., 1996) and Glycerol (Kojima et al., 1968), and n is the number of unique datapoints.

The weighted mean absolute percentage error also has shortcomings. Each study generally covers a limited range of equivalent spherical bubble radii. When $w_{sf}MAPE$ is used to fit the model, the quantity of datapoints is reduced, weighting the model towards the radii ranges that are covered within most studies rather than evenly weighting the fit across the full data range.

An alternative to this is to group the datapoints based on even intervals of their radius. The weighted mean absolute percentage error (listed as w_iMAPE in this case) can then be calculated

with an even weighting for each of these radius intervals. Using $w_i MAPE$ for analysis of the model produces a more even analysis, however, sudden changes, especially those within a single interval are poorly accounted for. This flaw can be reduced by using the minimum interval range such that each interval contains at least one data point. Experimental and systematic error can have a much greater impact with this method, with a single data point potentially having the same weighting as one thousand depending on the interval. All these methods of statistical forecasting analysis have merits, but also inherent biases that must be considered with their use.

3.3 Model Optimisation

The models currently used to calculate the terminal velocity of bubbles all contain empirical constants to fit the experimental data. This study has compiled the largest selection of data from bubble rising experiments, and therefore, can suggest optimised values for these empirical values. Minimising the $MAPE$, $w_{sf} MAPE$, and $w_i MAPE$ by adjusting the empirical values in the chosen model will produce optimal values for this dataset. In this study, the GRG Nonlinear engine in Microsoft® Excel® (Version 2402 Build 16.0.17328.20282) is used for optimisation. A pure water data set is used initially due to being the largest dataset of a single fluid within very similar experimental conditions. The results of this can then be compared against the full data set.

To produce an optimised model for isolated bubble terminal velocities in magma, the same method will be used. Minimising the values for statistical analysis, then considering any simplifications of the model as well as analysing the limitations of the model produced.

4. Analysis

4.1 General Bubble Terminal Velocity Model

4.1.1 Impurities in Fluids

One of the key challenges when analysing fluids is ensuring the purity of the fluid. In most experiments, it's impractical to constantly measure the viscosity and surface tension of the fluid. Many studies don't measure them at all, using known values at that temperature. However, this relies on the fluid being totally pure. In practice, that is rarely the case. The composition of the impurities determines the impact it has on the terminal velocity of the bubble. The addition of substances such as carboxymethyl cellulose (CMC), polyacrylamide (PAA), or polyethylene oxide (PEO) can cause the fluid to act with non-Newtonian properties (primarily shear-thinning), increasing the apparent viscosity in the experiments studied. The addition of 0.1% PAA to distilled water increased the zero-shear viscosity from 0.001-0.248 Pa.s (Zana 1975), an increase by over two orders of magnitude. This has the effect of reducing the terminal velocity for bubbles outside of the spherical-cap regime as shown in Figure 9. Within the spherical-cap regime, the inertial force is dominant, therefore the viscosity has minimal impact.

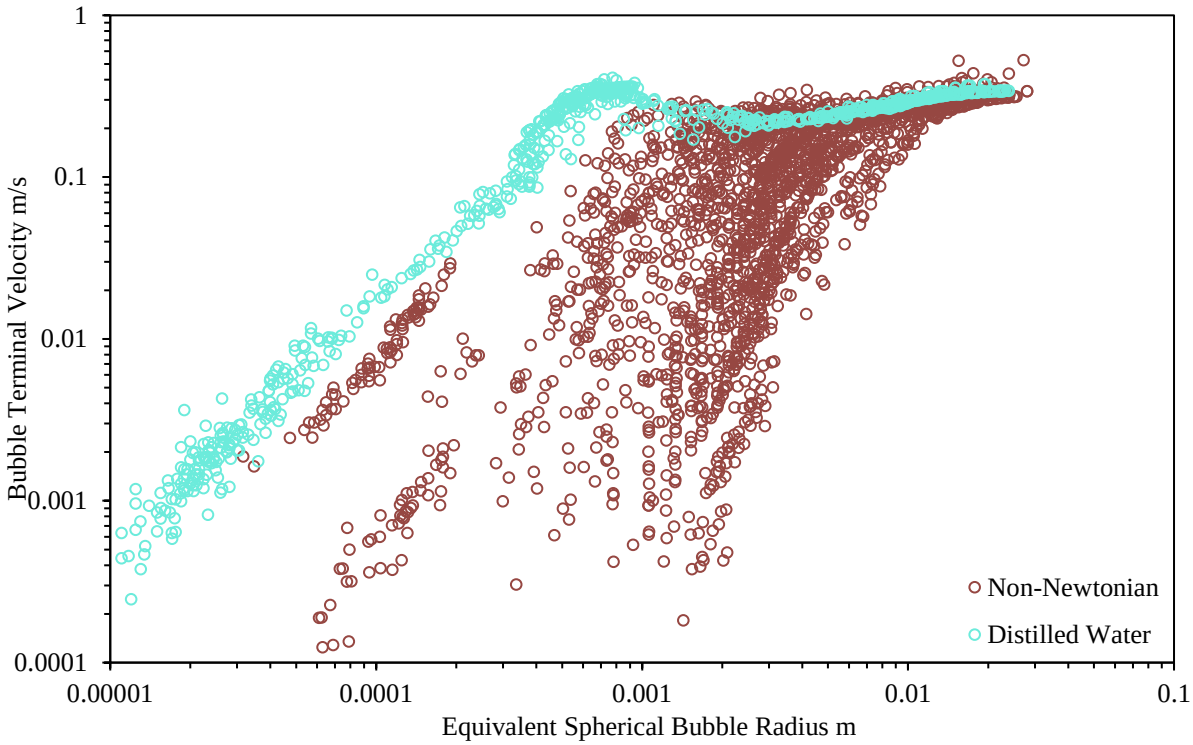

Figure 9. A comparison of the terminal velocities of non-Newtonian fluids to those of distilled water for similar bubble radii. The bubble terminal velocities can be seen to merge as the bubble enters the spherical-Cap regime (see Figure 3)

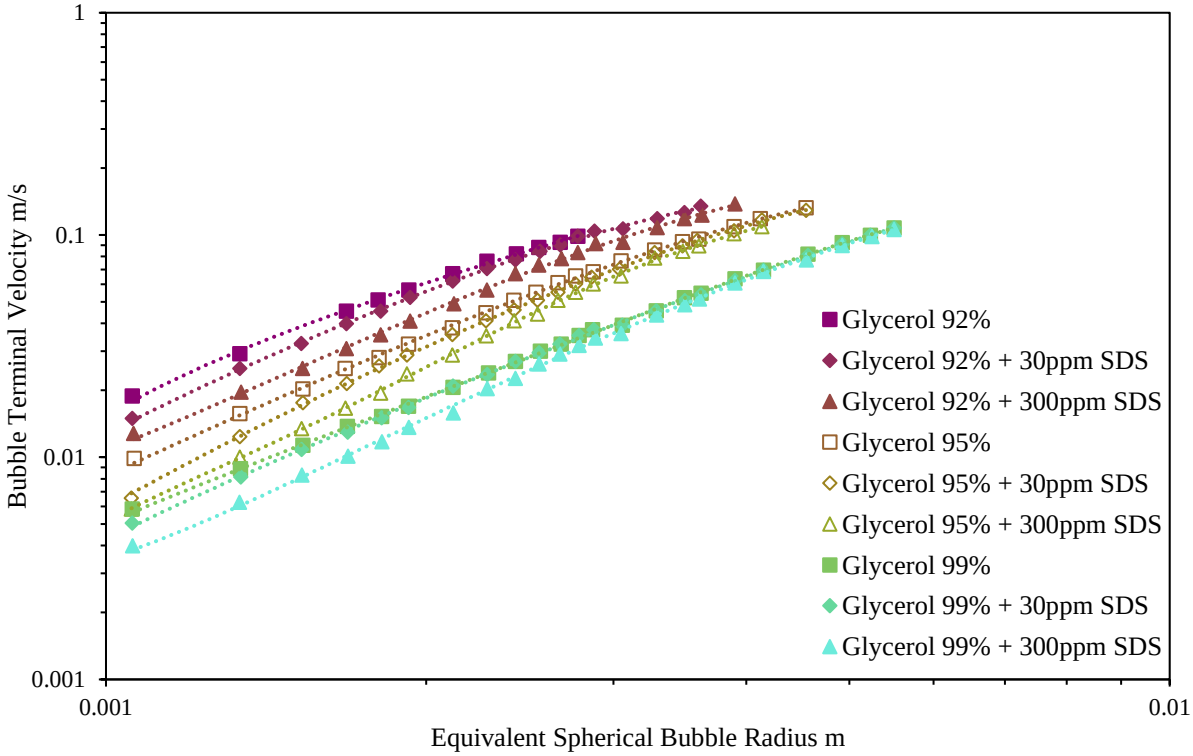

Figure 10. The impact of different concentrations of a surfactant (sodium dodecyl sulphate) on reducing bubble terminal velocity within mixtures of glycerol and water. As the bubble size decreases, the presence of surfactants has a greater impact on the terminal velocity.

Many impurities in the fluid act in a similar way to, or are, surfactants, such as heptanoic acid or long chain alcohols (n-Octanol, n-Heptanol etc.). This is particularly significant with water, which has a relatively high surface tension due to the molecular structure. The addition of other components will usually reduce the resulting surface tension. As discussed in Section 2.1.6.1, the surface of the bubble becomes less mobile. A surface tension gradient occurs as the surfactants migrate to the rear due to advection, inducing a tangential stress because of the Marangoni effect, and countering the viscous forces on the bubble. The reduction of the internal circulation increases the friction between the bubble and the fluid, reducing the velocity as seen in Figures 10 and 11 (Aybers & Tapucu, 1969; Kure 2021). Larger bubbles experience an increased shearing force, due to the increased rising velocity, reducing the accumulation of surfactants on the surface. Whereas smaller bubbles have a greater surface tension gradient, increasing the saturation of surfactants, and in turn reducing the relative velocity (Griffiths, 1962). The variation in purity of fluids explains some of the scattering of bubble terminal velocities within fluid systems and must be considered during the analysis of terminal velocity models for pure fluids.

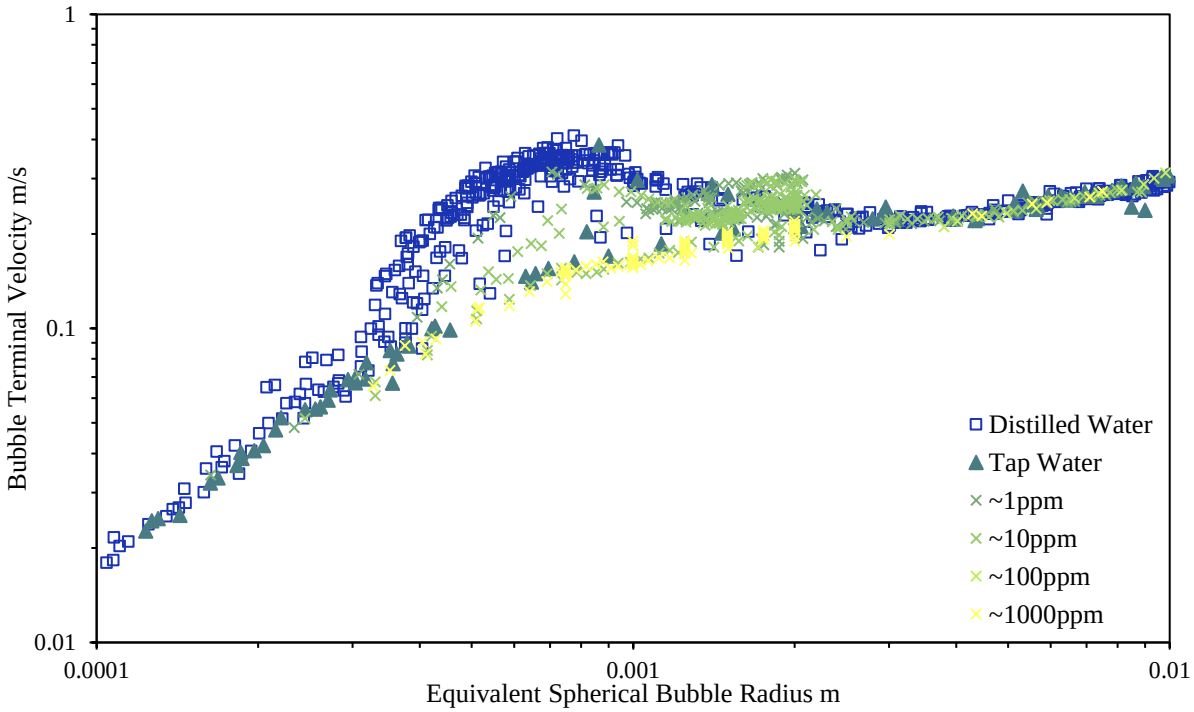

Figure 11. The impact of different concentrations of various surfactants on the rising rate of bubbles within water. Tap water follows a similar velocity-radius relationship as high concentrations of surfactants, further highlighting the issue of fluid purity when conducting experiments and producing models for the rising rate.

Studies are inconsistent in their description of their fluid medium. “Water” is commonly listed, without any additional information about its source or purity. As previously shown, the purity of these liquids has a significant impact on the bubble terminal velocity. Making the distinction between pure, or close to pure, liquids and those contaminated is crucial to produce an accurate model. Figure 11 shows that tap water is highly contaminated, therefore studies that do not explicitly state that the fluid is pure or distilled water cannot be used to analyse pure fluid systems and may have systematic error due to incorrect values of surface tension being used. Figure 12 shows the variability in velocity for fluids listed as “water”. Most of these fluids follow the highly contaminated results, such as tap water and the surfactant experiments. It is important to consider a range of fluids when analysing a general model, however, only a quarter of studies in the dataset collected test the fluid characteristics themselves. Many use solutions for the fluid medium, increasing the potential for error if we use known values for the fluid at different concentrations. Therefore, only studies that evaluate the fluid characteristics or use calibrated fluids would ideally be used to assess the accuracy of the model.

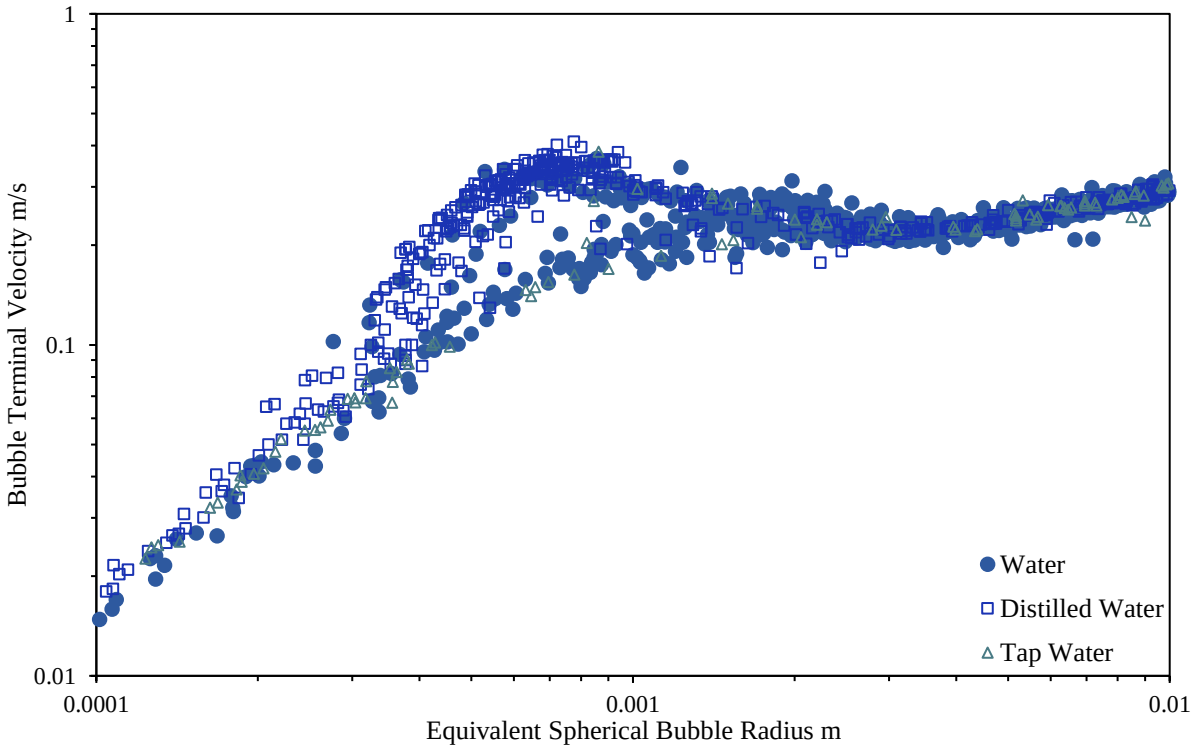

Figure 12. Experiments listing the fluid as “water” are shown to vary in their level of purity. Several experimental datasets follow a similar bubble velocity – radius relationship to pure water, whereas others display similar velocities to contaminated or tap water. This highlights the importance of ensuring the purity of the fluid medium in bubble rising experiments.

4.1.2 Data Constraints

To analyse proposed general models for bubble terminal velocity, we first tested the models against pure water datasets. Some models such as Fan and Tsuchiya (1990), Tomiyama et al. (2002), and Park et al. (2017) consider contaminated bubbles. Of note, the contaminated models produce a better fit of the bubble rising data in less than half of the "contaminated" studies, especially studies carried out in the early to mid-1900s (Allen, 1900; Shabalin et al., 1939; Datta et al., 1950; Garner & Hammerton, 1954). In these studies, the fluid is only listed as "water" and assumed to be pure when calculating the surface tension. More recent studies of contaminated water display an identical, or better, fit with the pure models (Baird and Davidson, 1962; Davenport, 1964; Guthrie, 1967; Sam et al., 1996; Zhang et al., 2005). If the impact of contaminants on surface tension is measured accurately, then the bubble terminal velocity follows the pure models; therefore, this study just focuses on a pure fluid model. As such, studies that list the fluid as "water" without any mention of the purity, or use tap water, have been discounted due to the issues highlighted in Figure 12 when initially analysing the general bubble terminal velocity model. Remaining "pure water" studies were compared against the rest of the dataset, and those with clear contamination or systematic error were also removed.

The temperature of the fluid impacts the viscosity, density, and surface tension. To graphically compare models against the dataset, a single fluid at a given temperature must be used. A significant proportion (12.3%) of the full data collected is pure water at 20±5°C, so this was chosen as the fluid for the general model, with the key properties being given in Table 3. The pure water dataset was then further constrained to temperatures from 15-25°C.

Fluid Composition	**Temperature** T °C	**Fluid Viscosity** μ_f Pa.s	**Fluid Density** ρ_f Kg/m^3	**Surface tension** σ N/m
Pure water	20	0.00100	998	0.0728

Table 3. The fluid properties used to calculate the bubble terminal velocity for the pure water models over a range of equivalent spherical bubble radii.

4.1.3 Current Models

A range of correlations have been proposed to calculate bubble terminal velocity. These can be divided into three groups: regime specific, general, and dimensionless. Most dimensionless models are based on a general parameterisation; therefore, we focus on the general correlation initially before considering a dimensionless version. The regime specific correlations are useful initial conditions, however, a general parameterisation of these is more applicable to modelling bubble terminal velocities. There are significant areas of transition between these regimes that must be accounted for, as seen in Figure 13. The Hadamard-Rybczynski solution for spherical bubbles is only valid up to values of $Re < 1$ which for pure water is a bubble radius of around 0.05mm. Bubbles in the transition between the spherical and ellipsoidal regimes are poorly described by the equations for either regime due to the presence of significant inertial and viscous forces. Wallis (1974) suggested the following equation as an improvement on the work of Peebles (1952), to calculate velocities of bubbles in the region $\sim 1 < Re < \sim 100$:

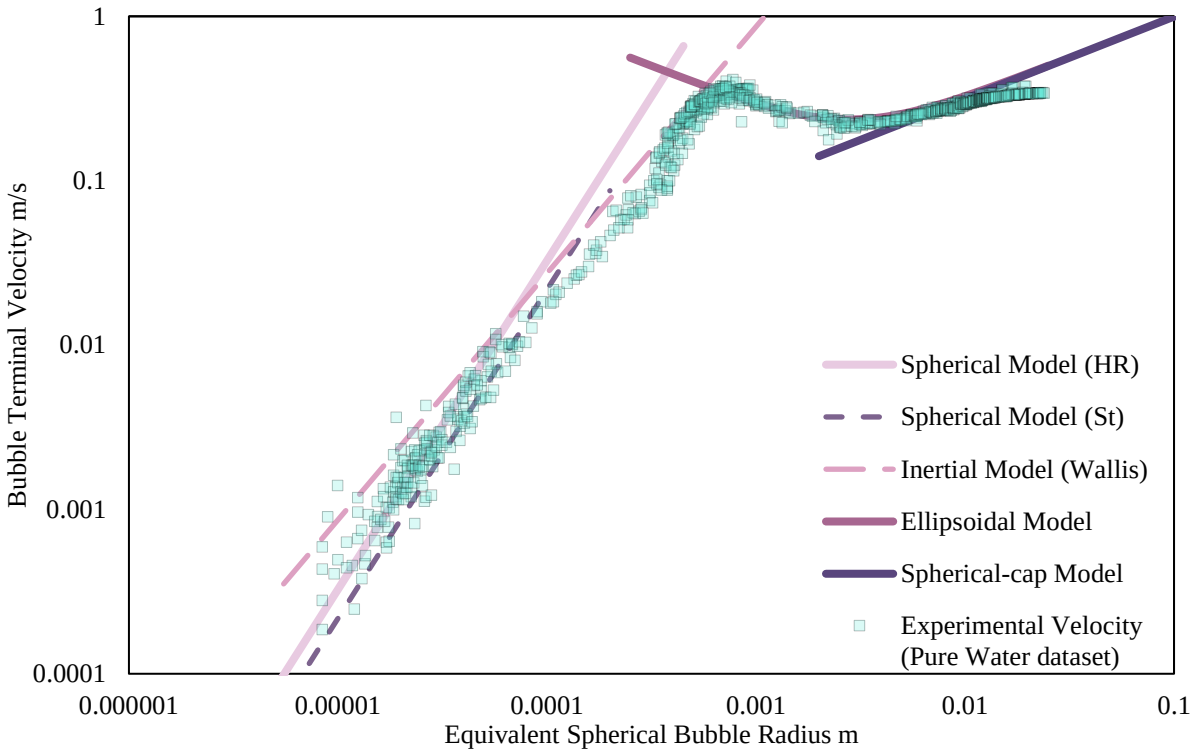

Figure 13. Models for each bubble rising regime given in Equations (9), (11) and (15) are overlaid by the experimental velocities for the constrained pure water dataset. Stokes' spherical model, Equation (20), and Wallis' model, Equation (33), for spherical bubbles under inertial forces have also been included as dashed lines for reference. The models are based on pure water at 20°C, fluid properties are listed in Table 3. The overestimation of velocity at the transition between spherical and ellipsoidal regimes can clearly be seen.

$$v_{b,W} = 0.14425 g^{\frac{5}{6}} \left(\frac{\rho_f}{\mu_f}\right)^{\frac{2}{3}} {d_{eb}}^{\frac{3}{2}}.$$

(33)

Some models, such as that proposed by Tomiyama et al. (2002), utilise the aspect ratio (E) to calculate the bubble terminal velocity,

$$v_{b,To} = \frac{\sin^{-1}\left(\sqrt{1-E^2}\right) - E\sqrt{1-E^2}}{1-E^2} \sqrt{\frac{8\sigma E^{\frac{4}{3}}}{\rho_f d_{eb}} + \frac{\Delta\rho g d_{eb}}{2\rho_f} + \frac{E^{\frac{2}{3}}}{1-E^2}},$$

(34)

where,

$$E = \frac{R_1}{R_2}.$$

(35)

Calculating the aspect ratio is not practical for calculating the bubble rise velocity, especially in magmatic settings. Correlations for the bubble aspect ratio have been proposed in terms of Eötvös and Weber numbers, with Moore's (1959) version being the best general approximation,

$$We = 4E^{\frac{4}{3}}\left(\frac{1}{E^3} + \frac{1}{E} - 2\right)\left(\frac{1}{E^2}\sin^{-1}\sin^{-1}\left(\frac{1}{E}\right) - \frac{1}{E}\sqrt{\frac{1}{E^2} - 1}\right)^2 \left(\frac{1}{E^2} - 1\right)^3,$$

(36)

which can be approximated to,

$$E \approx \frac{1}{1 + \frac{9}{64}We}.$$

(37)

The difficulty with using Moore's approximation is that the Weber number is dependent upon the bubble velocity and therefore cannot be determined. The correlations using the Eötvös number, such as Okawa et al. (2003) are limited to non-oscillatory, contaminated bubbles.

Investigations by Kure et al. (2021) suggest that the generalised model by Baz-Rodríguez et al. (2012) provides the next best fit to their dataset. The pure and contaminated parameterisations by Park et al. (2017) are also commonly used to calculate bubble terminal velocities. Both

models combine the equations for each bubble regime, along with Wallis' equation for spherical bubbles under inertial forces using a minimisation technique. The Baz-Rodríguez. model is given by,

$$v_{b,BR} = \frac{1}{\sqrt{\frac{1}{{v_1}^2} + \frac{1}{{v_2}^2}}},$$

$$v_1 = \frac{\Delta\rho g {d_{eb}}^2}{36\mu_f}\sqrt{1 + \left(0.73667\sqrt{g d_{eb}}\frac{36\mu_f}{\Delta\rho g {d_{eb}}^2}\right)},$$

$$v_2 = \sqrt{\frac{3\sigma}{\rho_f d_{eb}} + \frac{\Delta\rho g d_{eb}}{2\rho_f}}.$$

(38)

Park's pure model is calculated by,

$$v_{b,Park} = \frac{1}{\sqrt{\frac{1}{{v_{b,HR}}^2} + \frac{1}{{v_{b,W}}^2} + \frac{1}{{v_{b,E}}^2}}},$$

$$= \frac{1}{\sqrt{\frac{144{\mu_f}^2}{g^2{\rho_f}^2{d_{eb}}^4} + \frac{{\mu_f}^{\frac{4}{3}}}{0.14425^2 g^{\frac{5}{3}}{\rho_f}^{\frac{4}{3}}{d_{eb}}^3} + \frac{1}{\frac{2.14\,\sigma}{\rho_f d_{eb}} + 0.505 g d_{eb}}}}.$$

(39)

Park et al. (2017) also produced a formula for contaminated bubbles, by applying the following scaling factor to the viscous and inertial terms ($v_{b,HR}$ and $v_{b,W}$ respectively), producing the following equation,

$$f_{sc} = 1 + \frac{0.5}{1 + e^{\left(\frac{log_{10}(E_o)+1}{0.38}\right)}},$$

(40)

$$v_{b,Park} = \frac{1}{\sqrt{{f_{sc}}^2\left(\frac{144{\mu_f}^2}{g^2{\rho_f}^2{d_{eb}}^4} + \frac{{\mu_f}^{\frac{4}{3}}}{0.14425^2 g^{\frac{5}{3}}{\rho_f}^{\frac{4}{3}}{d_{eb}}^3}\right) + \frac{1}{\frac{2.14\,\sigma}{\rho_f d_{eb}} + 0.505 g d_{eb}}}}.$$

(41)

4.1.4 Pure Water Analysis

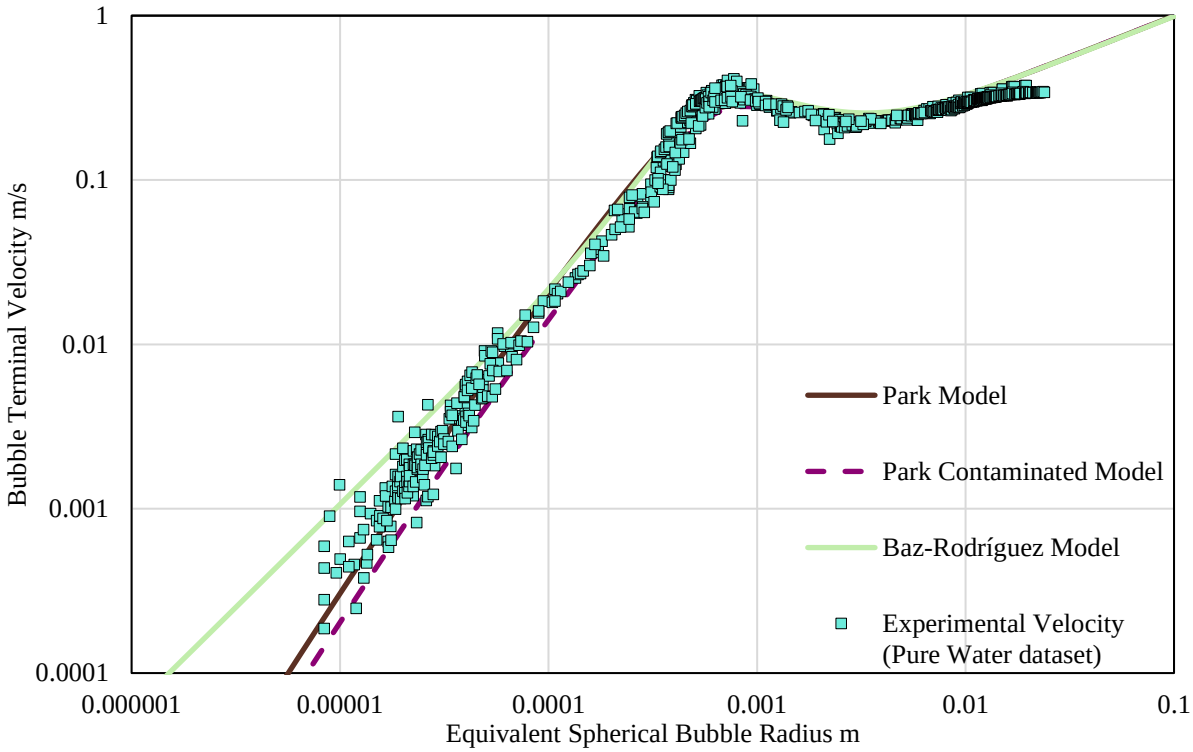

Figure 14. A comparison between terminal velocity models and the pure water dataset collected in this study. The velocity models are based on pure water at 20°C. The fluid properties are listed in table 3.

	Park Pure Model	Park Contaminated Model	Baz-Rodríguez Model
$MAPE$	19.0%	25.3%	26.4%
$w_{sf}MAPE$	18.2%	19.0%	23.8%
w_iMAPE	22.6%	27.7%	34.3%

Table 4. The mean absolute percentage error for each method of statistical analysis carried out on each model tested against the pure water dataset.

Figure 14 shows the pure water dataset with the bubble terminal velocity models of Park et al. (2017) and Baz-Rodríguez et al. (2012) overlaid. The Baz-Rodríguez model overestimates the bubble velocity in the spherical regime at bubble radii of less than 0.3 mm, with the relative error increasing as the bubble size decreases. Both models overestimate the velocity in the Spherical-Ellipsoidal transition, and similar overestimations can be seen in all pure models reviewed in the studies by Kure et al. (2021), Park et al. (2017), and Baz-Rodríguez et al (2012). The Park pure model provides a good statistical fit to the experimental data, with a $MAPE$ value of 19.0%, however, the Park contaminated, and Baz-Rodríguez models only forecast an

acceptable fit at 25.3% and 26.4% respectively. The $w_{sf}MAPE$ and w_iMAPE produce the same order of fit across the models as shown in Table 4.

If we limit the dataset to $Re > 1$ (around $r_{eb} > 60$ μm), we find that the Baz-Rodríguez model becomes the best fit ($MAPE$ 15.7% vs 17.1% for the Park pure model), especially around the onset of oscillatory motion in the ellipsoidal regime, at which point, the Park model underestimates the velocity. This is due to the method of parameterisation. A stationary point is produced by the transition from the Wallis velocity component to the Ellipsoidal velocity component, with the smoothing of this transition being too great in the Park model.

4.1.5 Experimental Precision

The $w_{sf}MAPE$ values are much closer across the models, ranging from 18.2% to 23.8%, with the Park pure model being the best fit. The tighter spread highlights how large datasets can skew the statistical analysis. In the case of the contaminated model, this is primarily the Parkinson et al. (2008) study, analysing 5-60 μm radius bubbles in purified water. The Parkinson study comprises 14.8% of the pure water dataset, an overweighted contribution when using the $MAPE$ statistical method, however, the contribution to the $w_{sf}MAPE$ value is only 5.9% as there are another 16 fluid studies contributing to the mean of the set. The opposite can be said of the w_iMAPE values (22.6% -34.3%), with the Parkinson study covering 34.6% of the radius intervals and consisting of 73.8% of the datapoints within them.

The bubbles in the Parkinson study are so small that any error in the measurement, or calculation, of the bubble size and velocity have a large impact on the relative error, with variations of up to ±17.8% in the radius over repeat measurements. Figures 13 and 14 display this, with an increase in scattering around the generally accepted values of the Hadamard-Rybczynski equation demonstrating the difficulties with experimental precision when working with such small bubbles. Only the study on water by Detsch (1991) covers bubble radii near the bottom of this range. The lack of very low Eötvös number studies can produce

parameterisations that immediately diverge away from accepted terminal velocity equations beyond the current experimental values, as seen with the Baz-Rodríguez model. This divergence will be more pronounced when considering highly viscous fluids that are well inside the spherical regime. It is therefore important to consider the forecasting of these models beyond the experimental data set they are analysed against, stating limits if required.

4.1.6 Optimised General Parameterisation

The divergence of the Baz-Rodríguez model at low Eötvös numbers for pure water, combined with the improved statistical fit of the Park model suggests that Park is the better model. Testing it against a larger dataset, containing fluids over a range of Morton numbers, is necessary to confirm this. To assess the fit of these models, we must be able to calculate the viscosity under rising conditions, therefore, non-Newtonian fluids and fluidized beds are discounted from this new dataset which will be referred to as the Newtonian dataset. Contaminated fluids have also been removed unless their surface tension has been measured as part of the experimental procedure. A full list of the included studies and fluids can be found in Appendix A.

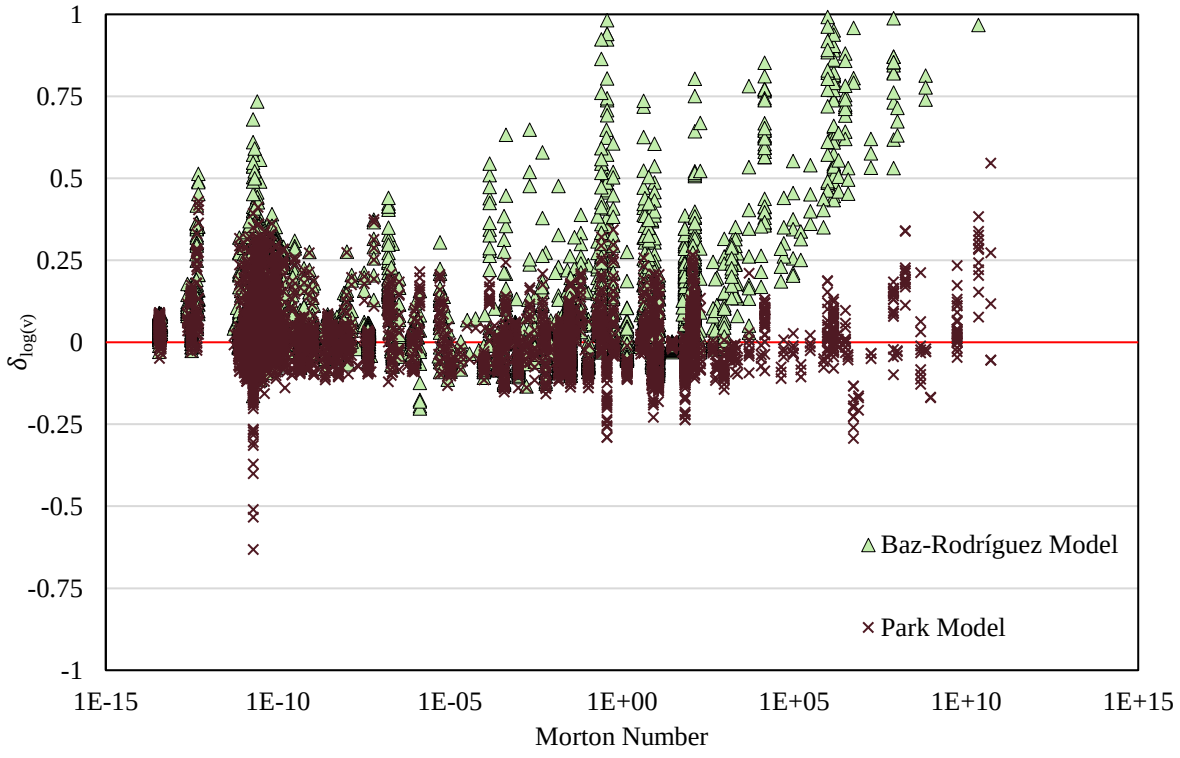

Figure 15. The relative error in the model calculated value for the Newtonian dataset against the Morton number. The divergence of the Baz-Rodríguez model from experimental values, as Morton number increases, can clearly be seen. An expanded, high contrast version is available in Appendix C

Calculating the relative error, $\delta_{\log(v)}$, for the Newtonian dataset across a range of Morton numbers (Figure 15) highlights that the Baz-Rodríguez model is not appropriate for highly viscous fluids such as soda-lime-silica glass, golden syrup, or glycerol. The $MAPE$ values confirm this, with the Park model again being a good fit at 16.8%, whereas the Baz-Rodríguez model is 31.6%. This is an acceptable fit with the range of fluids in this dataset, however, if just the highly viscous fluids were considered, it would become a statistically poor fit.

This study therefore shows that Park's pure model provides the most accurate fit of the experimental bubble rising data collected across a wide range of fluids. It contains three empirical fitting constants which can be optimised, designated A, B, and C,

$$v_{b,Optimised} = \frac{1}{\sqrt{\frac{144{\mu_f}^2}{g^2{\rho_f}^2{d_{eb}}^4} + \frac{{\mu_f}^{\frac{4}{3}}}{A^2 g^{\frac{5}{3}}{\rho_f}^{\frac{4}{3}}{d_{eb}}^3} + \frac{1}{\frac{B\,\sigma}{\rho_f d_{eb}} + Cgd_{eb}}}}. \tag{42}$$

Minimising the error values, through variance of the empirical fitting constants, produces the solutions listed in Table 5 and displayed in Figure 16 for the pure water dataset. The bias for each solution is discussed in Section 3.3. In this use case, we have 857 datapoints from 17 studies with the bubble radii covering 5 orders of magnitude. The $w_i MAPE$ minimisation is normally suited to this distribution; however, the data is not evenly distributed across the bubble radii range. The minimum interval while maintaining at least one datapoint per interval is 0.05 $\log(v)$, with the quartile 1 (Q1) of the data points containing 54% of the intervals, indicating that the distribution is heavily skewed and that $w_i MAPE$ is not suitable. This would also suggest that the $w_{sf} MAPE$ minimisation is unsuitable. Most of the studies included in this dataset are within a few specific ranges, primarily the transitions between each bubble regime. Therefore, that model is heavily overweighted towards those intervals.

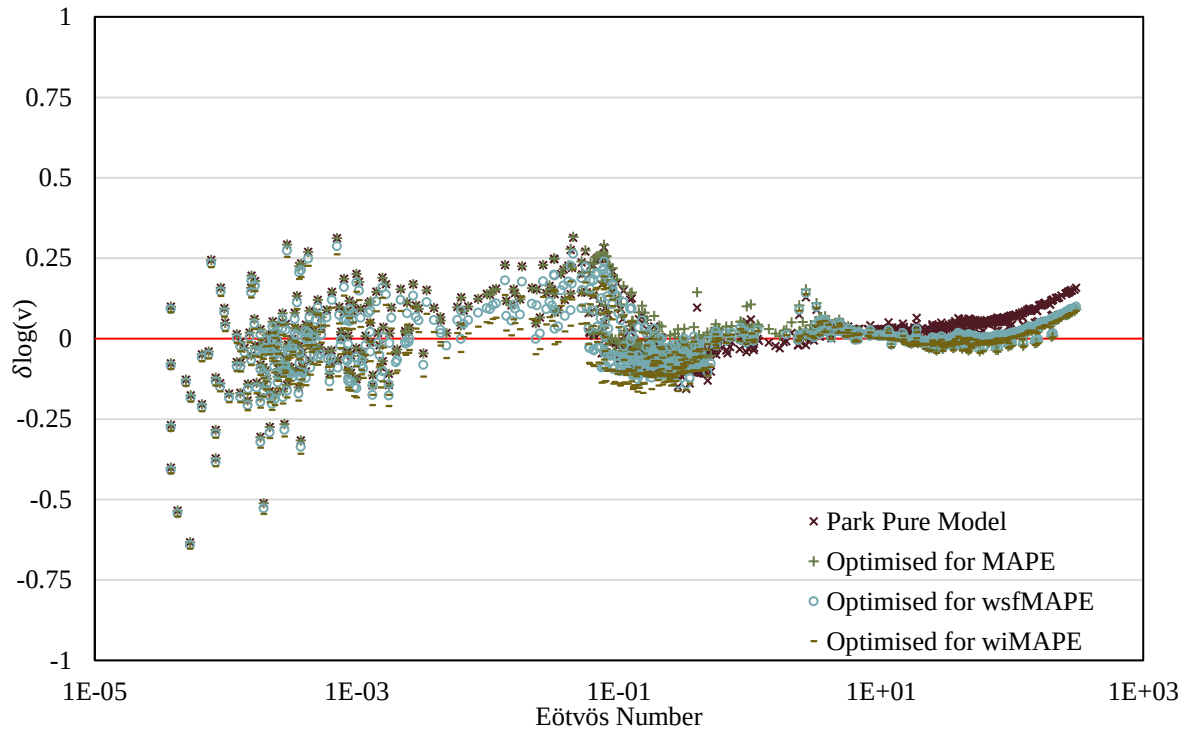

Figure 16. The relative error for each optimised model in comparison to the original Park model across the pure water dataset. An expanded, high contrast version is available in Appendix C

	Park Pure Model	**Optimised for MAPE**	**Optimised for w_{sf}MAPE**	**Optimised for w_{e}MAPE**
A	0.14425	0.14392	0.12424	0.10863
B	2.14	2.95	2.70	2.72
C	0.505	0.367	0.383	0.359
MAPE	19.0%	13.8%	14.6%	16.0%
$w_{sf}MAPE$	18.2%	16.3%	15.2%	15.7%
$w_{i}MAPE$	22.6%	19.7%	17.9%	17.4%

Table 5. The empirical fitting constants for Equation (45), obtained by minimisation of the statistical methods of error analysis, compared against those for the original Park model for the pure water dataset. The mean absolute percentage error values are included at the bottom and colour coded, from red for the largest error to green for the lowest percentage error within each row.

The $MAPE$ minimisation does overvalue certain larger studies, with Q1 containing 59% of the studies. The risk with this model bias is that systematic or experimental error in certain studies containing the majority of datapoints, in this case, the studies of Loudon (1968) and Parkinson et al. (2008), have a disproportionate effect on the model. Bubbles studied by Parkinson et al. (2008) are largely within the section of the spherical regime modelled by the Hadamard-Rybczynski section of the parameterisation, therefore the optimised empirical constants will not be significantly affected by that data. This further mitigates the bias of the $MAPE$ minimisation, and therefore it is the preferred optimised Park parameterisation.

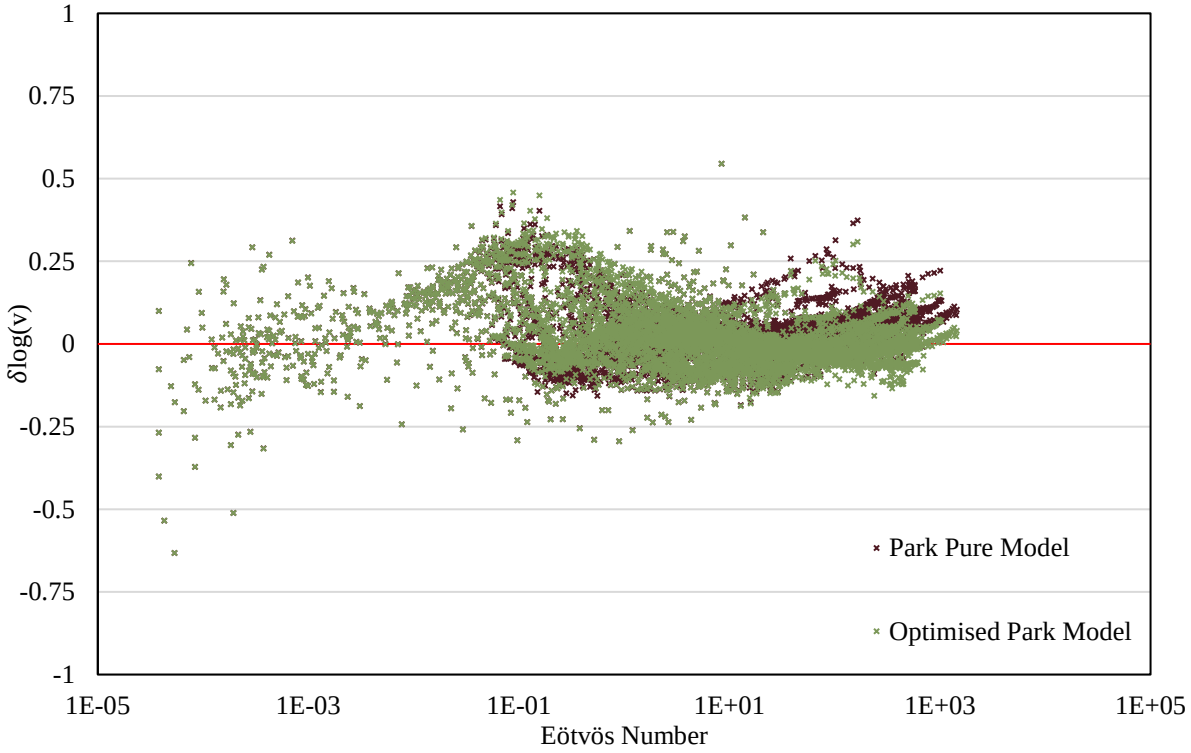

Figure 17. The relative error for the optimised Park model in comparison to the original Park pure model for the Newtonian dataset. The main improvement can be seen within the large Eötvös number range. An expanded, high contrast version is available in Appendix C

	Baz-Rodríguez Model	Park Contaminated Model	Park Pure Model	Optimised Park Model
$MAPE$	31.6%	16.9%	16.8%	15.5%
$w_{sf}MAPE$	38.7%	17.1%	17.5%	16.8%

Table 6. The mean absolute percentage error values for the various models using the Newtonian dataset. The values are colour coded from red for the largest percentage error to green for the lowest percentage error within each row.

Analysing the optimised Park parameterisation for the Newtonian dataset shows an improved fit for both $MAPE$ and $w_{sf}MAPE$ as shown in Table 6. Interestingly, the Park contaminated model shows an improved $w_{sf}MAPE$ than the Park pure model, but a slightly worse $MAPE$. This suggests that some of the studies may have contaminated or impure fluids within this dataset, further supporting the use of the pure water dataset for optimisation of the model before testing against the Newtonian dataset. The optimised Park model shows an improved fit of the dataset for Eötvös numbers greater than 10, with an almost identical fit for Eötvös numbers below 0.1. Therefore, this study proposes the following optimised Park parameterisation for isolated bubble terminal velocity:

$$v_{b,Optimised} = \frac{1}{\sqrt{\frac{144{\mu_f}^2}{g^2{\rho_f}^2{d_{eb}}^4} + \frac{{\mu_f}^{\frac{4}{3}}}{0.144^2 g^{\frac{5}{3}}{\rho_f}^{\frac{4}{3}}{d_{eb}}^3} + \frac{1}{\frac{2.95\,\sigma}{\rho_f d_{eb}} + 0.367 g d_{eb}}}}.$$

(43)

4.2 Container Impact

The container size varies significantly across different studies, ranging from 0.8 m to 4 mm in diameter, primarily due to issues with experimental setup. The cross-sectional shape also varies, and is usually circular, rectangular, or square. Different sizes and shape of the container can cause significant reductions in rising velocity. High temperature setups, such as those used for molten soda-lime-silica glass or metals, tend to minimise the size of the container to ensure consistent temperature throughout. A correction factor, such as Habermann & Sayre's in Equation (21), must be applied to experimental velocities obtained in confined setups such as these.

When constraining the pure water or Newtonian datasets, data with a significant wall diameter ratio (λ) that did not have a correction factor applied according to the study were removed. Experiments using fluids as a magmatic analogue regularly require highly confined setups that would otherwise lead to the data being discounted. Therefore, to ensure that the quantity of experimental datapoints is maximised, the Newtonian dataset was checked against the wall effect correction factors of Rosenberg (1950) and Habermann & Sayre (1958) as seen in Figure 18. This helped identify the Kočárková 2011 study as requiring a correction factor for the wall effect to be applied to the experimental velocities before the model can be tested against them. The corrected velocities are shown in Figure 19.

When analysing large bubbles ($E\ddot{o} > 100$), there appears to be a consistent overestimation by all the models tested against the experimental data. Figure 18 shows that this isn't due to a wall effect correction factor not being applied when required. However, the relative error follows a

linear relationship for increases of wall diameter ratio, suggesting that they may be linked. Further investigation into this could be carried out as an extension to this project.

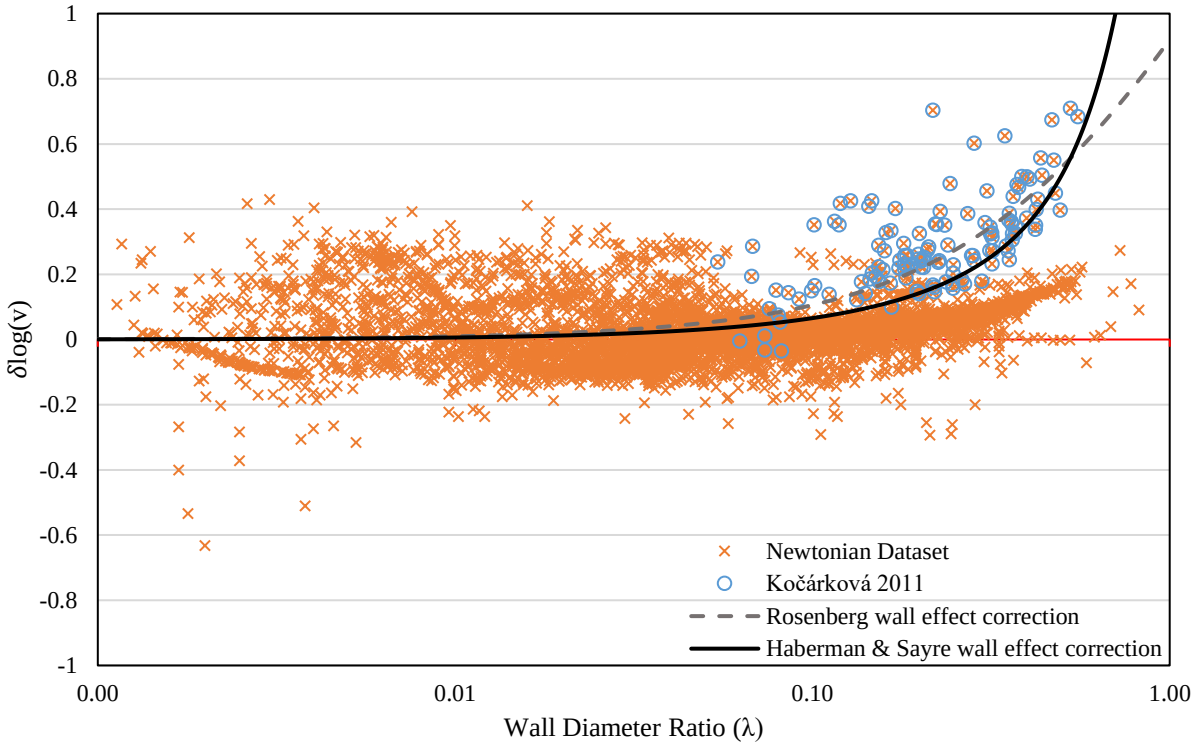

Figure 18. A comparison of the relative error for the Newtonian dataset to that of the wall effect correction factors for a range of wall diameter ratios.

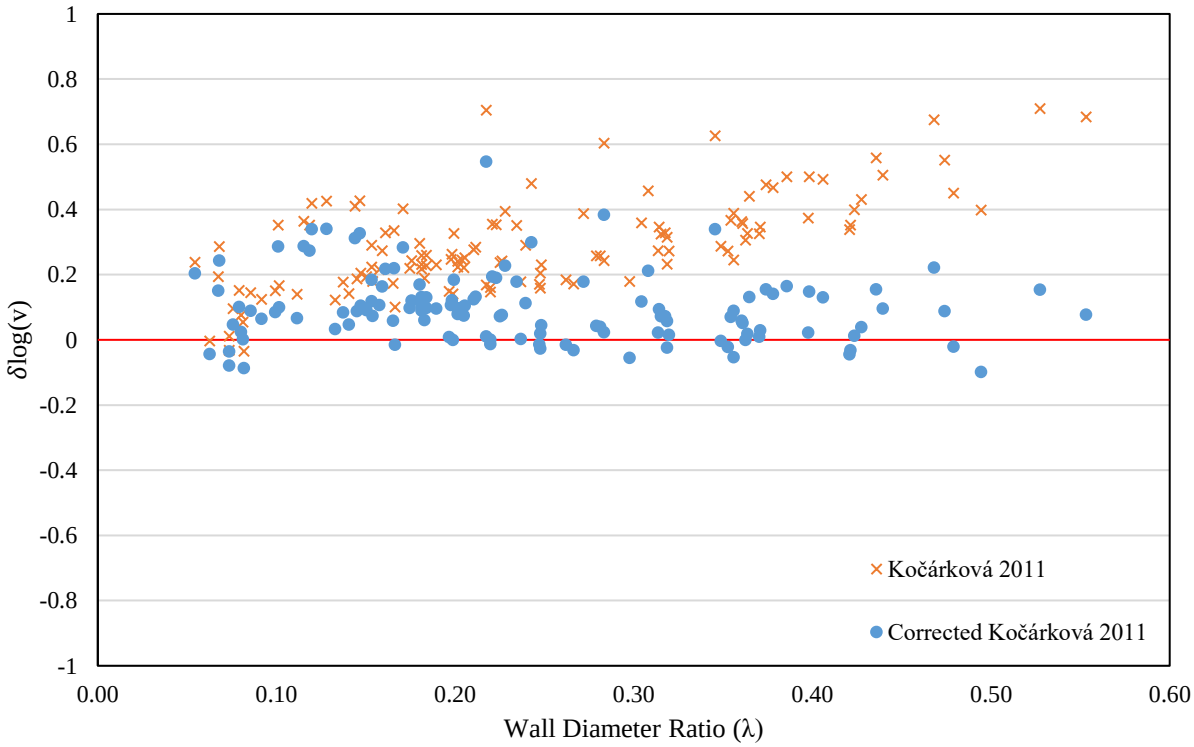

Figure 19. The bubble terminal velocities from the Kočárková 2011 study corrected using the Habermann & Sayre wall effect correction plotted against the original values.

4.3 Magmatic Bubble Terminal Velocity Model

4.3.1 Term Analysis

The Park and optimised Park models are parameterisations of several terms, covering each bubble shape regime. The spherical regime is split into the inertial and viscous force dominant regimes, using the Hadamard-Rybczynski and Wallis equations. The percentage contribution of each term for a single fluid can be calculated, shown in Figure 20 for pure water. The contribution of the ellipsoid and spherical-cap terms is minimal for bubbles rising slowly.

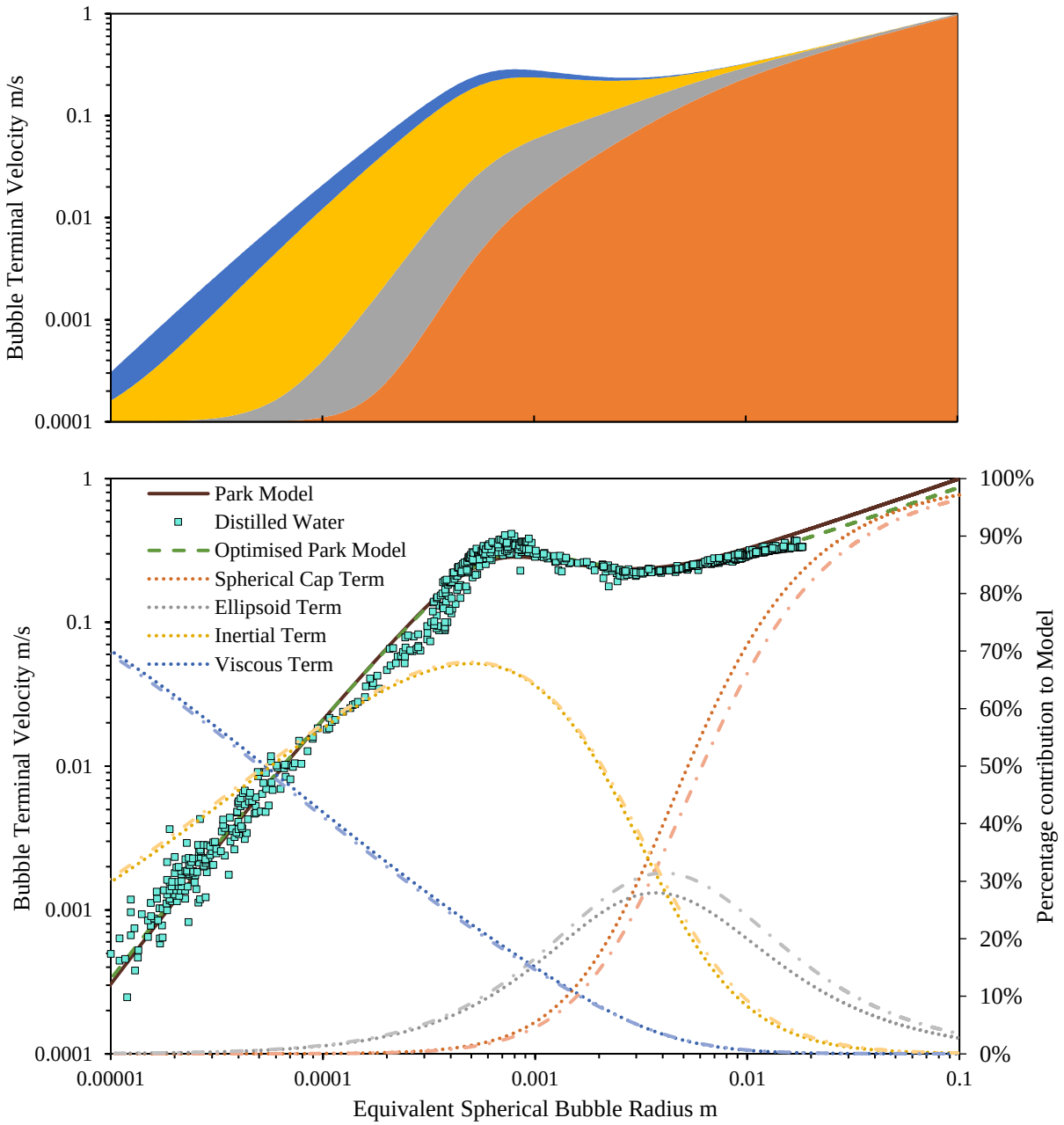

Figure 20. The cumulative (top) and percentage (bottom) contribution of each term to the Park and optimised Park models plotted against the calculated bubble terminal velocity. The main difference being the impact on the spheroid and spherical-cap terms due to the optimisation of the empirical fitting constants.

Taking a dimensionless approach to the analysis of each of these terms confirms that the contribution of the non-spherical terms is minimal for low Reynolds numbers ($Re < 0.1$), as shown for various fluids in Figure 21.

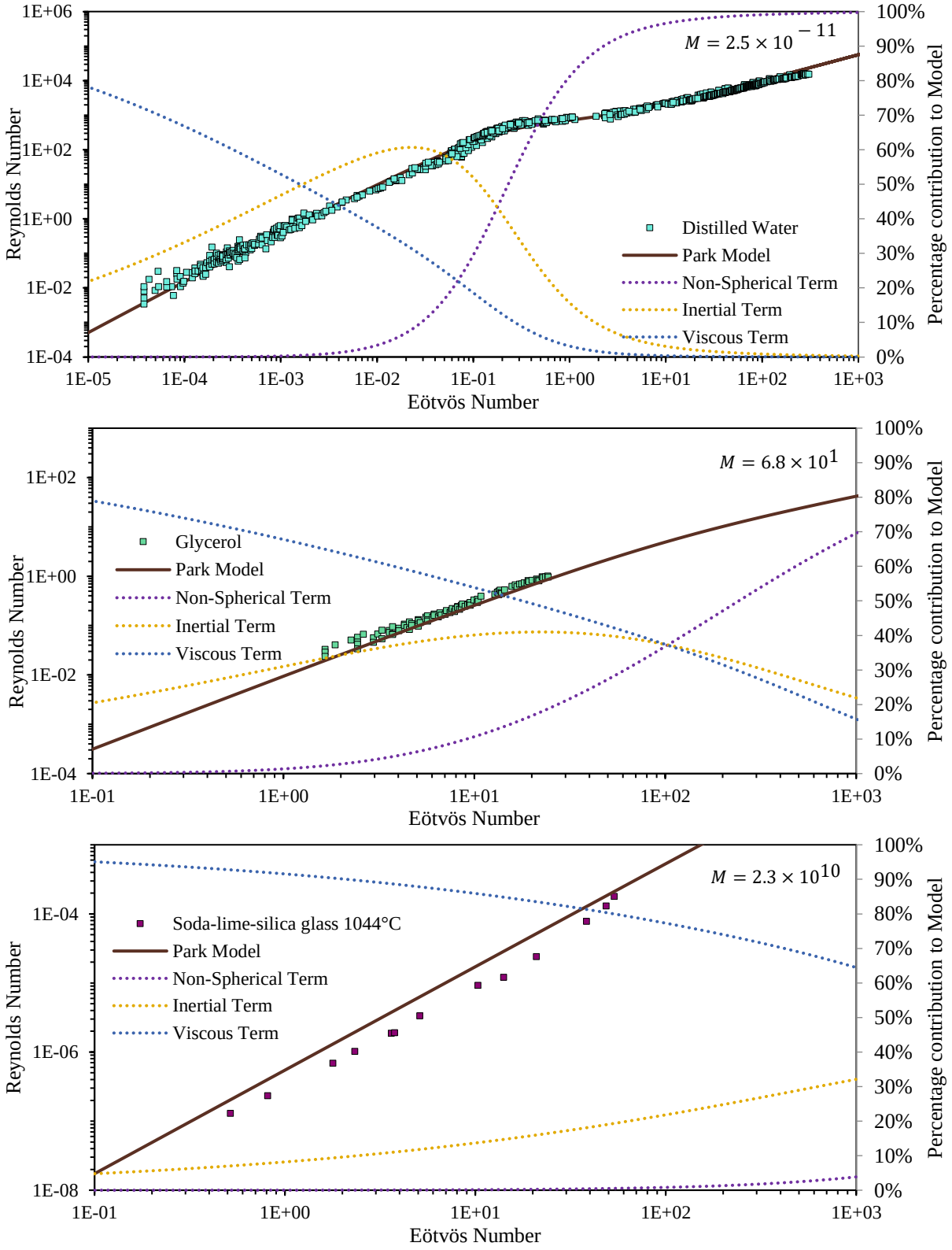

Figure 21. Percentage contribution of the non-spherical, inertial, and viscous terms to the Park model for bubble terminal velocity in various fluids, plotted for dimensionless numbers.

The contribution of the non-spherical terms decreases as the fluid viscosity, and therefore Morton number, increases. Silicate melt viscosity varies significantly depending on the composition and temperature. Even high-temperature komatiites and peridotite have viscosities greater than pure water, being similar to glycerol. Figure 21 shows how only the largest glycerol bubbles are utilising the non-spherical terms of the Park model, therefore they may be irrelevant for silicate melts.

4.3.2 Magmatic Dataset

To explore the hypothesis that non-spherical terms are irrelevant for silicate melts, the dataset must be limited to fluids analogous to silicate melts. By applying typical values for magmatic conditions and rheology, the range for each dimensionless number that occurs within silicate melts can be calculated as shown in Table 7. Therefore, the following conditions were imposed on the Newtonian dataset to produce a "magmatic dataset" analogous to silicate melts:

$$Re < 1, \qquad M < 0.1 \tag{44}$$

	Temperature T °C	**Fluid Viscosity** μ_f Pa.s	**Fluid Density** ρ_f Kg/m^3	**Surface tension** σ N/m	**Equivalent Spherical Bubble Radius** r_{eb} m	**Bubble Terminal Velocity** v_b m/s	**Eötvös Number** *Eö*	**Reynolds Number** *Re*	**Morton Number** *M*
Maximum	10^3	10^{10}	10^3	10^{-1}	10^0	10^0	10^5	10^0	10^{41}
Typical Basalt	1200	10^3	2600	0.1	-	-	-	-	10^{12}
Typical Rhyolite	850	10^8	2400	0.1	-	-	-	-	10^{32}
Minimum	10^3	10^0	10^3	10^{-2}	10^{-5}	10^{-3}	10^{-4}	10^{-9}	10^{-1}

Table 7. Maximum and minimum fluid properties used in calculating the constraints for the magmatic dataset, with the resulting maximum and minimum dimensionless numbers. The values for typical basaltic and rhyolitic melts are included for comparison and later use (Murase & McBirney, 1973).

The transitions between the bubble shape regimes can be calculated by equating dimensionless bubble regime terms. The dimensionless version of the optimised Park parameterisation, Equation (45), is used to calculate the transitions (values in Appendix B). Plotting the magmatic dataset from Equation (44) onto a Grace plot (Figure 22) with these transitions overlaid indicates that silicate melts only fall within the spherical regime, further supporting the hypothesis that the non-spherical terms of the Park model are irrelevant for silicate melts.

$$Re_{Optimised} = \frac{1}{\sqrt{\frac{144M}{E\ddot{o}^3} + \frac{M^{\frac{5}{6}}}{0.144^2 E\ddot{o}^{\frac{5}{2}}} + \frac{M^{\frac{1}{2}}}{E\ddot{o}^{\frac{1}{2}}(2.95 + 0.367E\ddot{o})}}} \quad (45)$$

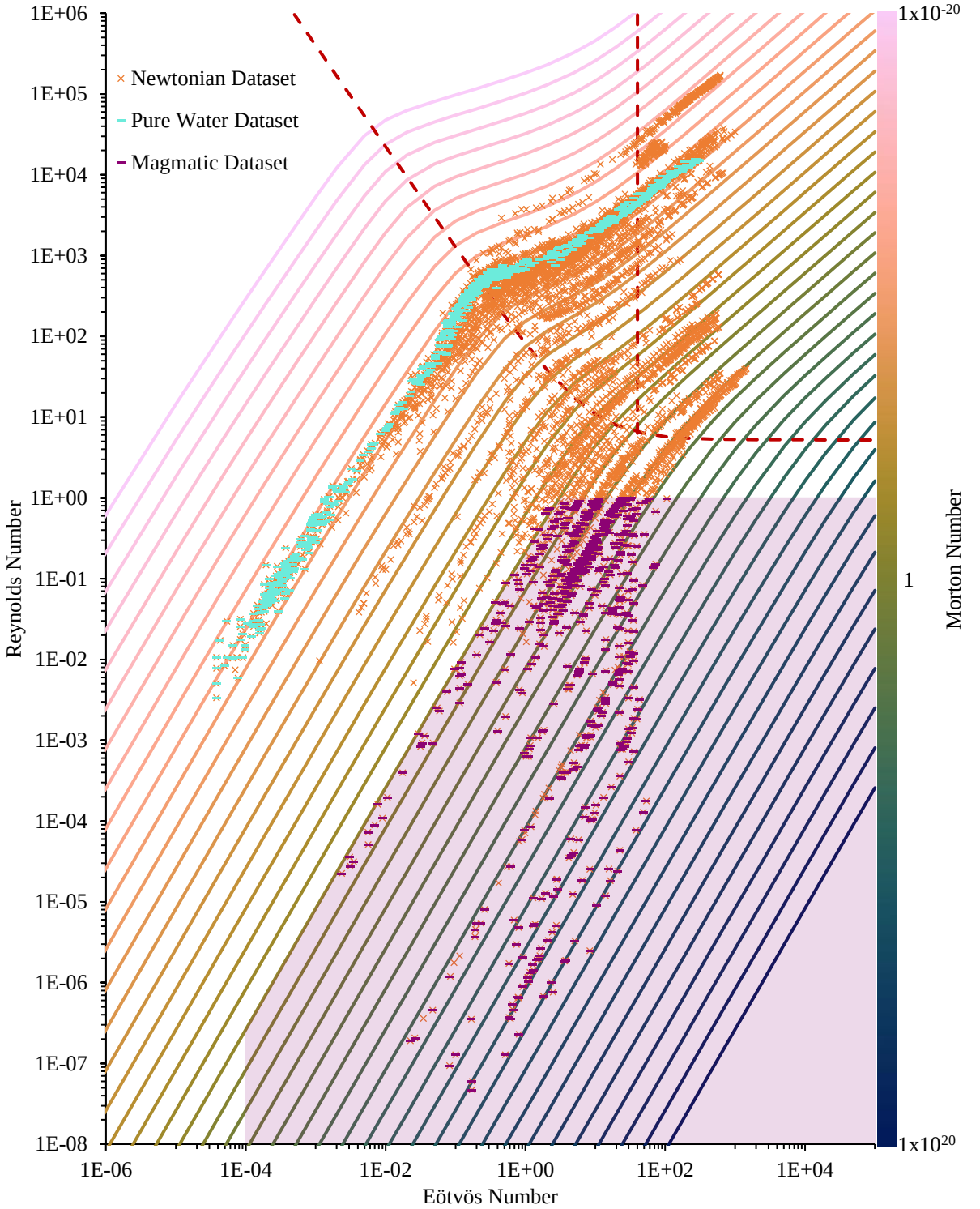

Figure 22. A Grace Plot of the Newtonian, pure water and magmatic datasets overlaid by Morton lines, the shape regime transition (red dotted), and the magmatic regime (shaded purple) calculated from the dimensionless optimised Park parameterisation and observations by Grace (1973).

4.3.3 Magmatic Model

Analysing the models against the magmatic dataset produces the mean absolute percentage error values shown in Table 8. The original Park pure model slightly outperforms the optimised Park Model suggested in Equation (43), with both providing good statistical fits of the dataset. To test the hypothesis that non-spherical terms of the Park model may be irrelevant for silicate melts, all the constants, including the Hadamard-Rybczynski constant of 144 are set as variables. Minimising the $MAPE$ value produces a solution, seen in Table 8, in which the constants belonging to the non-spherical terms (B & C) increase by several orders of magnitude. The reciprocal method of parameterisation used in the Park model, causes the minimum calculated velocity across each term to take precedence. Increasing the empirical constants of those terms, produces extremely large velocity values and therefore they do not contribute to the bubble terminal velocity calculated by the model.

The Hadamard-Rybczynski constant for the unconfined solution converged on 130. Considering the presence of impurities in these fluids and the experimental difficulties in testing fluids analogous to silicate melts, the value converging so close to the theoretical constant further supports the accuracy of the Hadamard-Rybczynski term. Removing the non-spherical terms from the Park model and optimising the empirical constant A produces an optimised model for isolated bubble terminal velocities in magma, shown in the equation below,

	Optimised Park Model	**Park Pure Model**	**Unconfined Optimised Park Model**	**Magmatic Model**
A	0.144	0.144	0.171	0.202
B	2.95	2.14	2626	-
C	0.367	0.505	468	-
H-R constant	144	144	130	144
$\boldsymbol{MAPE}$	21.8%	21.7%	20.2%	19.6%
$\boldsymbol{w_{sf}MAPE}$	21.3%	21.1%	18.9%	19.0%

Table 8. The empirical fitting constants for Equation (45) and resulting mean absolute percentage error values for various models assessed against the magmatic dataset. The Hadamard-Rybczynski (H-R) constant is also included and varied in the unconfined model to confirm the agreement with it. Constants B & C in the unconfined model increased by several orders of magnitude, minimising their respective terms' effect on the predicted bubble terminal velocity. The percentage error values are colour coded, from red for the largest to green for the lowest percentage error within each row.

$$v_{b,Magmatic} = \frac{1}{\sqrt{\frac{144{\mu_f}^2}{g^2{\rho_f}^2 d^4} + \frac{{\mu_f}^{\frac{4}{3}}}{0.202^2 g^{\frac{5}{3}} {\rho_f}^{\frac{4}{3}} d^3}}}. \quad (46)$$

The main improvement of the magmatic model's calculated velocities, over the Park and optimised Park models, is at the upper end of Eötvös and Reynolds number ranges within the magmatic dataset, as seen in Figures 23 and 24. This is the transitional phase in which both the viscous force and inertial force have a large effect on the spherical bubbles $\sim 1 < Re < \sim 100$. Figure 24 splits the magmatic dataset into ceramic fluids and oils, syrups, and glues. This highlights that all the models struggle with fluids at the extremities of Morton number within the magmatic dataset.

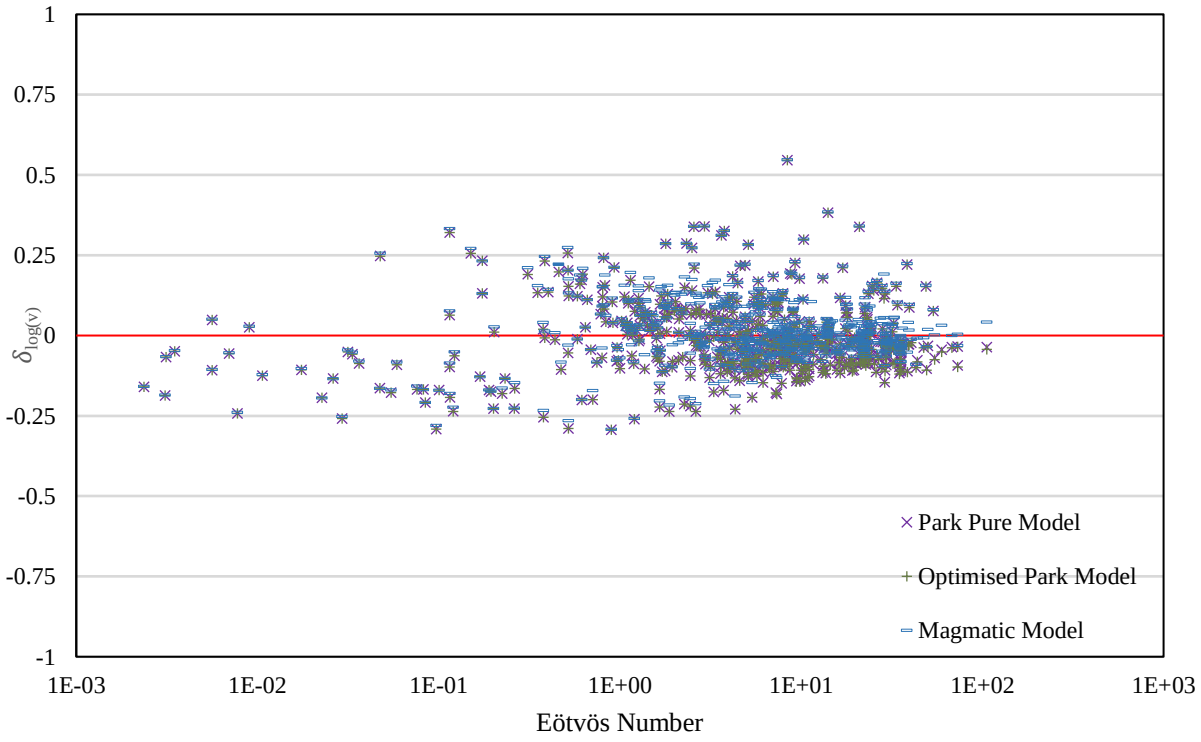

Figure 23. A comparison of the relative error of each model for the magmatic dataset. An expanded, high contrast version is available in Appendix C

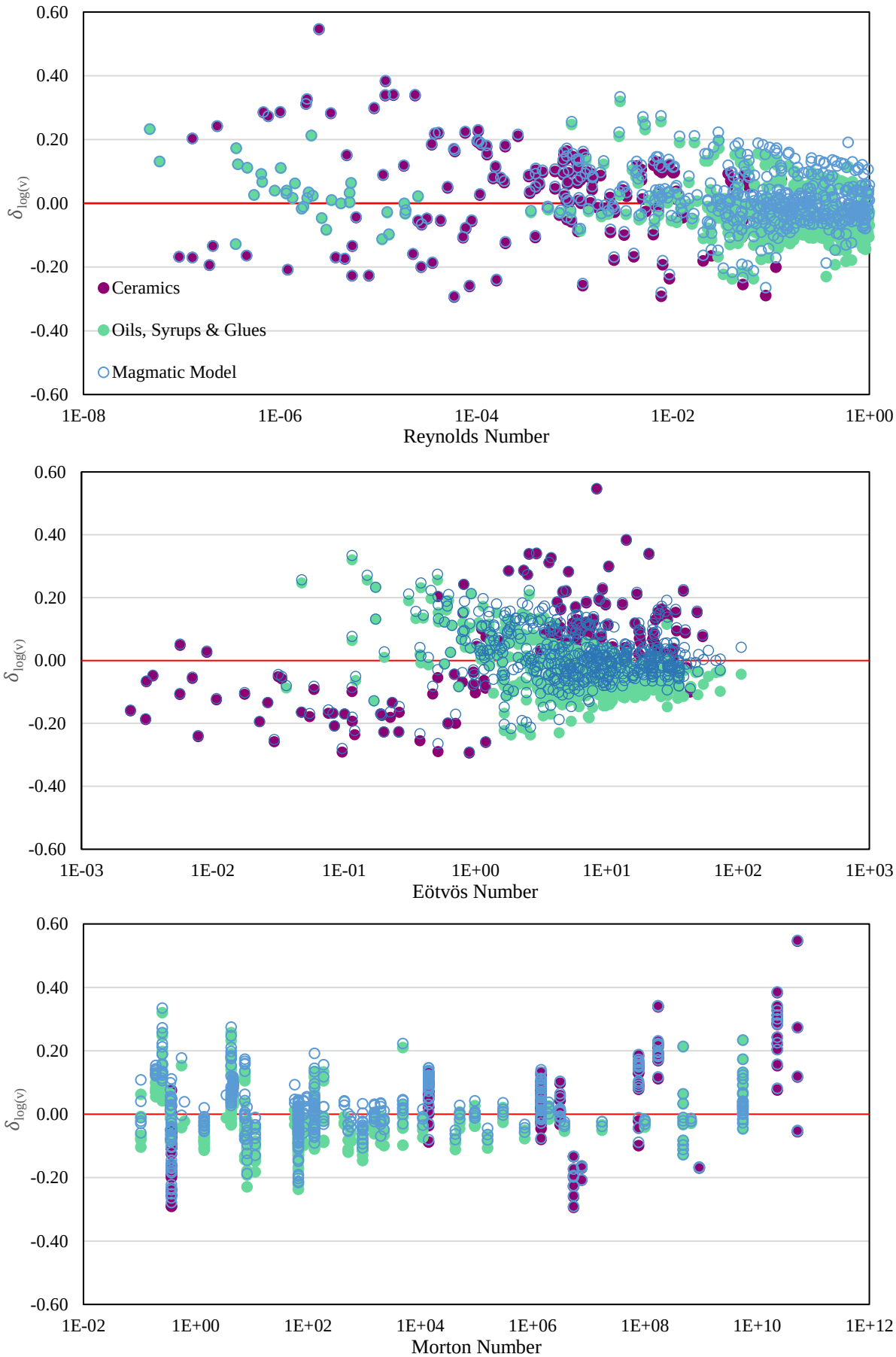

Figure 24. The relative error for the optimised Park model split into different fluid groups, along with the Magmatic model, for each dimensionless number.

4.3.4 Model Limitations

Checking the impact of each term of the Magmatic model against those of the Park Model (Figure 25) indicates that for high Morton number fluids, such as soda-lime-silica glass, there is almost no difference in the weighting of each term within the Eötvös number ranges of this dataset. As the Morton number approaches one, the increased empirical constant used in the inertial term maintains a linear relationship between the Eötvös and Reynolds numbers. The increased contribution of the inertial term to the model accounts for the lack of a non-spherical term, which would otherwise be present. As the Reynolds number increases beyond the scope of the magmatic dataset, the two models diverge, similarly to the effect seen with the Baz-Rodríguez model in Figure 15.

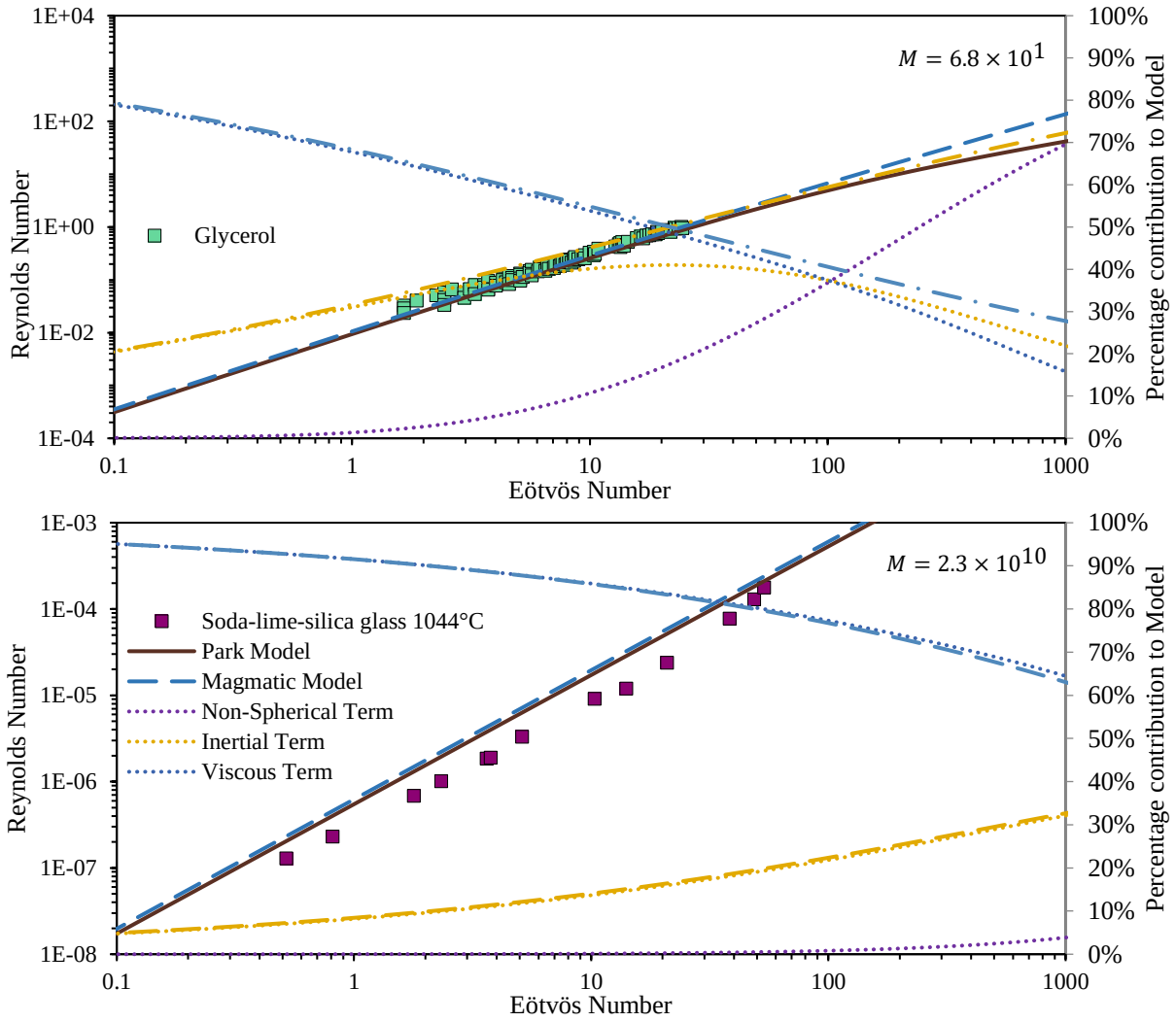

Figure 25. Percentage contribution of each term in the Park and Magmatic models for a glycerol and soda-lime-silica glass dataset. The beginning of the divergence between the two models can just be seen on the glycerol plot at high Reynolds numbers.

Plotting the predicted velocities for typical basaltic and rhyolitic melts, calculated from Table 7, the models only appear to diverge at $Re > 1$ (Figure 26). Expanding the range of Morton numbers out to less viscous fluids such as water ($M \approx 10^{-11}$) displays an increase in the Reynolds number at which divergence initially occurs.

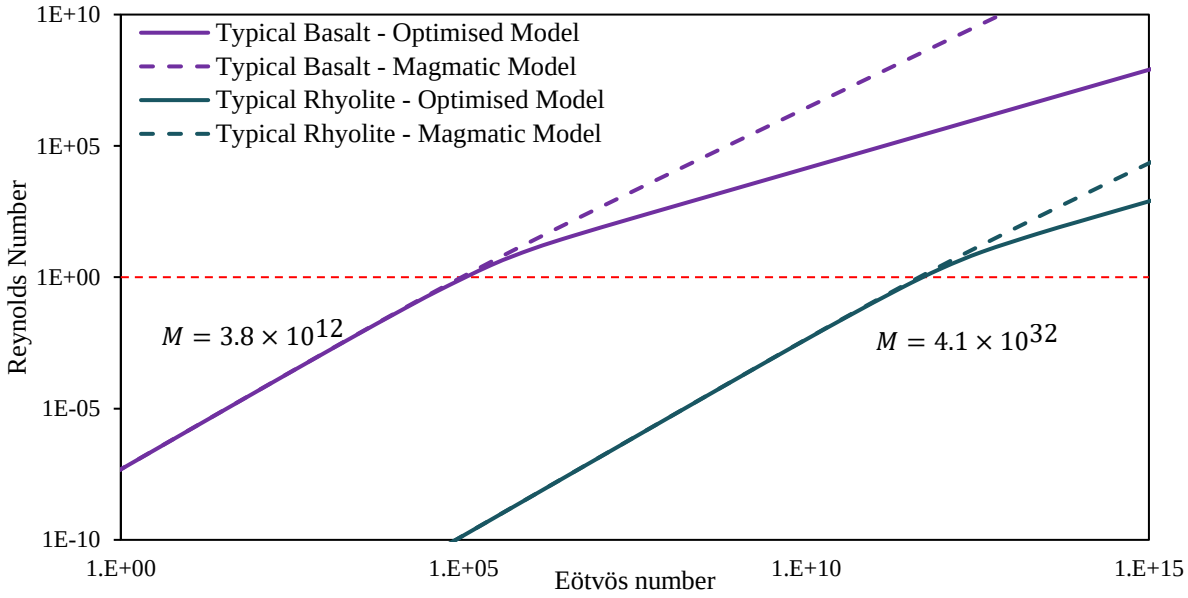

Figure 26. The divergence of the optimised Park and Magmatic models for typical silicate melts. There is a clear boundary at Re = 1, below which both models are almost identical.

Taking $Re = 1$, a limiting bubble radius can be calculated for any fluid viscosity, within which the Magmatic model produces a good fit for isolated bubble terminal velocity in silicate melts. This is displayed in Figure 27. Bubble exceeding a radius of 65 mm within low viscosity basaltic melts $\mu_f \approx 100$ Pa.s may show some deviation between the models, therefore the Optimised Park model would be recommended in these edge cases.

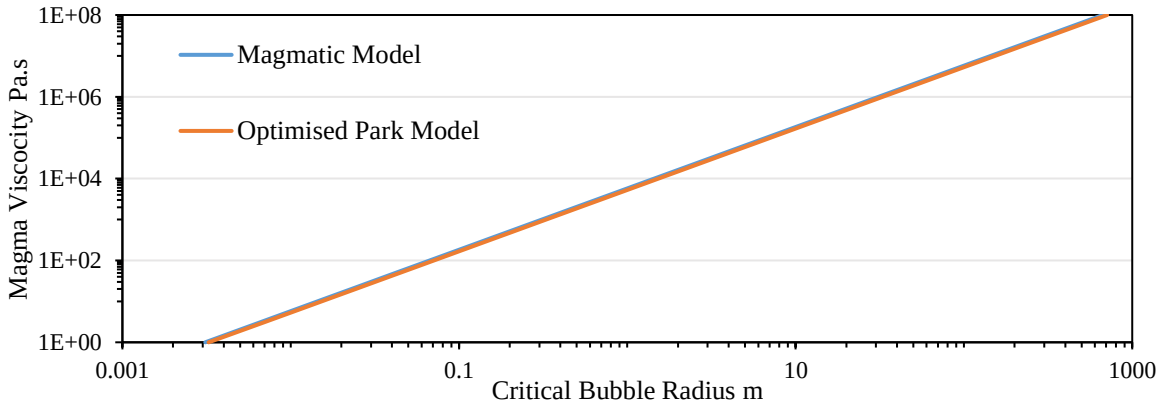

Figure 27. The critical bubble radius over a range of viscosities relevant for mafic melts. For bubbles larger than this value, the Magmatic model cannot be used to calculate the terminal velocity, and the optimised Park model should instead be used.

5. Implications and Conclusion

Within the full Newtonian dataset (Figure 17), there are three regions where our current terminal velocity models appear to provide a poor estimation: $E\ddot{o} < 10^{-3}$, $10^{-2} > E\ddot{o} > 10^{-1}$, and $E\ddot{o} > 10^{2}$. The low Eötvös number end of the dataset has issues with experimental precision due to the small size of the bubbles, as previously discussed. The Park models provide a good fit for this scattered data.

At the upper Eötvös number end, the bubbles are much larger and faster, requiring huge experimental setups to ensure the bubble reaches terminal velocity. The impact of any shape deformation due to the bubble injection or nucleation process is also substantial. Therefore, experimental error is likely to contribute. There is also more consideration required for the wall effect with large Eötvös number bubbles. Most experimental setups use just a single container, therefore, increasing the bubble radius also increases the wall diameter ratio. The Habermann & Sayre, and Rosenberg corrections that the dataset was tested against are for cylindrical containers. Many containers in the study had either square or rectangular cross-sections. These would reduce the impact of the wall force on the bubble terminal velocity. In Figure 18, some of the data at high wall diameter ratios displays a linear increase in model relative error. This increase in error is lower than expected for the wall effect in a cylindrical container but could match the expected error for a rectangular container. These datapoints were not included in the magmatic study unless a wall effect correction factor had already been applied within the original study. Some original studies may also have applied a cylindrical correction factor to bubbles in non-cylindrical containers. Applying a wall effect correction factor to studies using non-cylindrical containers was beyond the scope of this thesis but could be an avenue for future work, especially given the highly confined setups used for most magmatic analogues.

The relative error of all the models in the $10^{-2} > E\ddot{o} > 10^{-1}$ region is significant. In the case of pure water, this is the region around $10^{1} > Re > 10^{2}$ and $10^{-4} > r_{eb} > 4 \times 10^{-4}$ m, which

is beyond the scope of the Hadamard-Rybczynski solution due to the increase in inertial forces acting upon the bubble. The work by Peebles (1952), and then Wallis (1974), to bridge this gap before the ellipsoidal regime transition appears to fit well if the empirical constant A is adjusted. An example with $A = 0.95$ is shown in Figure 28 (based on Figure 13). A is larger than this in the Park, optimised Park, and Magmatic models, to bridge the gap to the ellipsoidal term, otherwise, the velocity would be underestimated by the models from $10^{-1} > E\ddot{o} > 10^{0}$.

This suggests that a term is missing from the parameterisation to adequately fit the $10^{-1} > E\ddot{o} > 10^{0}$ region. The empirical constants would then also need adjusting. An additional term covering the transition from spherical to ellipsoidal bubble regimes would also improve the fit of the Magmatic model for extremely low viscosity magmas. Therefore, further study into the $10^{-1} > E\ddot{o} > 10^{0}$ region of isolated rising bubble terminal velocities is strongly recommended. Additional experimental work with pure water would benefit the modelling of this transition.

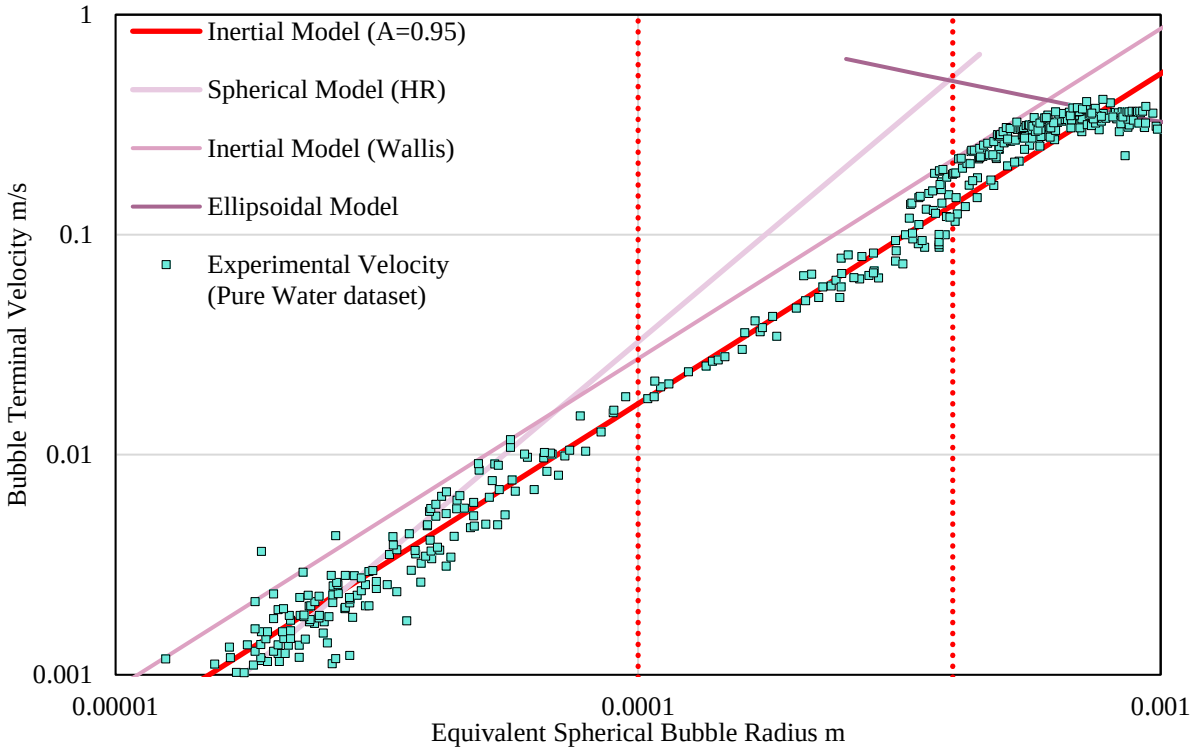

Figure 28. The terminal velocities within the poorly fitted $10^{-2} > E\ddot{o} > 10^{-1}$ region for the pure water dataset. The region is highlighted within the dotted red lines. The Wallis model with the empirical constant $A = 0.95$ is included, indicating that it is a good fit for that region.

The model proposed in this thesis for isolated bubble terminal velocities in magma produces an improved fit of experimental bubble rising data within fluids representative of silicate melts. It is also a simplification of the parameterisation proposed by Park et al. (2016) and, therefore, a more optimal model for use in quantitative models of bubble ascent in most magmas.

The terminal velocity of low Eötvös number bubbles in high Morton number fluids are overestimated by all models analysed in this thesis. Very few bubble rising experiments have high Morton number fluids, possibly due to the experimental difficulty and timescales involved. Further investigation into these fluids would help improve our understanding of this overestimation.

6. Appendices

6.1 Appendix A – Datasets

Newtonian dataset		Newtonian dataset	
Study	**Fluid**	**Study**	**Fluid**
Peebles 1952	Acetic Acid	Tsuge & Hibino 1977	Glycerol 50%
Tadaki & Maeda 1961	Acetic Acid 80%	Tsuge & Hibino 1977	Glycerol 52%
Allen 1900 Peebles 1952	Aniline	Bryn 1933	Glycerol 56%
		Maxworthy et al. 1996	Glycerol 60%
Jucha et al. 1982	Boron Trioxide	Raymond & Rosant 2000	Glycerol 60%
Gorodetskaya 1949	Butyl Alcohol	Raymond & Rosant 2000	Glycerol 69%
Kojima et al. 1968	Castor Oil	Gorring and Katz 1962	Glycerol 70.6%
Kojima et al. 1968	Corn Syrup	Tadaki & Maeda 1961	Glycerol 75%
Haberman & Morton 1953	Corn Syrup 62%	Raymond & Rosant 2000	Glycerol 76%
Haberman & Morton 1953	Corn Syrup 68%	Maxworthy et al. 1996	Glycerol 80%
Peebles 1952	Cottonseed Oil	Bryn 1933	Glycerol 81%
Redfield & Houghton 1965	Dextrose Solution 1-12	Raymond & Rosant 2000	Glycerol 82%
Tadaki & Maeda 1961 Davenport 1964	Ethanol	Zhang et al. 2004	Glycerol 85%
		Raymond & Rosant 2000	Glycerol 88%
Tadaki & Maeda 1961	Ethanol 8%	Zana 1975	Glycerol 89%
Bryn 1933	Ethanol 13%	Calderbank et al. 1970	Glycerol 90.6%
Tadaki & Maeda 1961	Ethanol 30%	Johnson 1969	Glycerol 90.6%
Peebles 1952 Tadaki & Maeda 1961	Ethyl Acetate	Rodrigue et al. 1996	Glycerol 92%
		Rodrigue et al. 1996	Glycerol 92% + 300ppm SDS
Peebles 1952	Ethyl Ether	Rodrigue et al. 1996	Glycerol 92% + 30ppm SDS
Wang et al. 2017 Zhang et al. 2005	Galinstan	Raymond & Rosant 2000	Glycerol 93%
		Rodrigue et al. 1996	Glycerol 95%
Angelino 1966 Garner & Hammerton 1954 Kojima et al. 1968 Raymond & Rosant 2000 Talaia 2007	Glycerol	Rodrigue et al. 1996	Glycerol 95% + 300ppm SDS
		Rodrigue et al. 1996	Glycerol 95% + 30ppm SDS
		Raymond & Rosant 2000	Glycerol 98%
		Calderbank et al. 1970	Glycerol 99%
		Johnson 1969	Glycerol 99%
Maxworthy et al. 1996	Glycerol 10%	Rodrigue et al. 1996	Glycerol 99%
Maxworthy et al. 1996	Glycerol 20%	Rodrigue et al. 1996	Glycerol 99% + 300ppm SDS
Maxworthy et al. 1996	Glycerol 30%	Rodrigue et al. 1996	Glycerol 99% + 30ppm SDS
Maxworthy et al. 1996	Glycerol 40%	Funfschilling & Li 2006	Glycerol 99.5%
Bryn 1933	Glycerol 42%	Liu et al. 2016	Glycerol Solutions 1-4
Tsuge & Hibino 1977	Glycerol 46%	Miyahara & Yamanaka 1993	Glycerol Solutions 2 & 4
Tsuge & Hibino 1977	Glycerol 48%		

Newtonian dataset		Newtonian dataset	
Study	**Fluid**	**Study**	**Fluid**
Bond & Newton 1928 Jackson et al. 2022	Golden Syrup Golden Syrup 80%	Hornyak & Weinberg 1984 Kočárková 2011	Soda-lime-silica Glass
Dong et al. 2010	Ionic Liquid [bmim] BF4	Tadaki & Maeda 1961	Sodium Chloride 3.5%
Dong et al. 2010	Ionic Liquid [bmim] PF6	Tadaki & Maeda 1961	Sodium Chloride 7%
Dong et al. 2010	Ionic Liquid [omim] BF4	Jucha et al. 1982	Sodium Diborate
Tadaki & Maeda 1961 Tsuge & Hibino 1977	Isoamyl Alcohol	Bond & Newton 1928	Sodium Silicate
		Tsuge & Hibino 1977	Soybean Oil 60% in Hexane
Mahmoudi et al. 2019	Kerosene	Tadaki & Maeda 1961	Toluene
Davenport 1964 Mori 1977 Paneni 1969	Mercury	Haberman & Morton 1953	Turpentine
		Haberman & Morton 1953	Varsol
		Viana et al. 2001	Viscous Liquid
Haberman & Morton 1953 Tsuge & Hibino 1977	Methanol	Allen 1900	Water
		Aybers and Tapucu 1969	
Tsuge & Hibino 1977	Methanol 30%	Blandín-Arrieta 1997	
Tsuge & Hibino 1977	Methanol 60%	Bryn 1933	
Haberman & Morton 1953 Leal et al. 1971	Mineral Oil	Calderbank & Lochiel 1964	
Gorodetskaya 1949	n-Amyl Alcohol	Coppock & Meiklejohn 1951	
Abou-el-Hassan 1983	Newtonian Fluid 1-22	Datta et al. 1950	
Davies & Taylor 1950 Peebles 1952 Tadaki & Maeda 1961	Nitrobenzene	Davies & Taylor 1950	
		Garner & Hammerton 1954	
		Haberman & Morton 1953	
Angelino 1966	Oil	Hoefer 1913	
Angelino 1966	Propylene Glycol mixture	Jamialahmadi & Müuller-Steinhagen 1993	
Guthrie 1967	PVA 0.1%	Leonard & Houghton 1963	
Davenport 1964	PVA 0.5%	Liu et al. 2015	
Guthrie 1967	PVA 4.19%	Luchsinger 1937	
Davenport 1964	PVA 4.5%	Merker et al. 2017	
Davenport 1964 PVA	PVA 5.4%	Miyagi 1925	
Guthrie 1967	PVA 5.64%	Miyahara & Yamanaka 1993	
Davenport 1964	PVA 6.1%		
Guthrie 1967	PVA 6.65%	Okawa et al. 2003	
Guthrie 1967	PVA 8.4%	Peebles 1952	
Peebles 1952	Pyridine	Rosenberg 1950	
Li & Schneider 1993	S-2000 Oil	Shabalin et al. 1939	
Li & Schneider 1993	S-8000 Oil	Stuke 1952 Water	
Jucha et al. 1982	Silicone Oil	Talaia 2007	
Davenport 1964	Silver	Uno & Kitner 1956	
Guthrie 1967	Silver 99.95%	Wang et al. 2017	

Newtonian dataset	
Study	**Fluid**
Sam et al. 1996	Water (30ppm MIBC)
Sam et al. 1996	Water (30ppm MPG)
Sam et al. 1996	Water (30ppm Pine Oil)
Haberman & Morton 1953	Water (4200ppm Glim)
Garner & Hammerton 1954	Water (Vaseline)
Calderbank et al. 1970 Davenport 1964 Detsch 1991 Duineveld 1995 Gorodetskaya 1949 Johnson 1969 Kure et al. 2021 Leifer et al. 2000 Loudon 1968 Mahmoudi et al. 2019 Maxworthy et al. 1996 Okazaki 1964 Paneni 1969 Parkinson et al. 2008 Pawliszak et al. 2019 Sam et al. 1996 Tsuge & Hibino 1977 Yan et al. 2017 Zawala & Niecikowska 2017 Zdonik 1942	Water (Distilled)
Leonard & Houghton 1963	Water (He saturated)
Leonard & Houghton 1963	Water (N_2O saturated)
Detsch 1991 Houghton et al. 1957	Water (Salt)
Baird and Davidson 1962 Davenport 1964 Detsch 1991 Gorodetskaya 1949 Gorring and Katz 1962 Guthrie 1967 Houghton et al. 1957 Sam et al. 1996 Zhang et al. 2005	Water (Tap)
Garner & Hammerton 1954	White Oil

Pure Water dataset	
Study	**Fluid**
Calderbank et al. 1970 Davenport 1964 Detsch 1991 Duineveld 1995 Gorodetskaya 1949 Johnson 1969 Kure et al. 2021 Leifer et al. 2000 Loudon 1968 Maxworthy et al. 1996 Merker et al. 2017 Okazaki 1964 Parkinson et al. 2008 Pawliszak et al. 2019 Tsuge & Hibino 1977 Yan et al. 2017 Zdonik 1942	Water (Distilled)

Magmatic dataset	
Study	**Fluid**
Jucha et al. 1982	Boron Trioxide
Kojima et al. 1968	Castor Oil
Kojima et al. 1968	Corn Syrup
Redfield & Houghton 1965	Dextrose Solutions 1-4
Garner & Hammerton 1954 Kojima et al. 1968 Raymond & Rosant 2000	Glycerol
Raymond & Rosant 2000	Glycerol 93%
Rodrigue et al. 1996	Glycerol 95%
Raymond & Rosant 2000	Glycerol 98%
Calderbank et al. 1970	Glycerol 99%
Johnson 1969	Glycerol 99%
Rodrigue et al. 1996	Glycerol 99%
Funfschilling & Li 2006	Glycerol 99.5%
Liu et al. 2016	Glycerol Solutions 1 & 2
Miyahara & Yamanaka 1993	Glycerol Solutions 2 & 4
Jackson et al. 2022	Golden Syrup 80%
Li & Schneider 1993	S-2000 Oil
Li & Schneider 1993	S-8000 Oil
Hornyak & Weinberg 1984 Kočárková 2011	Soda-Lime-Silica Glass
Jucha et al. 1982	Sodium Diborate
Bond & Newton 1928	Sodium Silicate
Garner & Hammerton 1954	White Oil

6.2 Appendix B – Dimensionless Equations for Grace Plot

Transition between spherical and ellipsoidal regimes:

$$Re = \frac{C^{\frac{5}{4}}}{A^{\frac{3}{2}}}\left(1 + \frac{B}{CE\ddot{o}}\right)^{\frac{5}{4}}$$

$$= 5.23\left(1 + \frac{8.04}{E\ddot{o}}\right)^{\frac{5}{4}}$$

Transition between spherical and spherical-cap regimes:

$$Re = 5.23$$

Transition between ellipsoidal and spherical-cap regimes from Grace (1973):

$$E\ddot{o} = 40$$

6.3 Appendix C – Expanded High Contrast Figures

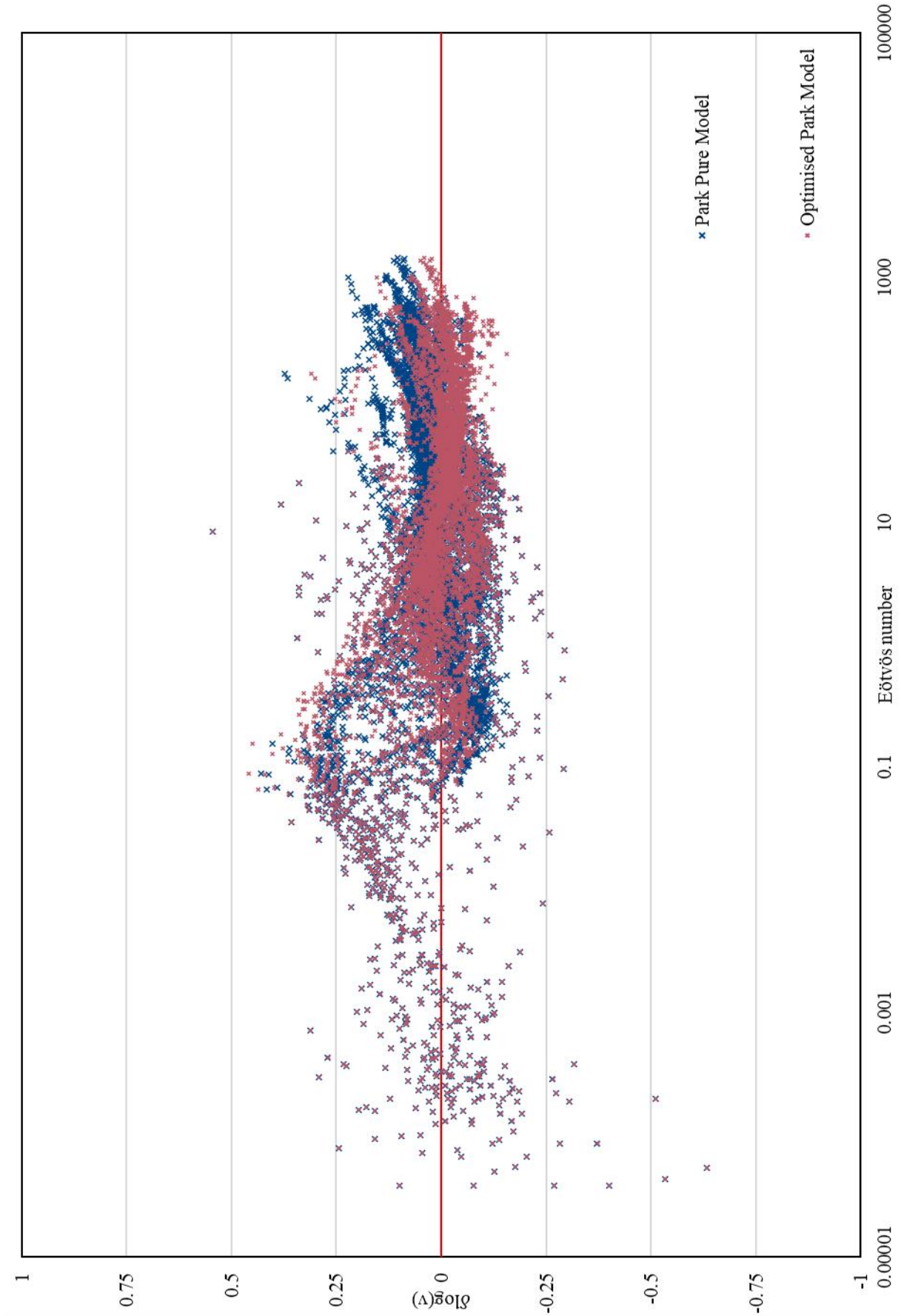

Figure 29. The relative error in the model calculated value for the Newtonian dataset against the Morton number. The divergence of the Baz-Rodríguez model from experimental values, as Morton number increases, can clearly be seen.

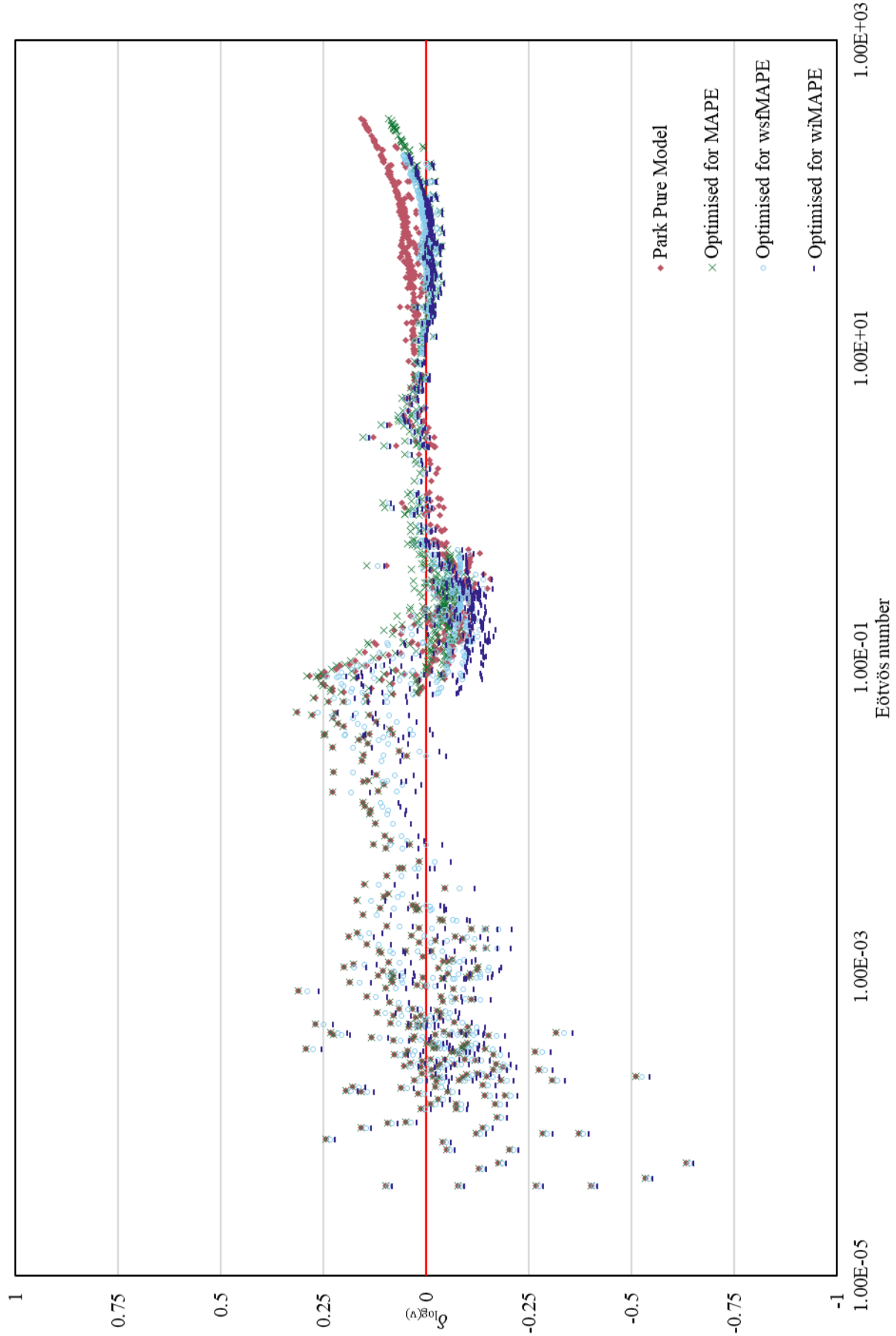

Figure 30. The relative error for each optimised model in comparison to the original Park model across the pure water dataset.

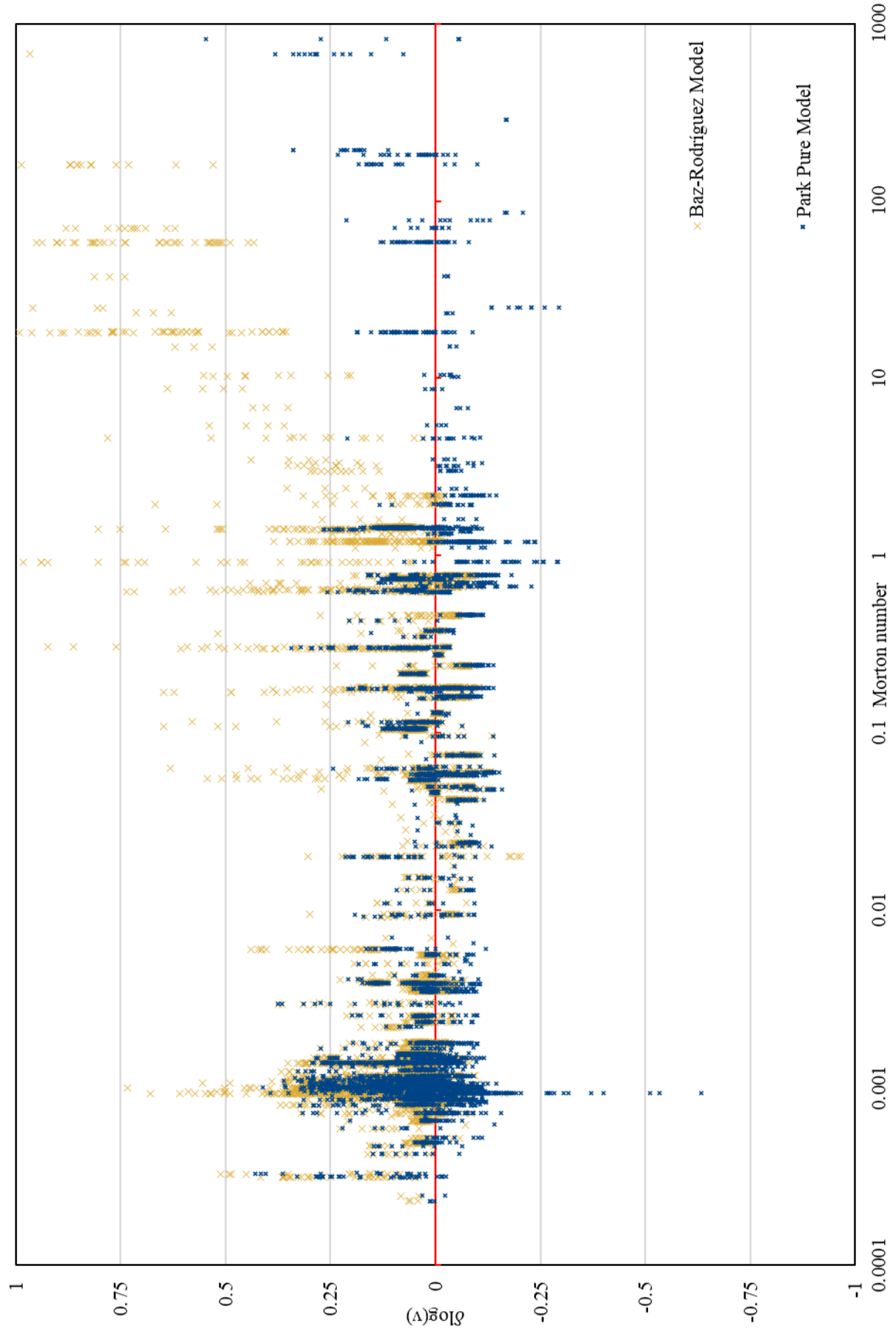

Figure 31. The relative error for the optimised Park model in comparison to the original Park pure model for the Newtonian dataset. The main improvement can be seen within the large Eötvös number range.

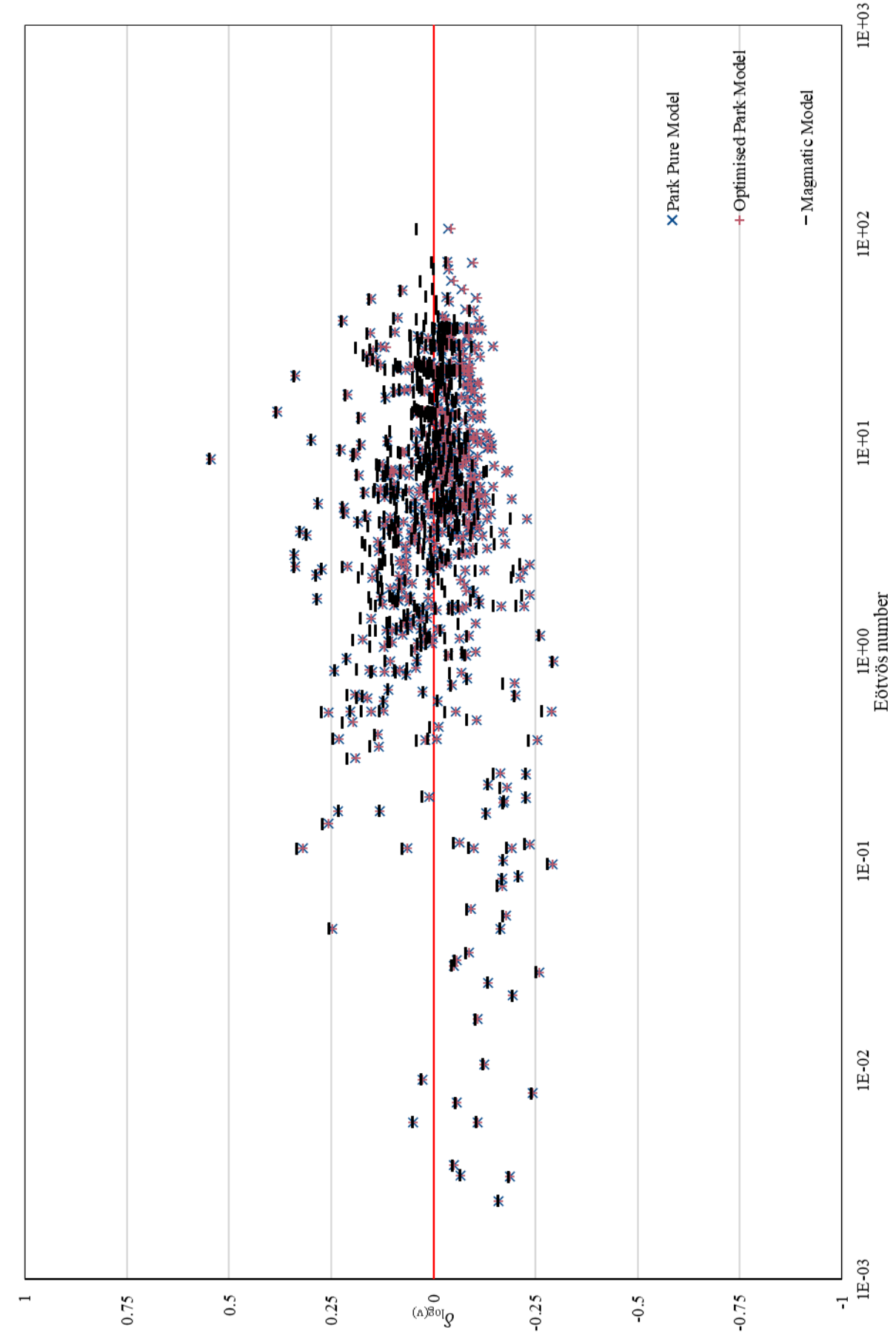

Figure 32. A comparison of the relative error of each model for the magmatic dataset.

7. Bibliography

Abou-El-Hassan, M. E. (1983). A generalized bubble rise velocity correlation. *Chemical Engineering Communications*, ***22*** (3-4), 243-250. https://doi.org/10.1080/00986448308940058

Acharya, A., Mashelkar, R. A., & Ulbrecht, J. (1977). Mechanics of bubble motion and deformation in non-Newtonian media. *Chemical Engineering Science*, ***32*** (8), 863-872. https://doi.org/10.1016/0009-2509(77)80072-9

Allen, H. S. (1900). XXXI. The motion of a sphere in a viscous fluid. *The London, Edinburgh, and Dublin Philosophical Magazine and Journal of Science*, ***50*** (304), 323-338. https://doi.org/10.1080/14786440009463920

Almani, S., Blel, W., Gadoin, E., & Gentric, C. (2021). Investigation of single bubbles rising in Newtonian and non-Newtonian fluids inside a thin-gap bubble column intended for microalgae cultivation. *Chemical Engineering Research and Design*, ***167***, 218-230. https://doi.org/10.1016/j.cherd.2021.01.010

Amirnia, S., de Bruyn, J. R., Bergougnou, M. A., & Margaritis, A. (2013). Continuous rise velocity of air bubbles in non-Newtonian biopolymer solutions. *Chemical Engineering Science*, ***94***, 60-68. https://doi.org/10.1016/j.ces.2013.02.032

Angelino, H. (1966). Hydrodynamique des grosses bulles dans les liquides visqueux. *Chemical Engineering Science*, ***21*** (6-7), 541-550. https://doi.org/10.1016/0009-2509(66)85068-6

Astarita, G., & Apuzzo, G. (1965). Motion of gas bubbles in non-Newtonian liquids. *AIChE Journal*, ***11*** (5), 815-820. https://doi.org/10.1002/aic.690110514

Aybers, N. M., & Tapucu, A. (1969). Studies on the drag and shape of gas bubbles rising through a stagnant liquid. *Wärme-und Stoffübertragung*, ***2*** (3), 171-177. https://doi.org/10.1007/BF00751164

Bachhuber, C., & Sanford, C. (1974). The rise of small bubbles in water. *Journal of Applied Physics*, ***45*** (6), 2567-2569. https://doi.org/10.1063/1.1663630

Bagdassarov, N., Dorfman, A., & Dingwell, D. B. (2000). Effect of alkalis, phosphorus, and water on the surface tension of haplogranite melt. *American Mineralogist*, ***85*** (1), 33-40. https://doi.org/10.2138/am-2000-0105

Baird, M. H. I., & Davidson, J. F. (1962). Annular jets-I: Fluid dynamics. *Chemical Engineering Science*, ***17*** (6), 467-472. https://doi.org/10.1016/0009-2509(62)85015-5

Bansal, N.P. & Doremus, R.H. (1986). Handbook of glass properties. *Academic Press* https://doi.org/10.1016/C2009-0-21785-5

Baz-Rodríguez, S., Aguilar-Corona, A., & Soria, A. (2012). Velocidad de ascenso de burbujas aisladas en líquidos puros. *Revista mexicana de ingeniería química*, ***11*** (2), 269-278.

Behrens, H., & Gaillard, F. (2006). Geochemical aspects of melts: volatiles and redox behavior. *Elements*, ***2*** (5), 275-280. https://doi.org/10.2113/gselements.2.5.275

Blandın-Arrieta, J. (1997). Visualization and Description of Bubble Dynamics. *MSc. Thesis, Universidad Autónoma Metropolitana-Iztapalapa, México*.

Bond, W. N., & Newton, D. A. (1928). LXXXII. Bubbles, drops, and Stokes' law. (Paper 2). *The London, Edinburgh, and Dublin Philosophical Magazine and Journal of Science*, ***5*** (30), 794-800. https://doi.org/10.1080/14786440408564523

Bottinga, Y., & Weill, D. F. (1972). The viscosity of magmatic silicate liquids; a model calculation. *American Journal of Science*, ***272*** (5), 438-475. https://doi.org/10.2475/ajs.272.5.438

Bourgue, E., & Richet, P. (2001). The effects of dissolved CO2 on the density and viscosity of silicate melts: a preliminary study. *Earth and Planetary Science Letters*, ***193*** (1-2), 57-68. https://doi.org/10.1016/S0012-821X(01)00491-5

Boussinesq, J. (1913). Vitesse de la chute lente, devenue uniforme, d'une goutte liquid sphérique, dans un fluide visqueux de poids spécifique moindre. *Annales de Chimie et de Physique*, ***29***, 364-372.

Bozzano, G., & Dente, M. (2001). Shape and terminal velocity of single bubble motion: a novel approach. *Computers & chemical engineering*, ***25*** (4-6), 571-576. https://doi.org/10.1016/S0098-1354(01)00636-6

Bryn, T. (1933). Steiggeschwindigkeit von Luftblasen in Flüssigkeiten. *Forschung auf dem Gebiet des Ingenieurwesens A*, ***4***, 27-30. https://doi.org/10.1007/BF02716943

Calderbank, P. H., & Lochiel, A. C. (1964). Mass transfer coefficients, velocities and shapes of carbon dioxide bubbles in free rise through distilled water. *Chemical Engineering Science*, ***19*** (7), 485-503. https://doi.org/10.1016/0009-2509(64)85075-2

Calderbank, P. H., Johnson, D. S. L., & Loudon, J. (1970). Mechanics and mass transfer of single bubbles in free rise through some Newtonian and non-Newtonian liquids. *Chemical Engineering Science*, ***25*** (2), 235-256. https://doi.org/10.1016/0009-2509(70)80018-5

Cassidy, M., Manga, M., Cashman, K., & Bachmann, O. (2018). Controls on explosive-effusive volcanic eruption styles. *Nature communications*, ***9***, 2839. https://doi.org/10.1038/s41467-018-05293-3

Chehata D. 2004. Estudio de la discontinuidad en la velocidad de ascenso de una burbuja en un liquido no-Newtoniano. MSc. Thesis, Universidad Nacional Autónoma de México.

Clanet, C., Héraud, P., & Searby, G. (2004). On the motion of bubbles in vertical tubes of arbitrary cross-sections: some complements to the Dumitrescu–Taylor problem. *Journal of Fluid Mechanics*, ***519***, 359-376. https://doi.org/10.1017/S0022112004001296

Clift, R., Grace, J. R., & Weber, M. E. (1978). Bubbles, drops, and particles. *Academic Press*

Collins, R. (1967). Experiments on large gas bubbles in liquids, *United Kingdom Atomic Energy Authority Research Group*, ***AERE-R-5402*** https://www.osti.gov/biblio/4420630

Coppock, P. D., & Meiklejohn, G. T. (1951). The behavior of gas bubbles in relation to mass transfer. *Transactions of the Institution of Chemical Engineers*, ***29***, 75-86.

Costa, A. (2005). Viscosity of high crystal content melts: dependence on solid fraction. *Geophysical Research Letters*, ***32*** (22). https://doi.org/10.1029/2005GL024303

Costa, A., & Macedonio, G. (2003). Viscous heating in fluids with temperature-dependent viscosity: implications for magma flows. *Nonlinear Processes in Geophysics*, ***10*** (6), 545-555. https://doi.org/10.5194/npg-10-545-2003

Costa, A., Melnik, O., & Vedeneeva, E. (2007). Thermal effects during magma ascent in conduits. *Journal of Geophysical Research: Solid Earth*, ***112*** (B12). https://doi.org/10.1029/2007JB004985

Costa, A., Caricchi, L., & Bagdassarov, N. (2009). A model for the rheology of particle-bearing suspensions and partially molten rocks. *Geochemistry, Geophysics, Geosystems*, ***10*** (3). https://doi.org/10.1029/2008GC002138

Couette, M. (1990). Etudes sur le frottement des liquids. *Ph.D. Thesis, Faculté des Sciences de Paris*.

Coumans, J. P., Llewellin, E. W., Wadsworth, F. B., Humphreys, M. C. S., Mathias, S. A., Yelverton, B. M., & Gardner, J. E. (2020). An experimentally validated numerical model for bubble growth in magma. *Journal of Volcanology and Geothermal Research*, ***402***, 107002. https://doi.org/10.1016/j.jvolgeores.2020.107002

Crozier, J., Tramontano, S., Forte, P., Oliva, S. J. C., Gonnermann, H. M., Lev, E., Manga, M., Myers, M., Rader, E., Ruprecht, P., Tuffen, H., Paisley, R., Houghton, B. F., Shea, T., Schipper, C. I., & Castro, J. M. (2022). Outgassing through magmatic fractures enables effusive eruption of silicic magma. *Journal of Volcanology and Geothermal Research*, ***430***, 107617. https://doi.org/10.1016/j.jvolgeores.2022.107617

Darton, R. C. & Harrison, D. (1974). The rise of single gas bubbles in liquid fluidised beds. *Transactions of the Institution of Chemical Engineers*, ***52***, 301-306.

Datta, R., Napier, D. H., & Newitt, D. M. (1950). The Property and Behavior of Gas Bubbles Formed at a Circular Orifice. *Transactions of the Institution of Chemical Engineers*, ***28***, 14-26.

Davenport, W.G. (1964). Bubbles in Liquids Including Liquid Metals. *Ph.D. Thesis, Royal School of Mines, Imperial College, London.*

Davenport, W. G., Richardson, F. D., & Bradshaw, A. V. (1967). Spherical cap bubbles in low density liquids. *Chemical Engineering Science*, ***22*** (9), 1221-1235. https://doi.org/10.1016/0009-2509(67)80188-X

Davies, R. M., & Taylor, G. I. (1950). The mechanics of large bubbles rising through extended liquids and through liquids in tubes. *Proceedings of the Royal Society of London. Series A. Mathematical and Physical Sciences*, ***200*** (1062), 375-390. https://doi.org/10.1098/rspa.1950.0023

Detsch, R. M. (1991). Small air bubbles in reagent grade water and seawater: 1. Rise velocities of 20-to 1000-μm-diameter bubbles. *Journal of Geophysical Research: Oceans*, ***96*** (C5), 8901-8906. https://doi.org/10.1029/91JC00484

Dingwell, D. B., Courtial, P., Giordano, D., & Nichols, A. R. L. (2004). Viscosity of peridotite liquid. *Earth and Planetary Science Letters*, ***226*** (1-2), 127-138. https://doi.org/10.1016/j.epsl.2004.07.017

Dong, H., Wang, X., Liu, L., Zhang, X., & Zhang, S. (2010). The rise and deformation of a single bubble in ionic liquids. *Chemical Engineering Science*, ***65*** (10), 3240-3248. https://doi.org/10.1016/j.ces.2010.02.011

Duineveld, P. C. (1995). The rise velocity and shape of bubbles in pure water at high Reynolds number. *Journal of Fluid Mechanics*, ***292***, 325-332. https://doi.org/10.1017/S0022112095001546

Dumitrescu, D. T. (1943). Strömung an einer Luftblase in senkrechten Rohr. *Zeitschrift für Angewandte Mathematik und Mechanik*, ***23***, 139-149. https://doi.org/10.1002/zamm.19430230303

Eichelberger, J. C., Carrigan, C. R., Westrich, H. R., & Price, R. H. (1986). Non-explosive silicic volcanism. *Nature*, ***323***, 598-602. https://doi.org/10.1038/323598a0

Einstein, A. (1906). Eine neue Bestimmung der Moleküldimensionen. *Annals of Physics*, ***19***, 289–306. http://doi.org/10.1002/andp.19063240204

Eötvös, R. (1886). Über den Zusammenhang der Oberflächenspannung der Flüssigkeiten mit ihrem Molecularvolumen. *Annalen der Physik*, ***263*** (3), 448-459. https://doi.org/10.1002/andp.19063240204

Epelbaum, M. B., Babashov, I. V., & Salova, T. P. (1973). Surface tension of acidic magmatic melts at high parameters. *Geokhimya*, ***3***, 461-464.

Faxén, H. (1922). Der Widerstand gegen die Bewegung einer starren Kugel in einer zähen Flüssigkeit, die zwischen zwei parallelen ebenen Wänden eingeschlossen ist. *Annalen der Physik*, ***373*** (10), 89-119. https://doi.org/10.1002/andp.19223731003

Feng, J., & Bolotnov, I. A. (2018). Effect of the wall presence on the bubble interfacial forces in a shear flow field. *International Journal of Multiphase Flow*, ***99***, 73-85. https://doi.org/10.1016/j.ijmultiphaseflow.2017.10.004

Fernandes, P. C., Risso, F., Ern, P., & Magnaudet, J. (2007). Oscillatory motion and wake instability of freely rising axisymmetric bodies. *Journal of Fluid Mechanics*, ***573***, 479-502. https://doi.org/10.1017/S0022112006003685

Francis, A. W. (1933). Wall effect in falling ball method for viscosity. *Physics*, ***4*** (11), 403-406. https://doi.org/10.1063/1.1745151

Frumkin, A.N., & Levich, V.G., (1947). Effect of surface-active substances on movement at the boundaries of liquid phases. *Zhurnal Fizicheskoi Khimii*, ***21***, 1183–1204

Fulcher, G. S. (1925). Analysis of recent measurements of the viscosity of glasses. *Journal of the American Ceramic Society*, ***8*** (6), 339-355. https://doi.org/10.1111/j.1151-2916.1925.tb16731.x

Funfschilling, D., & Li, H. Z. (2006). Effects of the injection period on the rise velocity and shape of a bubble in a non-Newtonian fluid. *Chemical Engineering Research and Design*, ***84*** (10), 875-883. https://doi.org/10.1205/cherd.01229

Gardner, J. E., Ketcham, R. A., & Moore, G. (2013). Surface tension of hydrous silicate melts: Constraints on the impact of melt composition. *Journal of Volcanology and Geothermal Research*, ***267***, 68-74. https://doi.org/10.1016/j.jvolgeores.2013.09.007

Gardner, J. E., Wadsworth, F. B., Carley, T. L., Llewellin, E. W., Kusumaatmaja, H., & Sahagian, D. (2023). Bubble formation in magma. *Annual Review of Earth and Planetary Sciences*, ***51***, 131-154. https://doi.org/10.1146/annurev-earth-031621-080308

Garner, F. H., & Hammerton, D. (1954). Circulation inside gas bubbles. *Chemical Engineering Science*, ***3*** (1), 1-11. https://doi.org/10.1016/0009-2509(54)80001-7

Giachetti, T., Gonnermann, H. M., Gardner, J. E., Burgisser, A., Hajimirza, S., Earley, T. C., Truong, N. & Toledo, P. (2019). Bubble coalescence and percolation threshold in expanding rhyolitic magma. *Geochemistry, Geophysics, Geosystems*, *20*(2), 1054-1074. https://doi.org/10.1029/2018GC008006

Giordano, D., & Dingwell, D. B. (2003). Non-Arrhenian multicomponent melt viscosity: a model. *Earth and Planetary Science Letters*, ***208*** (3-4), 337-349. https://doi.org/10.1016/S0012-821X(03)00042-6

Giordano, D., Mangiacapra, A., Potuzak, M., Russell, J. K., Romano, C., Dingwell, D. B., & Di Muro, A. (2006). An expanded non-Arrhenian model for silicate melt viscosity: A treatment for metaluminous, peraluminous and peralkaline liquids. *Chemical Geology*, ***229*** (1-3), 42-56. https://doi.org/10.1016/j.chemgeo.2006.01.007

Giordano, D., Russell, J. K., & Dingwell, D. B. (2008). Viscosity of magmatic liquids: a model. *Earth and Planetary Science Letters*, ***271*** (1-4), 123-134. https://doi.org/10.1016/j.epsl.2008.03.038

Gonnermann, H. M. (2015). Magma fragmentation. *Annual Review of Earth and Planetary Sciences*, ***43***, 431-458. https://doi.org/10.1146/annurev-earth-060614-105206

Gonnermann, H. M., & Manga, M. (2003). Explosive volcanism may not be an inevitable consequence of magma fragmentation. *Nature*, ***426***, 432-435. https://doi.org/10.1038/nature02138

Gonnermann, H. M., & Manga, M. (2007). The fluid mechanics inside a volcano. *Annual Review of Fluid Mechanics*, ***39***, 321-356. https://doi.org/10.1146/annurev.fluid.39.050905.110207

Gorodetskaya, A. (1949). The rate of rise of bubbles in water and aqueous solutions at great Reynolds numbers. *Russian Journal of Physical Chemistry*, **23**, 71-78.

Gorring, R. L., & Katz, D. L. (1962). Bubble rise in a packed bed saturated with liquids. *AIChE Journal*, ***8*** (1), 123-126. https://doi.org/10.1002/aic.690080128

Grace, J. R. (1973). Shapes and velocities of bubbles rising in infinite liquids. *Transactions of the Institution of Chemical Engineering*, ***54***, 116-120.

Grace, J. R., Wairegi, T., & Nguyen, T. H. (1976). Shapes and sizes of bubbles rising in infinite liquids. *Transactions of the Institution of Chemical Engineering*, ***54***, 167-173.

Griffith, R. M. (1962). The effect of surfactants on the terminal velocity of drops and bubbles. *Chemical Engineering Science*, ***17*** (12), 1057-1070. https://doi.org/10.1016/0009-2509(62)80084-0

Guthrie, R. I. L. (1967). Dynamic and mass transfer phenomena of spherical capped bubbles. *Ph.D. Thesis, Royal School of Mines, Imperial College, London.*

Guyer, A., & Pfister, X. (1946). Über die Absorption von Gasblasen I. *Helvetica Chimica Acta*, ***29*** (5), 1173-1183. https://doi.org/10.1002/hlca.19460290526

Haberman, W. L., & Morton, R. K. (1953). An experimental investigation of the drag and shape of air bubbles rising in various liquids. *David W. Taylor Model Basin. Navy Department, Washington DC, Report* ***802***.

Haberman, W. L., & Sayre, R. M. (1958). Motion of rigid and fluid spheres in stationary and moving liquids inside cylindrical tubes. *David W. Taylor Model Basin. Navy Department, Washington DC, Report* ***1143***.

Hadamard, J. S. (1911). Mouvement permanent lent d'une sphere liquide et visqueuse dans un liquide visqueux. *Comptes rendus de l'Académie des Sciences,* ***152***, 1735–1738

Haque, M. W., Nigam, K. D. P., Viswanathan, K., & Joshi, J. B. (1988). Studies on bubble rise velocity in bubble columns employing non-Newtonian solutions. *Chemical Engineering Communications*, ***73*** (1), 31-42. https://doi.org/10.1080/00986448808940431

Hoefer, K. (1913). Untersuchungen über die Strömungsvorgänge im Steigrohr eines Druckluft-Wasserhebers. *Forschungsarbeiten auf dem Gebiete des Ingenieurwesens****, 138***, 1-47. https://doi.org/10.1007/978-3-662-01995-5_1

Hornyak, E. J., & Weinberg, M. C. (1984). Velocity of a freely rising gas bubble in a soda-lime silicate glass melt. *Journal of the American Ceramic Society*, ***67*** (11), 244-246. https://doi.org/10.1111/j.1151-2916.1984.tb19498.x

Houghton, G., Ritchie, P. D., & Thomson, J. A. (1957). Velocity of rise of air bubbles in sea-water, and their types of motion. *Chemical Engineering Science*, ***7*** (1), 111-112. https://doi.org/10.1016/0009-2509(57)80026-8

Huber, C., Su, Y., Nguyen, C. T., Parmigiani, A., Gonnermann, H. M., & Dufek, J. (2014). A new bubble dynamics model to study bubble growth, deformation, and coalescence. *Journal of Geophysical Research: Solid Earth*, ***119*** (1), 216-239. https://doi.org/10.1002/2013JB010419

Hui, H., & Zhang, Y. (2007). Toward a general viscosity equation for natural anhydrous and hydrous silicate melts. *Geochimica et Cosmochimica Acta*, ***71*** (2), 403-416. https://doi.org/10.1016/j.gca.2006.09.003

Huppert, H. E., & Sparks, R. S. J. (1989). Chilled margins in igneous rocks. *Earth and Planetary Science Letters*, ***92*** (3-4), 397-405. https://doi.org/10.1016/0012-821X(89)90063-0

Jackson, L. E., Wadsworth, F. B., Mitchell, J., Rennie, C., Llewellin, E. W., Hess, K. U., & Dingwell, D. B. (2022). Bubble rise in molten glasses and silicate melts during heating and cooling cycles. *Journal of the American Ceramic Society*, ***105*** (12), 7238-7253. https://doi.org/10.1111/jace.18680

Jamialahmadi, M., & Müuller-Steinhagen, H. (1993). Effect of superficial gas velocity on bubble size, terminal bubble rise velocity and gas hold-up in bubble columns. *Developments in chemical engineering and mineral processing*, ***1*** (1), 16-31. https://doi.org/10.1002/apj.5500010103

Jamialahmadi, M., Branch, C. and Muller-Steinhagen, H. (1994). Terminal bubble rise velocity in liquids. *Chemical Engineering Research and Design*, ***72***, 119-122

Johnson, D. S. L. (1969). Mass transfer between single bubbles and Newtonian and non-Newtonian liquids. *Ph.D. Thesis, University of Edinburgh.*

Jucha, R. B., Powers, D., McNeil, T., Subramanian, R. S., & Cole, R. (1982). Bubble rise in glassmelts. *Journal of the American Ceramic Society*, ***65*** (6), 289-292. https://doi.org/10.1111/j.1151-2916.1982.tb10446.x

Karamanev, D. G. (1994). Rise of gas bubbles in quiescent liquids. *AIChE journal*, ***40*** (8), 1418-1421. https://doi.org/10.1002/aic.690400814

Karamanev, D. G., Chavarie, C., & Mayer, R. C. (1996). Dynamics of the free rise of a light solid sphere in liquid. *AIChE journal*, *42*(6), 1789-1792. https://doi.org/10.1002/aic.690420630

Kariyasaki, A. (1987). Behaviour of a gas bubble in a liquid flow with a linear velocity profile. *Transactions of the Japan Society of Mechanical Engineers. B*, ***53***, 744-749. https://doi.org/10.1299/kikaib.53.744

Kočárková, H. (2011). Stability of glass foams: experiments at the bubble scale and on vertical film. *Ph.D. Thesis, Université Paris-Est.* https://theses.hal.science/tel-00664444

Kojima, E., Akehata, T., & Shirai, T. (1968). Rising velocity and shape of single air bubbles in highly viscous liquids. *Journal of Chemical Engineering of Japan*, ***1*** (1), 45-50. https://doi.org/10.1252/jcej.1.45

Kosior, D., Wiertel-Pochopien, A., Kowalczuk, P. B., & Zawala, J. (2023). Bubble Formation and Motion in Liquids—A Review. *Minerals*, ***13*** (9), 1130. https://doi.org/10.3390/min13091130

Kozakevitch, P. (1959). Surface tension. In *Physicochemical measurements at high temperatures*, *Butterworths Scientific Publications*, 208–224.

Krieger, I.M., & Dougherty, T.J. (1959). A mechanism for non-Newtonian flow in suspensions of rigid spheres. *Transactions of The Society of Rheology*, ***3*** (1), 137–152. https://doi.org/10.1122/1.548848

Kubota, M., Akehata, T., & Shirai, T. (1967). The behaviour of single air bubbles in liquids of small viscosity. *Kagakudaf Kogaku*, ***31*** (11), 1074-1080. https://doi.org/10.1252/kakoronbunshu1953.31.1074

Kulkarni, A. A., & Joshi, J. B. (2005). Bubble formation and bubble rise velocity in gas− liquid systems: a review. *Industrial & engineering chemistry research*, ***44*** (16), 5873-5931. https://doi.org/10.1021/ie049131p

Kure, I. K., Jakobsen, H. A., La Forgia, N., & Solsvik, J. (2021). Experimental investigation of single bubbles rising in stagnant liquid: Statistical analysis and image processing. *Physics of Fluids*, ***33*** (10). https://doi.org/10.1063/5.0061581

La Spina, G., Burton, M., & Vitturi, M. D. M. (2015). Temperature evolution during magma ascent in basaltic effusive eruptions: A numerical application to Stromboli volcano. *Earth and Planetary Science Letters*, *426*, 89-100. https://doi.org/10.1016/j.epsl.2015.06.015

La Spina, G., Arzilli, F., Burton, M. R., Polacci, M., & Clarke, A. B. (2022). Role of volatiles in highly explosive basaltic eruptions. *Communications Earth & Environment*, ***3***, 156. https://doi.org/10.1038/s43247-022-00479-6

Ladenburg, R. (1907). Über den Einfluß von Wänden auf die Bewegung einer Kugel in einer reibenden Flüssigkeit. *Annals of Physics*, ***328*** (8), 447-458. https://doi.org/10.1002/andp.19073280806

Lavallée, Y., Hess, K. U., Cordonnier, B., & Bruce Dingwell, D. (2007). Non-Newtonian rheological law for highly crystalline dome lavas. *Geology*, ***35*** (9), 843-846. https://doi.org/10.1130/G23594A.1

Leal, L. G., Skoog, J., & Acrivos, A. (1971). On the motion of gas bubbles in a viscoelastic liquid. *The Canadian Journal of Chemical Engineering*, ***49*** (5), 569-575. https://doi.org/10.1002/cjce.5450490504

Legendre, D., Zenit, R., & Velez-Cordero, J. R. (2012). On the deformation of gas bubbles in liquids. *Physics of Fluids*, ***24*** (4). https://doi.org/10.1063/1.4705527

Leifer, I., Patro, R. K., & Bowyer, P. (2000). A study on the temperature variation of rise velocity for large clean bubbles. *Journal of Atmospheric and Oceanic Technology*, ***17*** (10), 1392-1402. https://doi.org/10.1175/1520-0426(2000)017<1392:ASOTTV>2.0.CO;2

Lejeune, A. M., & Richet, P. (1995). Rheology of crystal-bearing silicate melts: An experimental study at high viscosities. *Journal of Geophysical Research: Solid Earth*, ***100*** (B3), 4215-4229. https://doi.org/10.1029/94JB02985

Lensky, N. G., Navon, O., & Lyakhovsky, V. (2004). Bubble growth during decompression of magma: experimental and theoretical investigation. *Journal of Volcanology and Geothermal Research*, ***129*** (1-3), 7-22. https://doi.org/10.1016/S0377-0273(03)00229-4

Leonard, J. H., & Houghton, G. (1963). Mass transfer and velocity of rise phenomena for single bubbles. *Chemical Engineering Science*, ***18*** (2), 133-142. https://doi.org/10.1016/0009-2509(63)80022-6

Lesher, C.E., & Spera, F.J. (2015). Thermodynamic and Transport Properties of Silicate Melts and Magma. In *The Encyclopedia of Volcanoes (Second Edition)*, *Academic Press*, 113-141. https://doi.org/10.1016/B978-0-12-385938-9.00005-5

Levich, V. G. (1962). Physicochemical hydrodynamics. *Englewood Cliffs, N.J.: Prentice-Hall.*

Li, K. W. K., & Schneider, A. (1993). Rise velocities of large bubbles in viscous Newtonian liquids. *Journal of the American Ceramic Society*, ***76*** (1), 241-244. https://doi.org/10.1111/j.1151-2916.1993.tb03717.x

Liu, Y. J., Liao, T. Y., & Joseph, D. D. (1995). A two-dimensional cusp at the trailing edge of an air bubble rising in a viscoelastic liquid. *Journal of Fluid Mechanics*, ***304***, 321-342. https://doi.org/10.1017/S0022112095004447

Liu, L., Yan, H., & Zhao, G. (2015). Experimental studies on the shape and motion of air bubbles in viscous liquids. *Experimental Thermal and Fluid Science*, ***62***, 109-121. https://doi.org/10.1016/j.expthermflusci.2014.11.018

Liu, L., Yan, H., Zhao, G., & Zhuang, J. (2016). Experimental studies on the terminal velocity of air bubbles in water and glycerol aqueous solution. *Experimental Thermal and Fluid Science*, ***78***, 254-265. https://doi.org/10.1016/j.expthermflusci.2016.06.011

Llewellin, E. W., & Manga, M. (2005). Bubble suspension rheology and implications for conduit flow. *Journal of Volcanology and Geothermal Research*, ***143*** (1-3), 205-217. https://doi.org/10.1016/j.jvolgeores.2004.09.018

Loudon, J. (1968). Mass transfer between gas bubbles and liquids. *Ph.D. Thesis, University of Edinburgh*.

Luchsinger, W. (1937). Disperse Gase, III. [Blasengröße und Aufstiegzeit]. *Kolloid-Zeitschrift*, ***81***, 180-182. https://doi.org/10.1007/BF01518782

Luo, X., Zhang, J., Tsuchiya, K., & Fan, L. S. (1997). On the rise velocity of bubbles in liquid-solid suspensions at elevated pressure and temperature. *Chemical engineering science*, ***52*** (21-22), 3693-3699. https://doi.org/10.1016/S0009-2509(97)00215-7

Macedo, I. C., & Yang, W. J. (1974). The drag of air bubbles rising in non-Newtonian liquids. *Japanese Journal of Applied Physics*, ***13*** (3), 529. https://doi.org/10.1143/JJAP.13.529

Mader, H. M., Llewellin, E. W., & Mueller, S. P. (2013). The rheology of two-phase magmas: A review and analysis. Journal of Volcanology and geothermal Research, **257**, 135-158. https://doi.org/10.1016/j.jvolgeores.2013.02.014

Mahmoudi, S., Hashemi Shahraki, B., & Aghajani, M. (2019). Experimental and theoretical investigation of CO2 and air bubble rising velocity through kerosene and distilled water in bubble column. *Journal of Dispersion Science and Technology*, ***40*** (1), 33-42. https://doi.org/10.1080/01932691.2018.1464465

Mangan, M., & Sisson, T. (2005). Evolution of melt-vapor surface tension in silicic volcanic systems: Experiments with hydrous melts. *Journal of Geophysical Research: Solid Earth*, ***110*** (B1). https://doi.org/10.1029/2004JB003215

Margaritis, A., te Bokkel, D. W., & Karamanev, D. G. (1999). Bubble rise velocities and drag coefficients in non-Newtonian polysaccharide solutions. *Biotechnology and bioengineering*, ***64*** (3), 257-266. https://doi.org/10.1002/(SICI)1097-0290(19990805)64:3<257::AID-BIT1>3.0.CO;2-F

Mastin, L. G. (2005). The controlling effect of viscous dissipation on magma flow in silicic conduits. *Journal of Volcanology and Geothermal Research*, ***143*** (1-3), 17-28. https://doi.org/10.1016/j.jvolgeores.2004.09.008

Maxworthy, T., Gnann, C., Kürten, M., & Durst, F. (1996). Experiments on the rise of air bubbles in clean viscous liquids. *Journal of fluid mechanics*, ***321***, 421-441. https://doi.org/10.1017/S0022112096007781

Melnik, O., & Sparks, R. S. J. (1999). Nonlinear dynamics of lava dome extrusion. *Nature*, ***402***, 37-41. https://doi.org/10.1038/46950

Mendelson, H. D. (1967). The prediction of bubble terminal velocities from wave theory. *AIChE Journal*, ***13*** (2), 250-253. https://doi.org/10.1002/aic.690130213

Merker, D., Böhm, L., Oßberger, M., Klüfers, P., & Kraume, M. (2017). Mass Transfer in Reactive Bubbly Flows–A Single-Bubble Study. *Chemical Engineering & Technology*, ***40*** (8), 1391-1399. https://doi.org/10.1002/ceat.201600715

Miyagi, O. (1925). The motion of an air bubble rising in water. *Journal of the Society of Mechanical Engineers*, ***28*** (95), 97-128. https://doi.org/10.1299/jsmemagazine.28.95_97

Miyahara, T., & Yamanaka, S. (1993). Mechanics of motion and deformation of a single bubble rising through quiescent highly viscous Newtonian and non-Newtonian media. *Journal of chemical engineering of Japan*, ***26*** (3), 297-302. https://doi.org/10.1252/jcej.26.297

Moitra, P., & Gonnermann, H. M. (2015). Effects of crystal shape-and size-modality on magma rheology. *Geochemistry, Geophysics, Geosystems*, ***16*** (1), 1-26. https://doi.org/10.1002/2014GC005554

Moore, D. W. (1959). The rise of a gas bubble in a viscous liquid. *Journal of Fluid Mechanics*, ***6*** (1), 113-130. https://doi.org/10.1017/S0022112059000520

Moore, D. W. (1965). The velocity of rise of distorted gas bubbles in a liquid of small viscosity. *Journal of Fluid Mechanics*, ***23*** (4), 749-766. https://doi.org/10.1017/S0022112065001660

Mourtada-Bonnefoi, C. C., & Laporte, D. (2002). Homogeneous bubble nucleation in rhyolitic magmas: an experimental study of the effect of H2O and CO2. *Journal of Geophysical Research: Solid Earth*, ***107*** (B4), ECV-2. https://doi.org/10.1029/2001JB000290

Mourtada-Bonnefoi, C. C., & Laporte, D. (2004). Kinetics of bubble nucleation in a rhyolitic melt: an experimental study of the effect of ascent rate. *Earth and Planetary Science Letters*, ***218*** (3-4), 521-537. https://doi.org/10.1016/S0012-821X(03)00684-8

Moynihan, C. T. (1995). Structural relaxation and the glass transition. *Reviews in mineralogy*, ***32***, 1-20. https://doi.org/10.1515/9781501509384-003

Mori, Y., Hijikata, K., & Kuriyama, I. (1977). Experimental Study of Bubble Motion in Mercury With and Without a Magnetic Field. *ASME Journal of Heat Transfer*. ***99*** (3). 404–410. https://doi.org/10.1115/1.3450710

Murase, T., & McBirney, A. R. (1973). Properties of some common igneous rocks and their melts at high temperatures. *Geological Society of America Bulletin*, ***84*** (11), 3563-3592. https://doi.org/10.1130/0016-7606(1973)84<3563:POSCIR>2.0.CO;2

Narayanan, S., Goossens, L. H. J., & Kossen, N. W. F. (1974). Coalescence of two bubbles rising in line at low Reynolds numbers. *Chemical Engineering Science*, ***29*** (10), 2071-2082. https://doi.org/10.1016/0009-2509(74)80221-6

Neuville, D. R., Courtial, P., Dingwell, D. B., & Richet, P. (1993). Thermodynamic and rheological properties of rhyolite and andesite melts. *Contributions to Mineralogy and Petrology*, ***113***, 572-581. https://doi.org/10.1007/BF00698324

Newcombe, M. E., Plank, T., Zhang, Y., Holycross, M., Barth, A., Lloyd, A.S., Ferguson, D., Houghton, B.F. & Hauri, E. (2020). Magma pressure-temperature-time paths during mafic explosive eruptions. *Frontiers in Earth Science*, ***8***, 531911. https://doi.org/10.3389/feart.2020.531911

Nguyen, A. V. (1998). Prediction of bubble terminal velocities in contaminated water. *AIChE Journal*, ***44*** (1), 226-230. https://doi.org/10.1002/aic.690440124

O'Brien, M. P., & Gosline, J. E. (1935). Velocity of large bubbles in vertical tubes. *Industrial & Engineering Chemistry*, ***27*** (12), 1436-1440.

https://doi.org/10.1021/ie50312a013

Okawa, T., Tanaka, T., Kataoka, I., & Mori, M. (2003). Temperature effect on single bubble rise characteristics in stagnant distilled water. *International journal of heat and mass transfer*, ***46*** (5), 903-913. https://doi.org/10.1016/S0017-9310(02)00345-9

Okazaki, S. (1964). The velocity of ascending air bubbles in aqueous solutions of a surface active substance and the life of the bubble on the same solution. *Bulletin of the Chemical Society of Japan*, ***37*** (2), 144-150. https://doi.org/10.1246/bcsj.37.144

Owens, J. S. (1921). Experiments on Air-Lift Pumping. *Engineering*, ***112***, 458-461

Paneni, M. (1969). Hydrogen removal from steel., *MSc. Thesis, McGill University.*

Papale, P. (1999). Strain-induced magma fragmentation in explosive eruptions. *Nature*, ***397***, 425-428. https://doi.org/10.1038/17109

Park, S. H., Park, C., Lee, J., & Lee, B. (2017). *A simple parameterization for the rising velocity of bubbles in a liquid pool. Nuclear Engineering and Technology*, ***49*** (4), 692-699. https://doi.org/10.1016/j.net.2016.12.006

Parkinson, L., Sedev, R., Fornasiero, D., & Ralston, J. (2008). The terminal rise velocity of 10–100 μm diameter bubbles in water. *Journal of colloid and interface science*, ***322*** (1), 168-172. https://doi.org/10.1016/j.jcis.2008.02.072

Pawliszak, P., Ulaganathan, V., Bradshaw-Hajek, B. H., Manica, R., Beattie, D. A., & Krasowska, M. (2019). Mobile or immobile? Rise velocity of air bubbles in high-purity water. *The Journal of Physical Chemistry C*, ***123*** (24), 15131-15138. https://doi.org/10.1021/acs.jpcc.9b03526

Peebles, F. N. (1952). The Motion of Gas Bubbles in the HRE Reactor Core. *Atomic Energy Commission Reports*, ***ORNL-1171***.

Perkins, D. (2022). Petrology. *University of North Dakota* https://doi.org/10.31356/oers030

Prousevitch, A. A., Sahagian, D. L., & Anderson, A. T. (1993). Dynamics of diffusive bubble growth in magmas: Isothermal case. *Journal of Geophysical Research: Solid Earth*, ***98*** (B12), 22283-22307. https://doi.org/10.1029/93JB02027

Pyle, D. M., & Pyle, D. L. (1995). Bubble migration and the initiation of volcanic eruptions. *Journal of volcanology and geothermal research*, ***67*** (4), 227-232. https://doi.org/10.1016/0377-0273(94)00111-S

Räbiger, N., & Vogelpohl, A. (1986). Bubble formation and its movement in Newtonian and non-Newtonian liquids. *Encyclopedia of fluid mechanics*, ***3***, 58-88.

Raymond, F., & Rosant, J. M. (2000). A numerical and experimental study of the terminal velocity and shape of bubbles in viscous liquids. *Chemical Engineering Science*, ***55*** (5), 943-955. https://doi.org/10.1016/S0009-2509(99)00385-1

Raymond, D. R., & Zieminski, S. A. (1971). Mass transfer and drag coefficients of bubbles rising in dilute aqueous solutions. *AIChE Journal*, ***17*** (1), 57-65. https://doi.org/10.1002/aic.690170114

Redfield, J. A., & Houghton, G. (1965). Mass transfer and drag coefficients for single bubbles at Reynolds numbers of 0.02–5000. *Chemical Engineering Science*, ***20*** (2), 131-139. https://doi.org/10.1016/0009-2509(65)85006-0

Reynolds, O. (1883). XXIX. An experimental investigation of the circumstances which determine whether the motion of water shall be direct or sinuous, and of the law of resistance in parallel channels. *Philosophical Transactions of the Royal society of London*, ***174***, 935-982. https://doi.org/10.1098/rstl.1883.0029

Rodrigue, D. (2001). Generalized correlation for bubble motion. *AIChE journal*, ***47*** (1), 39-44. https://doi.org/10.1002/aic.690470106

Rodrigue, D. (2002). A simple correlation for gas bubbles rising in power-law fluids. *The Canadian Journal of Chemical Engineering*, ***80*** (2), 289-292. https://doi.org/10.1002/cjce.5450800214

Rodrigue, D. (2004). A general correlation for the rise velocity of single gas bubbles. *The Canadian Journal of Chemical Engineering*, ***82*** (2), 382-386. https://doi.org/10.1002/cjce.5450820219

Rodrigue, D., De Kee, D., & Fong, C. C. M. (1996). An experimental study of the effect of surfactants on the free rise velocity of gas bubbles. *Journal of non-newtonian fluid mechanics*, ***66*** (2-3), 213-232. https://doi.org/10.1016/S0377-0257(96)01486-3

Romine, W. L., & Whittington, A. G. (2015). A simple model for the viscosity of rhyolites as a function of temperature, pressure and water content. *Geochimica et cosmochimica acta*, ***170***, 281-300. https://doi.org/10.1016/j.gca.2015.08.009

Rosenberg, B. (1950). The drag and shape of air bubbles moving in liquids. *David W. Taylor Model Basin. Navy Department, Washington DC, Report* ***727***.

Rybczynski, W. (1911). Über die fortschreitende Bewegung einer flüssigen Kugel in einem zähen Medium. *Bulletin international de l'Académie des sciences de Cracovie A*, ***1***, 40–46

Sahagian, D. (2005). Volcanic eruption mechanisms: Insights from intercomparison of models of conduit processes. *Journal of Volcanology and Geothermal Research*, ***143*** (1-3), 1-15. https://doi.org/10.1016/j.jvolgeores.2004.12.006

Sam, A., Gomez, C. O., & Finch, J. A. (1996). Axial velocity profiles of single bubbles in water/frother solutions. *International Journal of Mineral Processing*, ***47*** (3-4), 177-196. https://doi.org/10.1016/0301-7516(95)00088-7

Sanada, T., Sugihara, K., Shirota, M., & Watanabe, M. (2008). Motion and drag of a single bubble in super-purified water. *Fluid dynamics research*, ***40*** (7-8), 534. https://doi.org/10.1016/j.fluiddyn.2007.12.005

Saper, L. M., & Stolper, E. M. (2020). Controlled cooling-rate experiments on olivine-hosted melt inclusions: Chemical diffusion and quantification of eruptive cooling rates on Hawaii and Mars. *Geochemistry, Geophysics, Geosystems*, ***21*** (2), 1-40. https://doi.org/10.1029/2019GC008772

Scriven, L. E. (1960). Dynamics of a fluid interface equation of motion for Newtonian surface fluids. *Chemical Engineering Science*, ***12*** (2), 98-108. https://doi.org/10.1016/0009-2509(60)87003-0

Serizawa, A., & Kataoka, I. (1994). Dispersed flow-I. *Multiphase science and technology*, ***8*** (1-4). https://doi.org/10.1615/MultScienTechn.v8.i1-4.40

Shabalin, K.N., Krylov, S.F., & Oborin, V.I. (1939). The rate of absorption under conditions of bubbling. *Journal of Chemical Industry USSR*, ***16***, 10-14.

Sharma, S. K., & Philbrook, W. O. (1970). Improved values of surface tension of calcium silicate melts. *Scripta Metallurgica*, ***4*** (2), 107-109. https://doi.org/10.1016/0036-9748(70)90173-0

Sparks, R. S. J. (1978). The dynamics of bubble formation and growth in magmas: a review and analysis. *Journal of Volcanology and Geothermal Research*, ***3*** (1-2), 1-37.

Sparks, R. S. J. (2003). Forecasting volcanic eruptions. *Earth and Planetary Science Letters*, ***210*** (1-2), 1-15. https://doi.org/10.1016/S0012-821X(03)00124-9

Sparks, R. S. J., Huppert, H. E., & Turner, J. S. (1984). The fluid dynamics of evolving magma chambers. *Philosophical Transactions of the Royal Society of London. Series A, Mathematical and Physical Sciences*, ***310***, 511-534. https://doi.org/10.1098/rsta.1984.0006

Sparks, R. S. J., Baker, L., Brown, R. J., Field, M., Schumacher, J., Stripp, G., & Walters, A. (2006). Dynamical constraints on kimberlite volcanism. *Journal of Volcanology and Geothermal Research*, ***155*** (1-2), 18-48. https://doi.org/10.1016/j.jvolgeores.2006.02.010

Spina, L., Cimarelli, C., Scheu, B., Di Genova, D., & Dingwell, D. B. (2016). On the slow decompressive response of volatile-and crystal-bearing magmas: An analogue experimental investigation. *Earth and Planetary Science Letters*, ***433***, 44-53. https://doi.org/10.1016/j.epsl.2015.10.029

Spina, L., Cannata, A., Morgavi, D., & Perugini, D. (2019). Degassing behaviour at basaltic volcanoes: New insights from experimental investigations of different conduit geometry and magma viscosity. *Earth-science reviews*, ***192***, 317-336. https://doi.org/10.1016/j.earscirev.2019.03.010

Stokes, G. G. (1851). On the effect of the internal friction of fluids on the motion of pendulums. *Transactions of the Cambridge Philosophical Society*, ***9*** (1), 1-62

Stuke, B. (1952). Das Verhalten der Oberfläche von sich in Flüssigkeiten bewegenden Gasblasen. *Naturwissenschaften*, ***39***, 325-326. https://doi.org/10.1007/BF00589374

Tadaki, R., & Maeda, S. (1961). On the shape and rate of rise of a single bubble rising in various stationary liquids. *Journal of Chemical Engineering of Japan*, ***25*** (4), 254-264. https://doi.org/10.1252/kakoronbunshu1953.25.254

Takemura, F., & Magnaudet, J. (2003). The transverse force on clean and contaminated bubbles rising near a vertical wall at moderate Reynolds number. *Journal of Fluid Mechanics*, ***495***, 235-253. https://doi.org/10.1017/S0022112003006232

Talaia, M. A. (2007). Terminal velocity of a bubble rise in a liquid column. *World Academy of Science, Engineering and Technology*, ***28***, 264-268. doi.org/10.5281/zenodo.1070173

Tammann, G. H. W. Z., & Hesse, W. (1926). Die Abhängigkeit der Viscosität von der Temperatur bie unterkühlten Flüssigkeiten. *Zeitschrift für anorganische und allgemeine Chemie*, ***156*** (1), 245-257. https://doi.org/10.1002/zaac.19261560121

Taylor, G. I. (1923). Stability of a Viscous Liquid Contained between Two Rotating Cylinders. *Philosophical Transactions of the Royal Society A: Mathematical, Physical and Engineering Sciences*, ***223*** (605-615), 289–343.

https://doi.org/10.1098/rsta.1923.0008

Tomiyama, A., Zun, I., Sou, A., & Sakaguchi, T. (1993). Numerical analysis of bubble motion with the VOF method. *Nuclear Engineering and Design*, ***141*** (1-2), 69-82. https://doi.org/10.1016/0029-5493(93)90093-O

Tomiyama, A., Kataoka, I., Zun, I., & Sakaguchi, T. (1998). Drag coefficients of single bubbles under normal and micro gravity conditions. *JSME International Journal Series B Fluids and Thermal Engineering*, ***41*** (2), 472-479. https://doi.org/10.1299/jsmeb.41.472

Tomiyama, A., Celata, G. P., Hosokawa, S., & Yoshida, S. (2002). Terminal velocity of single bubbles in surface tension force dominant regime. *International journal of multiphase flow*, ***28*** (9), 1497-1519. https://doi.org/10.1016/S0301-9322(02)00032-0

Tomiyama, A., Tamai, H., Zun, I., & Hosokawa, S. (2002). Transverse migration of single bubbles in simple shear flows. *Chemical Engineering Science*, ***57*** (11), 1849-1858. https://doi.org/10.1016/S0009-2509(02)00085-4

Taniguchi, H. (1988). Surface tension of melts in the system $CaMgSi_2O_6$-$CaAl_2Si_2O_8$ and its structural significance. *Contributions to Mineralogy and Petrology*, ***100*** (4), 484-489. https://doi.org/10.1007/BF00371377

Tsuge, H., & Hibino, S. I. (1977). The onset conditions of oscillatory motion of single gas bubbles rising in various liquids. *Journal of Chemical Engineering of Japan*, ***10*** (1), 66-68. https://doi.org/10.1252/jcej.10.66

Uno, S., & Kintner, R. C. (1956). Effect of wall proximity on the rate of rise of single air bubbles in a quiescent liquid. *AIChE Journal*, ***2*** (3), 420-425. https://doi.org/10.1002/aic.690020323

Vasseur, P., & Cox, R. G. (1977). The lateral migration of spherical particles sedimenting in a stagnant bounded fluid. *Journal of fluid mechanics*, ***80*** (3), 561-591. https://doi.org/10.1017/S0022112077001840

Vergniolle, S., & Gaudemer, Y. (2015). From reservoirs and conduits to the surface: Review of role of bubbles in driving basaltic eruptions. *Hawaiian volcanoes: from source to surface*, *American Geophysical Union, Geophysical Monograph*, ***208***, 289-321. https://doi.org/10.1002/9781118872079.ch14

Viana, F., Pardo, R., Rötzer, I., & Guzmán, N. (2001). Terminal rise velocity of various bubble sizes in a tube and an annular space through a viscous liquid. *Proceedings of Lacaflum 2001, 5th Latin American and Caribbean Congress of Fluid Mechanics, Caracas, Venezuela*, ***OAF-7***.

Vogel, H. (1921). Das temperaturabhangigkeitsgesetz der viskositat von flussigkeiten. *Physikalische Zeitschrift*, ***22***, 645-646.

Walker, D., & Mullins Jr, O. (1981). Surface tension of natural silicate melts from 1,200–1,500 C and implications for melt structure. *Contributions to Mineralogy and Petrology*, ***76*** (4), 455-462. https://doi.org/10.1007/BF00371487

Wallace, P. J., Plank, T., Edmonds, M., & Hauri, E. H. (2015). Volatiles in magmas. In *The Encyclopedia of Volcanoes (Second Edition)*, *Academic Press*, 163-183. https://doi.org/10.1016/B978-0-12-385938-9.00007-9

Wallis, G. B. (1974). The terminal speed of single drops or bubbles in an infinite medium. *International Journal of Multiphase Flow*, ***1*** (4), 491-511. https://doi.org/10.1016/0301-9322(74)90003-2

Wang, Z. H., Wang, S. D., Meng, X., & Ni, M. J. (2017). UDV measurements of single bubble rising in a liquid metal Galinstan with a transverse magnetic field. *International Journal of Multiphase Flow*, ***94***, 201-208. https://doi.org/10.1016/j.ijmultiphaseflow.2017.05.001

Weaver, J., Lavallée, Y., Ashraf, M., Kendrick, J. E., Lamur, A., Schauroth, J., & Wadsworth, F. B. (2022). Vesiculation and densification of pyroclasts: A clast-size dependent competition between bubble growth and diffusive outgassing. *Journal of Volcanology and Geothermal Research*, ***428***, 107550. https://doi.org/10.1016/j.jvolgeores.2022.107550

Webb, S. L., & Dingwell, D. B. (1990). The onset of non-Newtonian rheology of silicate melts: A fiber elongation study. *Physics and Chemistry of Minerals*, ***17***, 125-132. https://doi.org/10.1007/BF00199663

Wegener, P. P., & Parlange, J. Y. (1973). Spherical-cap bubbles. *Annual Review of Fluid Mechanics*, ***5*** (1), 79-100. https://doi.org/10.1146/annurev.fl.05.010173.000455

Weirauch Jr, D. A., & Ziegler, D. P. (1996). Surface tension of calcium aluminosilicate glass using computerized drop shape analysis. *Journal of the American Ceramic Society*, *79*(4), 920-926. https://doi.org/10.1111/j.1151-2916.1996.tb08526.x

Whittington, A. G., Hellwig, B. M., Behrens, H., Joachim, B., Stechern, A., & Vetere, F. (2009). The viscosity of hydrous dacitic liquids: implications for the rheology of evolving silicic magmas. *Bulletin of Volcanology*, ***71***, 185-199. https://doi.org/10.1007/s00445-008-0217-y

Will, J. B., Mathai, V., Huisman, S. G., Lohse, D., Sun, C., & Krug, D. (2021). Kinematics and dynamics of freely rising spheroids at high Reynolds numbers. *Journal of fluid mechanics*, ***912***, A16. https://doi.org/10.1017/jfm.2020.1104

Woods, A. W., & Cardoso, S. S. (1997). Triggering basaltic volcanic eruptions by bubble-melt separation. *Nature*, ***385***, 518-520. https://doi.org/10.1038/385518a0

Wu, T. Y. T. (1972). Cavity and wake flows. *Annual Review of Fluid Mechanics*, ***4*** (1), 243-284. https://doi.org/10.1146/annurev.fl.04.010172.001331

Yan, X., Jia, Y., Wang, L., & Cao, Y. (2017). Drag coefficient fluctuation prediction of a single bubble rising in water. *Chemical Engineering Journal*, ***316***, 553-562. https://doi.org/10.1016/j.cej.2017.01.137

Zana, E. (1975). The motion and associated mass transfer characteristics of gas bubbles in viscoelastic liquids. *Ph.D. Thesis, California Institute of Technology.*

Zaruba, A., Lucas, D., Prasser, H. M., & Höhne, T. (2007). Bubble-wall interactions in a vertical gas–liquid flow: Bouncing, sliding and bubble deformations. *Chemical engineering science*, ***62*** (6), 1591-1605. https://doi.org/10.1016/j.ces.2006.11.044

Zawala, J., & Niecikowska, A. (2017). "Bubble-on-demand" generator with precise adsorption time control. *Review of Scientific Instruments*, ***88*** (9).

https://doi.org/10.1063/1.5001846

Zeng, L., Balachandar, S., & Fischer, P. (2005). Wall-induced forces on a rigid sphere at finite Reynolds number. *Journal of Fluid Mechanics*, ***536***, 1-25. https://doi.org/10.1017/S0022112005004738

Zeng, L., Najjar, F., Balachandar, S., & Fischer, P. (2009). Forces on a finite-sized particle located close to a wall in a linear shear flow. *Physics of fluids*, ***21*** (3). https://doi.org/10.1063/1.3082232

Zdonik, S. B. (1942). The liquid-film coefficient and the mechanism of bubble absorption. *MSc. Thesis, Massachusetts Institute of Technology.*

Zhang, Y., Xu, Z., & Liu, Y. (2003). Viscosity of hydrous rhyolitic melts inferred from kinetic experiments, and a new viscosity model. *American Mineralogist*, ***88*** (11-12), 1741-1752. https://doi.org/10.2138/am-2003-11-1215

Zhang, C., Eckert, S., & Gerbeth, G. (2004). Gas and liquid velocity measurements in bubble chain driven two-phase flow by means of UDV and LDA. *Proceedings of 5th International Conference on Multiphase Flow, Yokohama*, ***ICMF04-260*.**

Zhang, C., Eckert, S., & Gerbeth, G. (2005). Experimental study of single bubble motion in a liquid metal column exposed to a DC magnetic field. *International journal of multiphase flow*, ***31*** (7), 824-842. https://doi.org/10.1016/j.ijmultiphaseflow.2005.05.001

Zhang, Y., Xu, Z., Zhu, M., & Wang, H. (2007). Silicate melt properties and volcanic eruptions. *Reviews of Geophysics*, ***45*** (4). https://doi.org/10.1029/2006RG000216

Zhou, W., Chrust, M., & Dušek, J. (2017). Path instabilities of oblate spheroids. *Journal of Fluid Mechanics*, ***833***, 445-468. https://doi.org/10.1017/jfm.2017.718

Ẑun, I. (1980). The transverse migration of bubbles influenced by walls in vertical bubbly flow. *International Journal of Multiphase Flow*, ***6*** (6), 583-588. https://doi.org/10.1016/0301-9322(80)90053-1